

Neutrino physics

Pilar Hernández

IFIC, Universidad de València and CSIC, E-46071 Valencia, Spain.

Email: Pilar.Hernandez@ific.uv.es

This is an update of the lectures previously published in [arXiv:1708.01046](https://arxiv.org/abs/1708.01046). The topics discussed in this lecture include: general properties of neutrinos in the SM, the theory of neutrino masses and mixings (Dirac and Majorana), neutrino oscillations both in vacuum and in matter, as well as an overview of the experimental evidence for neutrino masses and of the prospects in neutrino oscillation physics. We also briefly comment on the relevance of neutrinos in leptogenesis and in beyond-the-Standard-Model physics.

1	Introduction	140
2	Neutrinos in the Standard Model	143
2.1	Chiral structure of the weak interactions	143
2.2	Family structure	145
3	Massive neutrinos	146
3.1	Massive Dirac neutrinos	147
3.2	Massive Majorana neutrinos	149
3.3	Neutrino masses and physics beyond the Standard Model	150
4	Neutrino masses and lepton mixing	150
5	Majorana versus Dirac	152
6	Neutrino oscillations	154
6.1	Plane wave derivation	155
6.2	Wave packet derivation	156
6.3	QFT derivation	157
6.4	Neutrino oscillations in vacuum	159
6.5	Neutrino propagation in matter	161
6.6	Neutrino oscillations in constant matter	162
6.7	Neutrino oscillations in variable matter	162
7	Evidence for neutrino oscillations	165
7.1	Solar neutrinos	165
7.2	Atmospheric neutrinos	170
8	The three-neutrino mixing scenario	173
9	Prospects in determining unknown neutrino parameters	177

This article should be cited as: Neutrino physics, Pilar Hernández, DOI: [10.23730/CYRSP-2025-001.139](https://doi.org/10.23730/CYRSP-2025-001.139), in: Proceedings of the 2022 European School of High-Energy Physics, CERN Yellow Reports: School Proceedings, CERN-2025-001, DOI: [10.23730/CYRSP-2025-001](https://doi.org/10.23730/CYRSP-2025-001), p. 139. © CERN, 2025. Published by CERN under the [Creative Commons Attribution 4.0 license](https://creativecommons.org/licenses/by/4.0/).

9.1	Neutrino ordering	177
9.2	Leptonic CP violation	179
9.3	Absolute neutrino mass scale	182
10	Outliers: the LSND anomaly	182
11	Neutrinos and BSM physics	184
11.1	One example: Type I seesaw model	188
12	Low-scale leptogenesis	193
13	Conclusions	200

1 Introduction

Neutrinos made their first *invisible* appearance at the beginning of the 20th century as *dark* particles in radioactive β -decay. In this process a nucleus undergoes a transition



emitting an electron, which, by energy–momentum conservation, should have an energy approximately equal to the difference of the parent and daughter nuclear masses, Q , see Fig. 1.

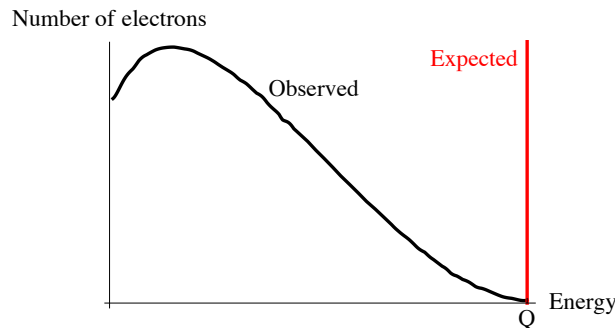


Fig. 1: Electron spectrum of β -decay.

The spectrum of the electrons was measured to be instead continuous with an end-point at Q . It took almost 20 years to come up with an explanation to this apparent violation of energy–momentum conservation. W. Pauli called for a *desperate remedy*, suggesting that in the decay, a neutral and light particle was being emitted together with the electron and escaped undetected. In that case the spectrum of the electron would indeed be continuous since only the sum of the energy of the electron and the phantom particle should equal Q . The dark particle got an Italian name: *neutrino* in honour of E. Fermi, who was among the first to take seriously Pauli’s hypothesis, from which he constructed the famous theory of β -decay [1]. In this theory, the interaction responsible for β -decay is shown in Fig. 2, a four-fermion interaction with strength given by G_F , the Fermi constant.

Such interaction implies that neutrinos should also scatter off matter through the inverse beta

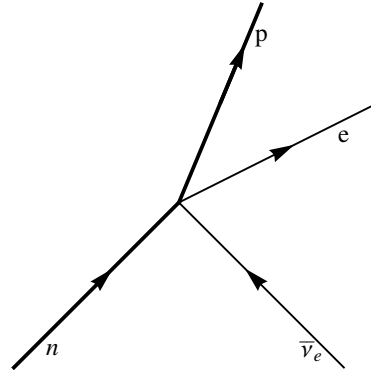


Fig. 2: Fermi four-fermion coupling responsible for β -decay.

process, $\bar{\nu} p \rightarrow n e^+$. Bethe and Pearls [2] estimated the cross section for such process to be

$$\sigma_{\bar{\nu}} \leq 10^{-44} \text{ cm}^2, \quad E_{\bar{\nu}} \simeq 2 \text{ MeV}, \quad (1.2)$$

and concluded that “*it is absolutely impossible to observe processes of this kin*”. Indeed this tiny cross section implies that a neutrino has a mean free path of thousands of light-years in water.

Pontecorvo [3] however was among the first to realise that it was not so hopeless. One could get a few events per day in a ton-mass scale detector with a neutrino flux of $10^{11} \nu/\text{cm}^2/\text{s}$. Such is the neutrino flux from a typical nuclear reactor at a few tens of meters distance from its core. Reines and Cowen (RC) succeeded in detecting reactor neutrinos [4, 5]. They were able to detect neutrinos via inverse beta decay in a very massive detector thanks to the extremely clean signal which combines the detection of the positron and the neutron in delayed coincidence, see Fig. 3. This experiment not only led to the discovery of anti-neutrinos, but introduced a detection technique that is still being used today in state-of-the-art reactor neutrino experiments and continues to make fundamental discoveries in neutrino physics.

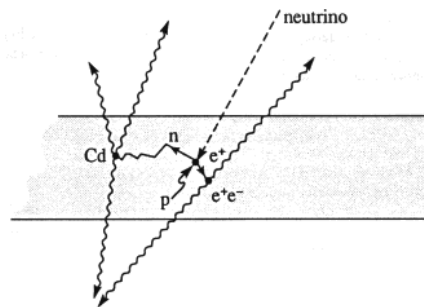


Fig. 3: Detection technique in the Reines–Cowan experiment.

Shortly after anti-neutrinos were discovered, it was realised that they come in flavours or families. The muon had been discovered in cosmic rays much earlier, and pion decay to muons is an analogous

process to β -decay:

$$\pi^- \rightarrow \mu^- \bar{\nu}_\mu. \quad (1.3)$$

It was understood that also in this case a (anti-)neutrino is emitted but, accompanying a μ instead of an electron, it had a different identity to that in β -decay. Since the energy transfer in this process is higher than in β -decay, and the neutrino cross-sections grow fast with energy in the Fermi theory, it would actually be easier to detect this new type of neutrino.

In 1962 Lederman, Schwartz and Steinberger (LSS) detected for the first time neutrinos from pion decay by creating the first accelerator neutrino beam [6]. The accelerated proton beam is made to hit a fixed target producing pions and other hadrons that decay into neutrinos and other particles, mimicking what happens in cosmic rays. If a thick shield intercepts the secondary particles, all particles except the neutrinos are stopped, see Fig. 4. Finally a neutrino detector is located behind the shield. A neutrino event will induce the appearance of a muon in the detector. Again this was such a great idea that we are still making discoveries with the modern versions of the LSS experiment, in the so-called conventional accelerator neutrino beams.

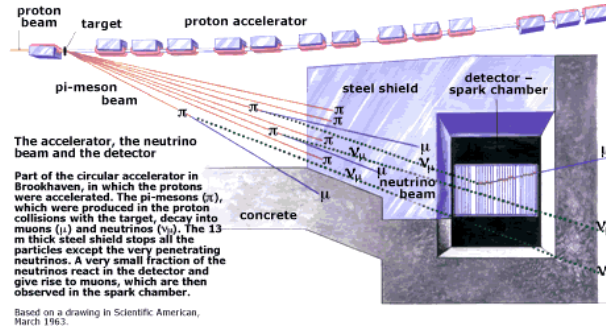


Fig. 4: Lederman, Schwartz, Steinberger experiment.

Kinematical effects of neutrino masses were searched for by measuring very precisely the end-point of the lepton energy spectrum in weak decays, that gets modified if neutrinos are massive. In particular the most stringent limit is obtained from tritium β -decay for the “electron” neutrino:

$${}^3\text{H} \rightarrow {}^3\text{He} + e^- + \bar{\nu}_e. \quad (1.4)$$

Figure 5 shows the effect of a neutrino mass in the end-point electron energy spectrum in this decay.

The best limit has been recently improved by the Katrin experiment [7]:

$$m_{\nu_e} < 0.8 \text{ eV} (90\% \text{CL}), \quad (1.5)$$

which aims at reaching a sensitivity of 0.2 eV. The direct limits from processes involving μ, τ leptons are much weaker. The best limit on the ν_μ mass ($m_{\nu_\mu} < 170 \text{ keV}$ [8]) was obtained from the end-point spectrum of the decay $\pi^+ \rightarrow \mu^+ \nu_\mu$, while that on the ν_τ mass was obtained at LEP ($m_{\nu_\tau} <$

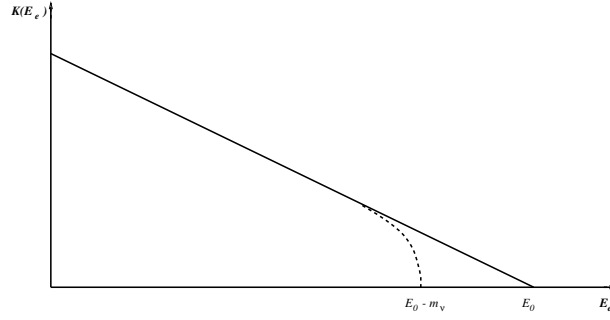


Fig. 5: Effect of a neutrino mass in the end-point of the lepton energy spectrum in β decay.

Table 1: Irreducible fermionic representations in the Standard Model: $(d_{SU(3)}, d_{SU(2)})_Y$.

$(\mathbf{1}, \mathbf{2})_{-\frac{1}{2}}$	$(\mathbf{3}, \mathbf{2})_{\frac{1}{6}}$	$(\mathbf{1}, \mathbf{1})_{-1}$	$(\mathbf{3}, \mathbf{1})_{\frac{2}{3}}$	$(\mathbf{3}, \mathbf{1})_{-\frac{1}{3}}$
$\begin{pmatrix} \nu_e \\ e \end{pmatrix}_L$	$\begin{pmatrix} u^i \\ d^i \end{pmatrix}_L$	e_R	u^i_R	d^i_R
$\begin{pmatrix} \nu_\mu \\ \mu \end{pmatrix}_L$	$\begin{pmatrix} c^i \\ s^i \end{pmatrix}_L$	μ_R	c^i_R	s^i_R
$\begin{pmatrix} \nu_\tau \\ \tau \end{pmatrix}_L$	$\begin{pmatrix} t^i \\ b^i \end{pmatrix}_L$	τ_R	t^i_R	b^i_R

18.2 MeV [9]) from the decay $\tau \rightarrow 5\pi\nu_\tau$. Neutrinos in the Standard Model were therefore conjectured to be massless.

2 Neutrinos in the Standard Model

The Standard Model (SM) is a gauge theory based on the gauge group $SU(3) \times SU(2) \times U_Y(1)$. All elementary particles arrange in irreducible representations of this gauge group. The quantum numbers of the fermions $(d_{SU(3)}, d_{SU(2)})_Y$ are listed in Table 1.

Under gauge transformations neutrinos transform as doublets of $SU(2)$, they are singlets under $SU(3)$ and their hypercharge is $-1/2$. The electric charge, given by $Q = T_3 + Y$, vanishes. They are therefore the only particles in the SM that carry no conserved charge.

The two most intriguing features of Table 1 are its left–right or chiral asymmetry, and the three-fold repetition of family structures. Neutrinos have been essential in establishing both features.

2.1 Chiral structure of the weak interactions

The left and right entries in Table 1 have well defined chirality, negative and positive respectively. They are two-component spinors or Weyl fermions, the smallest irreducible representation of the Lorentz group representing spin $1/2$ particles. Only fields with negative chirality carry the $SU(2)$ charge. For free fermions moving at the speed of light (i.e., massless), the chiral states have a well defined helicity,

i.e they are eigenstates of the helicity operator, $\Sigma = \frac{\mathbf{s} \cdot \mathbf{p}}{|\mathbf{p}|}$, that measures the component of the spin in the direction of the momentum. This is not inconsistent with Lorentz invariance, since for a fermion travelling at the speed of light, the helicity is the same in any reference frame. In other words, the helicity operator commutes with the Hamiltonian for a massless fermion and is thus a good quantum number.

The discrete symmetry under CPT (charge conjugation, parity, and time reversal), which is a basic building block of any Lorentz invariant and unitary quantum field theory (QFT), requires that for any left-handed particle, there exists a right-handed antiparticle, with opposite charge, but the right-handed particle state may not exist. A Weyl fermion field represents therefore a particle of negative helicity and an antiparticle with positive one.

Parity however transforms left and right fields into each other, thus the left-handedness of the weak interactions implies that parity is maximally broken in the SM. The breaking is nowhere more obvious than for neutrinos since the parity partner of the neutrino does not exist. All the remaining fermions in the SM come in parity pairs, albeit with different $SU(2) \times U(1)$ charges. Since this gauge symmetry is spontaneously broken, the left and right fields combine into massive Dirac fermions, that is a four component representation of the Lorentz group and parity, which represents a particle and an antiparticle with either helicity. The chirality components are recovered from the four-component Dirac spinor by the chiral projectors

$$\psi_L = P_L \psi = \frac{1 - \gamma_5}{2} \psi, \quad \psi_R = P_R \psi = \frac{1 + \gamma_5}{2} \psi. \quad (2.1)$$

The SM resolved the Fermi interaction as being the result of the exchange of the $SU(2)$ massive W boson as in Fig. 6.

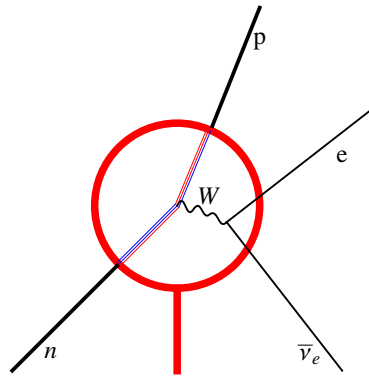


Fig. 6: β -decay process in the SM.

Neutrinos interact in the SM via charged and neutral currents:

$$\mathcal{L}_{SM} \supset -\frac{g}{\sqrt{2}} \sum_{\alpha} \bar{\nu}_{\alpha} \gamma_{\mu} P_L l_{\alpha} W_{\mu}^{+} - \frac{g}{2 \cos \theta_W} \sum_{\alpha} \bar{\nu}_{\alpha} \gamma_{\mu} P_L \nu_{\alpha} Z_{\mu}^{+} + h.c. \quad (2.2)$$

The weak current is therefore $V-A$ since it only couples to the left fields: $\gamma_{\mu} P_L \propto \gamma_{\mu} - \gamma_{\mu} \gamma_5$. This structure is clearly seen in the kinematics of weak decays involving neutrinos, such as the classic

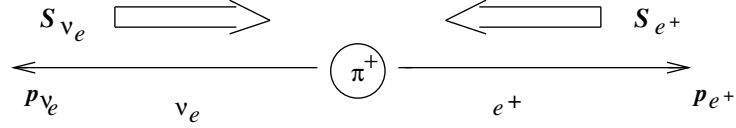


Fig. 7: Kinematics of pion decay: two recoiling particles must have same helicity to ensure angular momentum conservation.

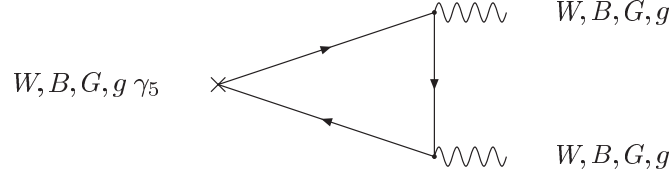


Fig. 8: Triangle diagrams that can give rise to anomalies. W, B, G are the gauge bosons associated to the $SU(2), U_Y(1), SU(3)$ gauge groups, respectively, and g is the graviton

example of pion decay to $e\bar{\nu}_e$ or $\mu\bar{\nu}_\mu$. In the limit of vanishing electron or muon mass, this decay is forbidden, because the spin of the initial state is zero and thus it is impossible to conserve simultaneously momentum and angular momentum if the two recoiling particles must have opposite helicities, as shown in Fig. 7. The decay amplitude is therefore proportional to the lepton mass and the ratio of the decay rates to electrons and muons, in spite of the larger phase space in the former, is strongly suppressed by the factor $\left(\frac{m_e}{m_\mu}\right)^2 \sim 2 \times 10^{-5}$.

Another profound consequence of the chiral nature of the weak interaction is anomaly cancellation. The chiral coupling of fermions to gauge fields leads generically to inconsistent gauge theories due to chiral anomalies: if any of the diagrams depicted in Fig. 8 is non-vanishing, the weak current which is conserved at tree level is not at one loop, implying a catastrophic breaking of gauge invariance. Anomaly cancellation is the requirement that all these triangle diagrams vanish, which imposes strong constraints on the hypercharge assignments of the fermions in the SM, which are *miraculously* satisfied:

$$\overbrace{\sum_{i=\text{quarks}} Y_i^L - Y_i^R}^{GGB} = \overbrace{\sum_{i=\text{doublets}} Y_i^L}^{WWB} = \overbrace{\sum_i Y_i^L - Y_i^R}^{Bgg} = \overbrace{\sum_i (Y_i^L)^3 - (Y_i^R)^3}^{B^3} = 0, \quad (2.3)$$

where $Y_i^{L/R}$ are the hypercharges of the left/right components of the fermionic field i , and the triangle diagram corresponding to each of the sums is indicated above the bracket.

2.2 Family structure

Concerning the family structure, we know, thanks to neutrinos, that there are exactly three families in the SM. An extra SM family with quarks and charged leptons so heavy that cannot be produced at the energies explored so far in colliders, would also have massless neutrinos that would contribute to the

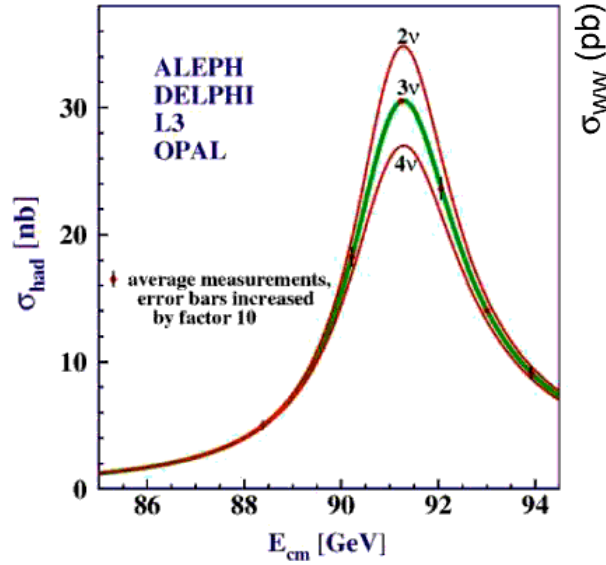


Fig. 9: Z^0 resonance from the LEP experiments. Data are compared to the case of $N_\nu = 2, 3$ and 4

invisible Z^0 decay:

$$Z^0 \rightarrow \bar{\nu}_\alpha \nu_\alpha. \quad (2.4)$$

The invisible width of the Z^0 has been measured at LEP with an impressive precision, as shown in Fig. 9 [10]. This measurement has been recently revised [11, 12] with a reduced systematic error and excludes any number of standard families different from three:

$$N_\nu = \frac{\Gamma_{\text{inv}}}{\Gamma_{\bar{\nu}\nu}} = 2.9963 \pm 0.00074. \quad (2.5)$$

3 Massive neutrinos

Neutrinos are ubiquitous in our surroundings. If we open our hand, it will be crossed each second by about $\mathcal{O}(10^{12})$ neutrinos from the sun, about $\mathcal{O}(10)$ from the atmosphere, about $\mathcal{O}(10^9)$ from natural radioactivity in the earth and even $\mathcal{O}(10^{12})$ relic neutrinos from the Big Bang. In 1987, the Kamiokande detector in Japan observed the neutrino burst from a SuperNova that exploded in the Large Magellanic Cloud, at a distance of 160 thousand light years from earth. For a few seconds, the supernova neutrino flux was of the same order of magnitude as the flux of solar neutrinos!

Using many of these sources as well as others from reactors and accelerators, a decade of revolutionary neutrino experiments have demonstrated that, for the time being, neutrinos are the less standard of the SM particles. They have tiny masses and this necessarily requires new degrees of freedom with respect to those in Table 1.

A massive fermion necessarily has two states of helicity, since it is always possible to reverse the helicity of a state that moves at a slower speed than light by looking at it from a boosted reference frame. What is the right-handed state of the neutrino? It turns out there are two ways to proceed.

Let us consider the case of free fermions. A four-component Dirac fermion can be made massive adding the following mass term to the Lagrangian:

$$-\mathcal{L}_m^{\text{Dirac}} = m\bar{\psi}\psi = m(\overline{\psi_L + \psi_R})(\psi_L + \psi_R) = m(\overline{\psi_L}\psi_R + \overline{\psi_R}\psi_L). \quad (3.1)$$

A Dirac mass term couples the left-handed and right-handed chiral components of the fermion field, and therefore this coupling vanishes identically in the case of a Weyl fermion.

Can one give a mass to a two-component Weyl fermion? As first noticed by Majorana, this indeed can be done with the following mass term:

$$-\mathcal{L}_m^{\text{Majorana}} = \frac{m}{2}\bar{\psi}^c\psi + \frac{m}{2}\bar{\psi}\psi^c = \frac{m}{2}\psi^T C\psi + \frac{m}{2}\bar{\psi}C\bar{\psi}^T, \quad (3.2)$$

where

$$\psi^c \equiv C\bar{\psi}^T = C\gamma_0\psi^*. \quad (3.3)$$

It is easy to check that the Majorana mass term satisfies the required properties:

- 1) It can be constructed with a two-component spinor or Weyl fermion: if $\psi = P_L\psi$

$$\psi^T C\psi = \psi_L^T i\sigma_2\psi_L, \quad (3.4)$$

which does not vanish in the absence of the right chiral component.

- 2) It is Lorentz invariant. It is easy to show, using the properties of the gamma matrices that under a Lorentz transformation ψ and ψ^c transform in the same way,

$$\psi \rightarrow e^{-\frac{i}{4}\omega_{\mu\nu}\sigma^{\mu\nu}}\psi \equiv S(\Lambda)\psi, \quad \psi^c \rightarrow S(\Lambda)\psi^c, \quad (3.5)$$

with $\sigma_{\mu\nu} \equiv \frac{i}{4}[\gamma_\mu, \gamma_\nu]$, and therefore the bilinear $\bar{\psi}^c\psi$ is Lorentz invariant.

- 3) The equation of motion derived from Eq. (3.2) for a free majorana fermion has plane wave solutions satisfying the relativistic relation for a massive fermion:

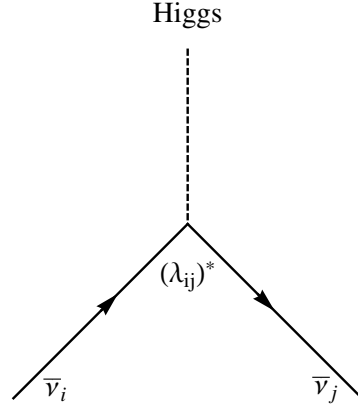
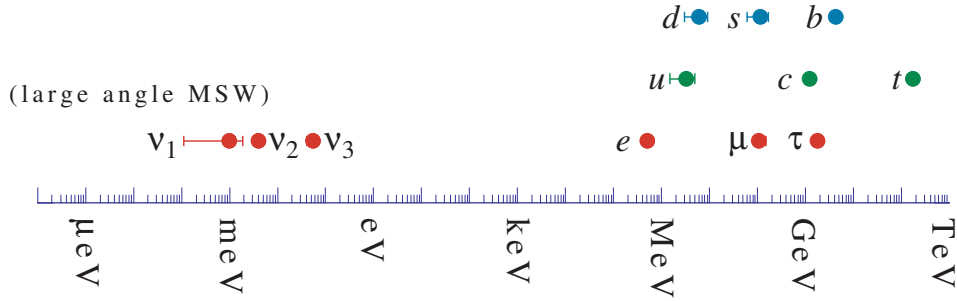
$$E^2 - \mathbf{p}^2 = m^2.$$

In the SM none of the mass terms of Eqs. (3.1) and (3.2) are gauge invariant. Spontaneous symmetry breaking allows to generate the Dirac mass term from Yukawa couplings for all fermions in the SM, while the Majorana mass term can only be generated for neutrinos. Let us see how this works.

3.1 Massive Dirac neutrinos

We can enlarge the SM by adding a set of three right-handed neutrino, ν_R states, with quantum numbers $(1, 1)_0$, i.e. singlets under all the gauge groups. A new Yukawa (Fig. 10) coupling of these new states with the lepton doublet is exactly gauge invariant and therefore can be added to the SM:

$$-\mathcal{L}_m^{\text{Dirac}} = \bar{L} \lambda \tilde{\Phi} \nu_R + \text{h.c.} \quad (3.6)$$


Fig. 10: Neutrino Yukawa coupling.

Fig. 11: Fermion spectrum in the Standard Model.

where $L = (\nu \ l)$ is the lepton doublet, $\tilde{\Phi} \equiv i\sigma_2\phi^*$ and ϕ is the Higgs field, with quantum numbers $(\mathbf{1}, \mathbf{2})_{-\frac{1}{2}}$. Upon spontaneous symmetry breaking the scalar doublet gets a vacuum expectation value $\langle \tilde{\Phi} \rangle = (\frac{v}{\sqrt{2}} \ 0)$, and therefore a neutrino Dirac mass term is generated

$$-\mathcal{L}_m^{\text{Dirac}} \rightarrow -\bar{\nu}_L \lambda \frac{v}{\sqrt{2}} \nu_R + \text{h.c.} \quad (3.7)$$

The neutrino mass matrix is proportional to the Higgs vacuum expectation value, in complete analogy to the remaining fermions:

$$m_\nu = \lambda \frac{v}{\sqrt{2}}. \quad (3.8)$$

There are two important consequences of Dirac neutrinos. First, there is a new hierarchy problem in the SM to be explained: why are neutrinos so much lighter than the remaining leptons, even those in the same family (see Fig. 11), if they get the mass in the same way? This requires a large hierarchy in the Yukawa couplings that should differ in many orders of magnitude. Secondly, an accidental global symmetry, lepton number L , that counts the number of leptons minus that of antilepton, remains exactly conserved at the classical level,¹ just as baryon number, B , is.

¹As usual $B + L$ is broken by the anomaly and only $B - L$ remains exact at all orders.

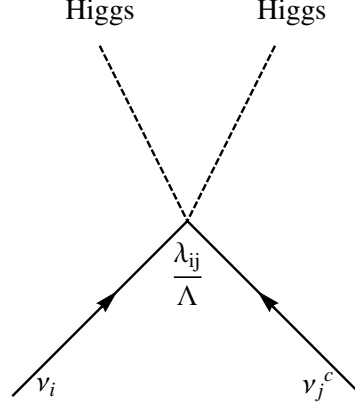


Fig. 12: Weinberg operator.

3.2 Massive Majorana neutrinos

Since the combination $\bar{L}\tilde{\phi}$ is a singlet under all gauge groups, the Majorana-type contraction (see Fig. 12):

$$-\mathcal{L}_m^{\text{Majorana}} = \bar{L}\tilde{\phi} \alpha C \tilde{\phi}^T \bar{L}^T + h.c., \quad (3.9)$$

is gauge invariant. This term, first written down by Weinberg [13], gives rise to a Majorana mass term for neutrinos upon spontaneous symmetry breaking:

$$-\mathcal{L}_m^{\text{Majorana}} \rightarrow \bar{\nu}_L \alpha \frac{v^2}{2} C \bar{\nu}_L^T + h.c., \quad (3.10)$$

The neutrino mass matrix in this case is given by:

$$m_\nu = \alpha v^2. \quad (3.11)$$

The Weinberg operator has dimension 5, and therefore the coupling $[\alpha] = -1$. We can write it in terms of a dimensionless coupling as

$$\alpha = \frac{\lambda}{\Lambda}, \quad (3.12)$$

where Λ is a new physics scale, in principle unrelated to the electroweak scale.

The consequences of the SM neutrinos being massive Majorana particles are profound. If the scale Λ is much higher than the electroweak scale v , a strong hierarchy between the neutrino and the charged lepton masses arises naturally. If all dimensionless couplings λ are of the same order, neutrino masses are suppressed by a factor v/Λ with respect to the charged fermions. On the other hand, Weinberg's operator violates lepton number L and provides a new seed for generating the matter/antimatter asymmetry in the Universe as we will see.

Even though the Majorana mechanism to generate neutrino masses does not involve any extra degree of freedom with respect to those in the SM, the existence of the Weinberg coupling implies that cross sections involving for example the scattering of neutrinos and the Higgs will grow with energy,

ultimately violating unitarity. The situation is analogous to that of the Fermi interaction of Fig. 2. The SM resolved this interaction at higher energies as being the result of the interchange of a heavy vector boson, Fig. 6. The Majorana coupling, if it exists, should also represent the effect at low energies of the exchange of one or more unknown massive states. What those states are remains one of the most interesting open questions in neutrino physics.

Finally, it is interesting to note that the anomaly cancellation conditions fix all the hypercharges in this case (i.e., there is only one possible choice for the hypercharges that satisfies Eq. (2.3)), which implies that electromagnetic charge quantization is the only possibility in a field theory with the same matter content as the SM.

3.3 Neutrino masses and physics beyond the Standard Model

Any new physics beyond the standard model (BSM) characterized by a high scale, Λ , will induce effects at low energies $E \ll \Lambda$ that can be described by an effective field theory [14, 15] of the form:

$$\mathcal{L}_{\text{eff}} = \mathcal{L}_{\text{SM}} + \sum_i \frac{\alpha_i}{\Lambda} O_i^{d=5} + \sum_i \frac{\beta_i}{\Lambda^2} O_i^{d=6} + \dots \quad (3.13)$$

It is the most general Lagrangian which includes the SM and an infinite tower of operators constructed out of the SM fields respecting Lorentz and gauge symmetries. In principle such a theory depends on infinite new couplings, one per new independent operator, and it is therefore not predictive. However, if we are interested in describing processes at energies $E \ll \Lambda$, we can truncate the sum of operators up to a given dimension d in such a way that our predictions are correct up to order $(\frac{E}{\Lambda})^{d-4}$.

The operators of lowest dimension are the most relevant at low energies. It turns out that there is only one such operator of the lowest possible dimension, $d = 5$, which is precisely the Weinberg operator of Eq. (3.9). In this perspective, it is natural to expect that the first indication of BSM physics is precisely Majorana neutrino masses. While many types of BSM theories can give rise to neutrino masses, generically they will induce other new physics effects represented by the operators of $d = 6$ and higher.

4 Neutrino masses and lepton mixing

Neutrino masses, whether Dirac or Majorana, imply lepton mixing [16, 17]. The Yukawa coupling in Eq. (3.6) is a generic complex matrix in flavour space, while that in Eq. (3.9) is a generic complex symmetric matrix, and the same holds for the corresponding leptonic mass matrices:

$$-\mathcal{L}_m^{\text{Dirac}} = \overline{\nu}_L^i (M_\nu)_{ij} \nu_R^j + \overline{l}_L^i (M_l)_{ij} l_R^j + \text{h.c.} \quad (4.1)$$

$$-\mathcal{L}_m^{\text{Majorana}} = \frac{1}{2} \overline{\nu}_L^i (M_\nu)_{ij} \nu_L^{cj} + \overline{l}_L^i (M_l)_{ij} l_R^j + \text{h.c.} \quad (4.2)$$

In the Dirac case, the two mass matrices can be diagonalized by a bi-unitary rotation:

$$M_\nu = U_\nu^\dagger \text{Diag}(m_1, m_2, m_3) V_\nu, \quad M_l = U_l^\dagger \text{Diag}(m_e, m_\mu, m_\tau) V_l, \quad (4.3)$$

while in the Majorana case, the neutrino mass matrix, being symmetric, can be taken to a diagonal form by

$$M_\nu = U_\nu^\dagger \text{Diag}(m_1, m_2, m_3) U_\nu^*. \quad (4.4)$$

We can go to the mass basis by rotating the fields as:

$$\nu'_R = V_\nu \nu_R, \quad \nu'_L = U_\nu \nu_L, \quad l'_R = V_l l_R, \quad l'_L = U_l l_L. \quad (4.5)$$

In this basis the charged-current interactions are no longer diagonal, in complete analogy with the quark sector (see Fig. 13):

$$\mathcal{L}_{CC}^{\text{lepton}} = -\frac{g}{\sqrt{2}} \bar{l}_i \gamma_\mu P_L W_\mu^+ \underbrace{(U_l^\dagger U_\nu)_{ij}}_{U_{\text{PMNS}}} \nu'_j + \text{h.c.} \quad (4.6)$$

The mixing matrix in the lepton sector is referred to as the Pontecorvo–Maki–Nakagawa–Sakata (PMNS) matrix, analogous to the CKM one in the quark sector.

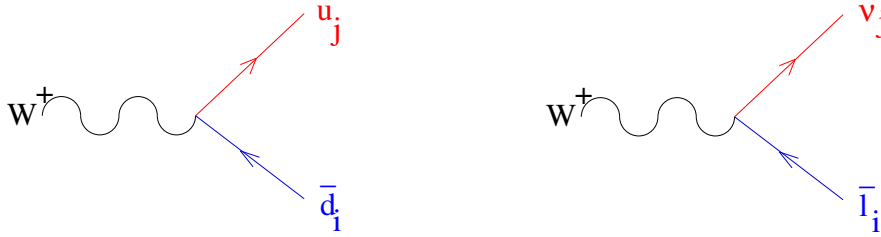


Fig. 13: Quark and lepton mixing.

The number of physical parameters in the lepton mixing matrix, U_{PMNS} , can easily be computed by counting the number of independent real and imaginary elements of the Yukawa matrices and eliminating those that can be absorbed in field redefinitions. The allowed field redefinitions are the unitary rotations of the fields that leave the rest of the Lagrangian invariant (only those that are not symmetries of the full Lagrangian when lepton masses are included are efficient in absorbing flavour parameters).

In the Dirac case, it is possible to rotate independently the left-handed lepton doublet, together with the right-handed charged leptons and neutrinos, that is $U(n)^3$, for a generic number of families n . However, this includes total lepton number which remains a symmetry of the massive theory and thus cannot be used to reduce the number of physical parameters in the mass matrix. The parameters that can be absorbed in field redefinitions are thus the parameters of the group $U(n)^3/U(1)$ (that is $\frac{3(n^2-n)}{2}$ real, $\frac{3(n^2+n)-1}{2}$ imaginary).

In the case of Majorana neutrinos, there is no independent right-handed neutrino field, nor is lepton number a good symmetry. Therefore the number of field redefinitions is the number of parameters of the elements in $U(n)^2$ (that is $n^2 - n$ real and $n^2 + n$ imaginary).

The resulting real physical parameters are the mass eigenstates and the mixing angles, while the resulting imaginary parameters are CP-violating phases. All this is summarized in Table 2. Dirac and Majorana neutrinos differ only in the number of observable phases. For three families ($n = 3$), there is

Table 2: Number of real and imaginary parameters in the Yukawa matrices, of those that can be absorbed in field redefinitions. The difference between the two is the number of observable parameters: the lepton masses (m), mixing angles (θ), and imaginary phases (ϕ).

	Yukawas	Field redefinitions	No. m	No. θ	No. ϕ
Dirac Real, Im	λ_l, λ_ν $2n^2, 2n^2$	$U(n)^3/U(1)$ $\frac{3(n^2 - n)}{2}, \frac{3(n^2 + n) - 1}{2}$	$2n$	$\frac{n^2 - n}{2}$	$\frac{(n - 2)(n - 1)}{2}$
Majorana Real, Im	$\lambda_l, \alpha_\nu^T = \alpha_\nu$ $n^2 + \frac{n(n+1)}{2}, n^2 + \frac{n(n+1)}{2}$	$U(n)^2$ $n^2 - n, n^2 + n$	$2n$	$\frac{n^2 - n}{2}$	$\frac{n^2 - n}{2}$

just one Dirac phase and three in the Majorana case.

A standard parametrization of the mixing matrices for Dirac, U_{PMNS} , and Majorana, \tilde{U}_{PMNS} , is given by

$$\begin{aligned}
 U_{\text{PMNS}} &= \begin{pmatrix} 1 & 0 & 0 \\ 0 & c_{23} & s_{23} \\ 0 & -s_{23} & c_{23} \end{pmatrix} \begin{pmatrix} c_{13} & 0 & s_{13}e^{-i\delta} \\ 0 & 1 & 0 \\ -s_{13}e^{i\delta} & 0 & c_{13} \end{pmatrix} \begin{pmatrix} c_{12} & s_{12} & 0 \\ -s_{12} & c_{12} & 0 \\ 0 & 0 & 1 \end{pmatrix}, \\
 \tilde{U}_{\text{PMNS}} &= U_{\text{PMNS}}(\theta_{12}, \theta_{13}, \theta_{23}, \delta) \begin{pmatrix} 1 & 0 & 0 \\ 0 & e^{i\alpha_1} & 0 \\ 0 & 0 & e^{i\alpha_2} \end{pmatrix}, \tag{4.7}
 \end{aligned}$$

where in all generality $\theta_{ij} \in [0, \pi/2]$ and $\delta, \alpha_1, \alpha_2 \in [0, 2\pi]$.

5 Majorana versus Dirac

It is clear that establishing the Majorana nature of neutrinos is of great importance, since it would imply the existence of a new physics scale. In principle there are very clear signatures, such as the one depicted in Fig. 14, where a ν_μ beam from π^+ decay is intercepted by a detector, D . In the Dirac case, the interaction of neutrinos on the detector via a charged current interaction will produce only a μ^- in the final state. If neutrinos are Majorana, a wrong-sign muon in the final state is also possible. Unfortunately the rate for μ^+ production is suppressed by m_ν/E in amplitude with respect to the μ^- . For example, for $E_\nu = \mathcal{O}(1)$ GeV and $m_\nu \sim \mathcal{O}(1)$ eV the cross section for this process will be roughly 10^{-18} times the usual CC neutrino cross section.

The best hope of observing a rare process of this type seems to be the search for neutrinoless double-beta decay ($2\beta 0\nu$), the right diagram of Fig. 15. The background to this process is the standard double-beta decay depicted on the left of Fig. 15, which has been observed to take place for various isotopes with a lifetime of $T_{2\beta 2\nu} > 10^{19} - 10^{21}$ years.

If the source of this process is just the Majorana ν mass, the inverse lifetime for this process is

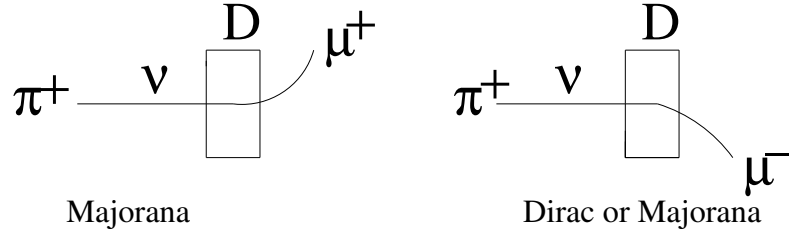


Fig. 14: A neutrino beam from π^+ decay (ν_μ) could interact in the magnetized detector producing a μ^+ only if neutrinos are Majorana.

given by

$$T_{2\beta 0\nu}^{-1} \simeq \underbrace{G^{0\nu}}_{\text{Phase}} \underbrace{|M^{0\nu}|^2}_{\text{Nuclear M.E.}} \underbrace{\left| \sum_i (\tilde{U}_{PMNS}^{ei})^2 m_i \right|^2}_{|m_{ee}|^2}. \quad (5.1)$$

In spite of the suppression in the neutrino mass (over the energy of this process), the neutrinoless mode has a phase factor orders of magnitude larger than the 2ν mode, and as a result present experiments searching for this rare process have already set bounds on neutrino masses in the eV range as shown in Table 3.



Fig. 15: 2β decay: normal (left) and neutrinoless (right).

Table 3: Present bounds at 90%CL from some recent neutrinoless double-beta-decay experiments [18].

Experiment	Nucleus	$ m_{ee} $
EXO-200	^{136}Xe	$< 0.093\text{--}0.286$ eV
AMoRE	^{100}Mo	$< 1.2\text{--}2.1$ eV
GERDA	^{76}Ge	$< 0.079\text{--}0.18$ eV
KamLAND-Zen	^{136}Xe	$< 0.061\text{--}0.165$ eV
CUORE	^{130}Te	$< 0.11\text{--}0.52$ eV

6 Neutrino oscillations

The most spectacular implication of neutrino masses and mixings is the macroscopic quantum phenomenon of neutrino oscillations, first introduced by B. Pontecorvo [19]. The Nobel Prize of 2015 was awarded to T. Kajita (from the SuperKamiokande collaboration) and A. B. McDonald (from the SNO collaboration) for the *discovery of neutrino oscillations, which shows that neutrinos have a mass*.

We have seen that if neutrinos are massive the neutrino flavour fields $(\nu_e, \nu_\mu, \nu_\tau)$, that couple via CC to the leptons (e, μ, τ) , are unitary combinations of the mass eigenstates fields (ν_1, ν_2, ν_3) :

$$\begin{pmatrix} \nu_e \\ \nu_\mu \\ \nu_\tau \end{pmatrix} = U_{\text{PMNS}}(\theta_{12}, \theta_{13}, \theta_{23}, \text{phases}) \begin{pmatrix} \nu_1 \\ \nu_2 \\ \nu_3 \end{pmatrix}. \quad (6.1)$$

In a neutrino oscillation experiment, neutrinos are produced by a source (e.g. pion or μ decays, nuclear reactions, etc) and are detected some macroscopic distance, L , away from the production point. They are produced and detected via weak processes in combination with a given lepton flavour, that is in flavour states or a combination of mass eigenstates. As these states propagate undisturbed in space-time from the production to the detection regions, the different mass eigenstates, having slightly different phase velocities, pick up different phases, resulting in a non-zero probability that the state that arrives at the detector is in a different flavour combination to the one originally produced, see Fig. 16. The probability for this flavour transition oscillates with the distance travelled.

Two ingredients are mandatory for this phenomenon to take place:

- neutrinos must keep quantum coherence in propagation over macroscopic distances, which is only possible because they are so weakly interacting
- there is sufficient uncertainty in momentum at production and detection so that a coherent flavour state can be produced².

The master formula for the oscillation probability of ν_α turning into a ν_β is

$$P(\nu_\alpha \rightarrow \nu_\beta) = \sum_{i,j} U_{\alpha i}^* U_{\beta i} U_{\alpha j} U_{\beta j}^* e^{-i \frac{\Delta m_{ji}^2 L}{2|\mathbf{p}|}}, \quad (6.2)$$

where $\Delta m_{ji}^2 \equiv m_i^2 - m_j^2$, $U_{\alpha i}$ are the elements of the PMNS matrix, L is the baseline and \mathbf{p} is the neutrino momentum.

There are many ways to derive this formula. The simplest way that appears in most textbooks uses simple quantum mechanics, where neutrinos are treated as plane waves. A slightly more rigorous method treats neutrinos as wave packets. Finally, it is also possible to derive it from QFT, where neutrinos are treated as intermediate virtual states. The different methods make more or less explicit the basic necessary conditions of neutrino oscillations mentioned above, and therefore are more or less prone to quantum paradoxes.

²If the momentum uncertainty is sufficiently small one could kinematically distinguish the mass eigenstate being produced/detected.



Fig. 16: Neutrino oscillations.

6.1 Plane wave derivation

Let us suppose that a neutrino of flavor α is produced at t_0 . It is therefore a superposition of the mass eigenstates that we assume to be plane waves with spatial momentum \mathbf{p} :

$$|\nu_\alpha(t_0)\rangle = \sum_i U_{\alpha i}^* |\nu_i(\mathbf{p})\rangle. \quad (6.3)$$

The mass eigenstates are eigenstates of the free Hamiltonian:

$$\hat{H}|\nu_i(\mathbf{p})\rangle = E_i(\mathbf{p})|\nu_i(\mathbf{p})\rangle, \quad E_i(\mathbf{p})^2 = \mathbf{p}^2 + m_i^2. \quad (6.4)$$

The time evolution operator from $t_0 \rightarrow t$ is given by $e^{-i\hat{H}(t-t_0)}$ and therefore the state at time t is given by

$$|\nu_\alpha(t)\rangle = e^{-i\hat{H}(t-t_0)}|\nu_\alpha(t_0)\rangle = \sum_i U_{\alpha i}^* e^{-iE_i(\mathbf{p})(t-t_0)} |\nu_i(\mathbf{p})\rangle. \quad (6.5)$$

The probability that at time t the state is in flavour β is

$$P(\nu_\alpha \rightarrow \nu_\beta)(t) = |\langle \nu_\beta | \nu_\alpha(t) \rangle|^2 = \left| \sum_i U_{\beta i} U_{\alpha i}^* e^{-iE_i(\mathbf{p})(t-t_0)} \right|^2, \quad (6.6)$$

where we have used the orthogonality relation $\langle \nu_i(\mathbf{p}) | \nu_j(\mathbf{p}) \rangle = \delta_{ij}$.

Since the neutrinos are ultrarelativistic, we can approximate

$$E_i(\mathbf{p}) - E_j(\mathbf{p}) \simeq \frac{1}{2} \frac{m_i^2 - m_j^2}{|\mathbf{p}|} + \mathcal{O}(m^4), \quad (6.7)$$

and $L \simeq (t - t_0)$, so that the master formula in Eq. (6.2) is recovered.

The well-founded criticism to this derivation can be summarized in the following questions: 1) why are all mass eigenstates of equal spatial momentum, \mathbf{p} ? 2) is the plane wave treatment justified when the production and detection regions are localized? 3) why is it necessary to do the $t - t_0 \rightarrow L$ conversion?

A number of quantum paradoxes can be formulated from these questions, that can be resolved only when the two basic conditions for neutrino oscillations above are made explicit. This can be achieved in

a wave packet treatment.

6.2 Wave packet derivation

Many authors have derived the master formula treating neutrinos involved as wave packets. For examples, see Refs. [20, 21].

A neutrino of flavour α is produced at time and position $(t_0, \mathbf{x}_0) = (0, \mathbf{0})$ as a superposition of *source* wave packets, $f_i^S(\mathbf{p})$, one for each mass eigenstate. The state at time and position (t, \mathbf{x}) is therefore

$$|\nu_\alpha(t, \mathbf{x})\rangle = \sum_i U_{\alpha i}^* \int_{\mathbf{p}} f_i^S(\mathbf{p}) e^{-iE_i(\mathbf{p})t} e^{i\mathbf{p}\mathbf{x}} |\nu_i\rangle. \quad (6.8)$$

For simplicity we will assume Gaussian wave packets, with an average momentum \mathbf{Q}_i and width σ_S :

$$f_i^S(\mathbf{p}) \propto e^{-(\mathbf{p}-\mathbf{Q}_i)^2/2\sigma_S^2}. \quad (6.9)$$

Note that we have lifted the assumption that all mass eigenstates have the same spatial momentum.

A neutrino of flavour β is detected at time and position (T, \mathbf{L}) as a superposition of *detector* wave packets, $f_j^D(\mathbf{p})$, created at this space-time position. The state detected is therefore

$$|\nu_\beta(t, \mathbf{x})\rangle = \sum_j U_{\beta j}^* \int_{\mathbf{p}} f_j^D(\mathbf{p}) e^{-iE_j(\mathbf{p})(t-T)} e^{i\mathbf{p}(\mathbf{x}-\mathbf{L})} |\nu_j\rangle, \quad (6.10)$$

where we also assume Gaussian wave packets at detection, with average momentum \mathbf{Q}'_j and width σ_D :

$$f_j^D(\mathbf{p}) \propto e^{-(\mathbf{p}-\mathbf{Q}'_j)^2/2\sigma_D^2}. \quad (6.11)$$

The probability amplitude for the first state to turn into the second is therefore

$$\mathcal{A}(\nu_\alpha \rightarrow \nu_\beta) \propto \int d\mathbf{x} \langle \nu_\beta(t, \mathbf{x}) | \nu_\alpha(t, \mathbf{x}) \rangle = \sum_i U_{\alpha i}^* U_{\beta i} \int_{\mathbf{p}} e^{-iE_i(\mathbf{p})T} e^{i\mathbf{p}\mathbf{L}} f_i^S(\mathbf{p}) f_i^{D*}(\mathbf{p}) \quad (6.12)$$

For Gaussian wave packets we can rewrite the product of the *S* and *D* wave packets as a Gaussian wave packet:

$$f_i^{D*}(\mathbf{p}) f_i^S(\mathbf{p}) \propto f_i^{ov}(\mathbf{p}) e^{-(\mathbf{Q}_i - \mathbf{Q}'_i)^2/4(\sigma_S^2 + \sigma_D^2)}, \quad (6.13)$$

where the overlap wave packet

$$f_i^{ov}(\mathbf{p}) \equiv e^{-(\mathbf{p}-\bar{\mathbf{Q}}_i)^2/2\sigma_{ov}^2}, \quad \bar{\mathbf{Q}}_i \equiv \left(\frac{\mathbf{Q}_i}{\sigma_S^2} + \frac{\mathbf{Q}'_i}{\sigma_D^2} \right) \sigma_{ov}^2, \quad \sigma_{ov}^2 \equiv \frac{1}{1/\sigma_S^2 + 1/\sigma_D^2}. \quad (6.14)$$

The momentum integral in Eq. (6.12) can be done analytically if we approximate

$$E_i(\mathbf{p}) \simeq E_i(\bar{\mathbf{Q}}_i) + \sum_k \left. \frac{\partial E_i}{\partial p_k} \right|_{\bar{\mathbf{Q}}_i} (p_k - (\bar{\mathbf{Q}}_i)_k) + \dots = E_i(\bar{\mathbf{Q}}_i) + \mathbf{v}_i(\mathbf{p} - \bar{\mathbf{Q}}_i) + \dots, \quad (6.15)$$

where \mathbf{v}_i is the overlap wave packet group velocity.

The amplitude obtained is

$$\mathcal{A}(\nu_\alpha \rightarrow \nu_\beta) \propto \sum_i U_{\alpha i}^* U_{\beta i} e^{-iE_i(\bar{\mathbf{Q}}_i)T} e^{i\bar{\mathbf{Q}}_i \mathbf{L}} e^{-(\mathbf{Q}_i - \mathbf{Q}'_i)^2 / 4(\sigma_S^2 + \sigma_D^2)} e^{-(\mathbf{L} - \mathbf{v}_i T)^2 \sigma_{\text{ov}}^2 / 2}. \quad (6.16)$$

Note that the two last exponential factors impose momentum conservation (the average momentum of the source and detector wave packets should be equal up to the momentum uncertainty) and the classical relation $\mathbf{L} = \mathbf{v}_i T$ within the spatial uncertainty, σ_{ov}^{-1} .

Since we usually do not measure the detection time T in a neutrino oscillation experiment, we should integrate the probability over this variable. For simplicity we assume $\mathbf{Q}_i \simeq \mathbf{Q}'_i$ and parallel to \mathbf{L} . In this case, the integral gives:

$$\begin{aligned} P(\nu_\alpha \rightarrow \nu_\beta) &\propto \int_{-\infty}^{\infty} dT |\mathcal{A}(\nu_\alpha \rightarrow \nu_\beta)|^2 \\ &\propto \sum_{i,j} U_{\alpha i}^* U_{\beta i} U_{\alpha j} U_{\beta j}^* e^{-i \frac{\Delta m_{ji}^2 L}{2|\mathbf{p}|}} \underbrace{e^{-\left(\frac{L}{L_{\text{coh}}(i,j)}\right)^2}}_{\text{coherence}} \underbrace{e^{-\left(\frac{E_i(\mathbf{Q}_i) - E_j(\mathbf{Q}_j)}{2\sigma_{\text{ov}}}\right)^2}}_{\text{momentum uncertainty}} \end{aligned} \quad (6.17)$$

where the coherence length

$$L_{\text{coh}}(i,j) \simeq \sigma_{\text{ov}} \frac{|\mathbf{v}_i - \mathbf{v}_j|}{\sqrt{\mathbf{v}_i^2 + \mathbf{v}_j^2}}, \quad (6.18)$$

represents the distance travelled by the two wave packets, moving at slightly different group velocities \mathbf{v}_i and \mathbf{v}_j , such that the center of the two wave packets have separated spatially a distance of the order of the spatial uncertainty σ_{ov}^{-1} . For $L \geq L_{\text{coh}}(i,j)$ the coherence between the wave packets i, j is lost and the corresponding terms in the oscillation probability exponentially suppressed. The last exponential factor in Eq. (6.17) leads to a suppression of the oscillation probability when the difference in average energies of the two wave packets i, j is larger than the momentum uncertainty of the overlap wave packet, σ_{ov} . Note that σ_{ov} is dominated by the smallest of the production and detection uncertainties, and therefore both should be large enough to ensure that the wave packets of the different mass eigenstates remain coherent. To the extent that $L \ll L_{\text{coh}}$ and $|E_i - E_j| \ll \text{Min}(\sigma_S, \sigma_D)$, the probability reduces to the master formula, with one caveat: we have lost the normalization along the way. This is usually unavoidable in the wave packet derivation. The right normalization can be imposed only a posteriori, for example, from unitarity, $\sum_\beta P(\nu_\alpha \rightarrow \nu_\beta) = 1$.

In summary, the wave packet derivation is clearly more physical, as it makes explicit the two necessary conditions for neutrino oscillations to take place: coherence and sufficient momentum uncertainty.

6.3 QFT derivation

Since we are dealing with relativistic quantum mechanics, QFT should be the appropriate framework to derive the oscillation probability.

In QFT we consider scattering processes where some asymptotic *in-states* that we can prepare

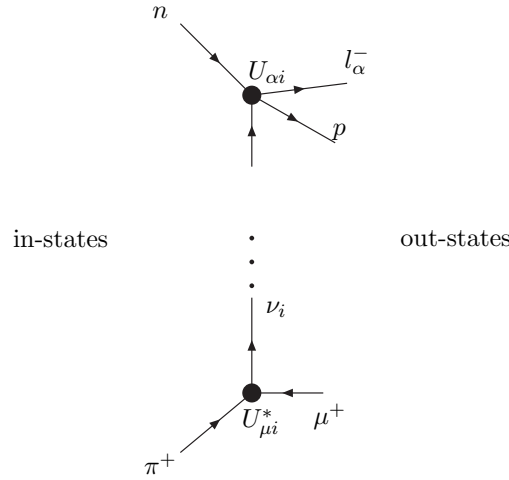


Fig. 17: Neutrino oscillations in QFT.

in the infinite past come close together at some finite time in an interaction region and scatter off into other asymptotic *out-states* at time $t \rightarrow \infty$. The probability amplitude for this process is just the scalar product of the in and out states. In computing this amplitude we usually idealise the asymptotic states as plane waves, which is a good approximation provided the interaction region is small compared to the Compton wavelength of the scattering states. In reality however the proper normalization of the scattering probability as a probability per unit time and volume requires that the initial states are normalized wave packets.

In a neutrino oscillation experiment, the asymptotic states are not the neutrinos, we cannot really prepare the neutrino states, but the particles that produce the neutrino at the source and those that interact with the neutrino in the detector. The neutrino is just a virtual particle being exchanged between the source and detector, see Fig. 17, and in this perspective the interaction region is as large as the baseline and therefore macroscopic, in particular much larger than the Compton wavelength of the asymptotic states involved. It is mandatory therefore to consider the in-states as wave packets to ensure the localization of the source and detector.

Consider for example a neutrino beam produced from pions at rest and a detector some distance apart, where neutrinos interact with nucleons that are also at rest, via a quasi-elastic event:

$$\pi n \rightarrow p \mu l_{\beta}. \quad (6.19)$$

The in-states therefore will be the two wave packets representing a static pion that decays and is localized at time and position $(0, \mathbf{0})$ within the uncertainty better defined than the decay tunnel, and a nucleon that is static and localized within the detector, at time and position (T, \mathbf{L}) , when the interaction takes place. The out-states are the muon produced in pion decay and the lepton and hadron produced in the quasi-elastic event. The probability amplitude for the whole process includes the pion decay amplitude, the neutrino propagation and the scattering amplitude at the detector. Therefore in order to extract from the full amplitude an oscillation probability, it must be the case that there is factorization of the whole probability into three factors that can be identified with the flux of neutrino from pion decay, an oscillation

probability and a neutrino cross section.

By explicit calculation [22], it is possible to show that such factorization does indeed take place as long as kinematical effects of neutrino masses can be neglected. The oscillation probability defined as the ratio of the probability for the whole process and the product of the neutrino flux from pion decay and the neutrino scattering cross-section is properly normalized.

6.4 Neutrino oscillations in vacuum

Let us analyse more closely the master formula Eq. (6.2). The probability is a superposition of oscillatory functions of the baseline with wavelengths that depend on the neutrino mass differences $\Delta m_{ij}^2 = m_j^2 - m_i^2$, and amplitudes that depend on different combinations of the mixing matrix elements. Defining $W_{\alpha\beta}^{ij} \equiv [U_{\alpha i} U_{\beta i}^* U_{\alpha j}^* U_{\beta j}]$ and using the unitarity of the mixing matrix, we can rewrite the probability in the more familiar form:

$$\begin{aligned} P(\nu_\alpha \rightarrow \nu_\beta) &= \delta_{\alpha\beta} - 4 \sum_{j>i} \text{Re}[W_{\alpha\beta}^{ij}] \sin^2 \left(\frac{\Delta m_{ij}^2 L}{4E_\nu} \right) \\ &\mp 2 \sum_{j>i} \text{Im}[W_{\alpha\beta}^{ij}] \sin \left(\frac{\Delta m_{ij}^2 L}{2E_\nu} \right), \end{aligned} \quad (6.20)$$

where the \mp refers to neutrinos/antineutrinos and $|\mathbf{p}| \simeq E_\nu$.

We refer to an *appearance* or *disappearance* oscillation probability when the initial and final flavours are different ($\alpha \neq \beta$) or the same ($\alpha = \beta$), respectively. Note that oscillation probabilities show the expected GIM suppression of any flavour changing process: they vanish if the neutrinos are degenerate.

In the simplest case of two-family mixing, the mixing matrix depends on just one mixing angle:

$$U_{\text{PMNS}} = \begin{pmatrix} \cos \theta & \sin \theta \\ -\sin \theta & \cos \theta \end{pmatrix}, \quad (6.21)$$

and there is only one mass square difference Δm^2 . The oscillation probability of Eq. (6.20) simplifies to the well-known expression where we have introduced convenient physical units:

$$\begin{aligned} P(\nu_\alpha \rightarrow \nu_\beta) &= \sin^2 2\theta \sin^2 \left(1.27 \frac{\Delta m^2 (\text{eV}^2) L (\text{km})}{E_\nu (\text{GeV})} \right), \quad \alpha \neq \beta. \\ P(\nu_\alpha \rightarrow \nu_\alpha) &= 1 - P(\nu_\alpha \rightarrow \nu_\beta). \end{aligned} \quad (6.22)$$

The probability is the same for neutrinos and antineutrinos, because there cannot be CP violation when there are only two families. Indeed CPT implies that the disappearance probabilities are the same for neutrinos and antineutrinos, and therefore according to Eq. (6.22) the same must hold for the appearance probability. The latter is a sinusoidal function of the distance between source and detector, with a period determined by the oscillation length:

$$L_{\text{osc}} (\text{km}) = \pi \frac{E_\nu (\text{GeV})}{1.27 \Delta m^2 (\text{eV}^2)}, \quad (6.23)$$

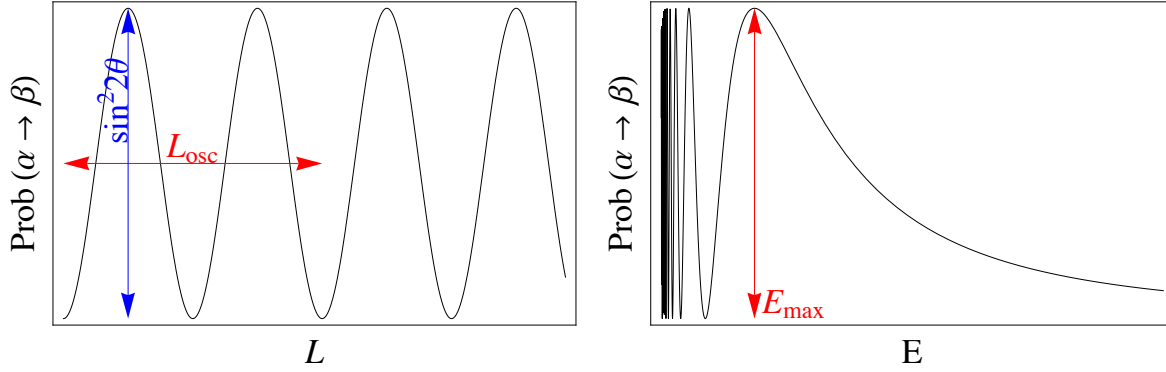


Fig. 18: Left: two-family appearance oscillation probability as a function of the baseline of L at fixed neutrino energy. Right: same probability shown as a function of the neutrino energy for fixed baseline.

which is proportional to the neutrino energy and inversely proportional to the neutrino mass square difference. The amplitude of the oscillation is determined by the mixing angle. It is maximal for $\sin^2 2\theta = 1$ or $\theta = \pi/4$. The oscillation probability as a function of the baseline is shown on the left plot of Fig. 18.

In many neutrino oscillation experiments the baseline is not varied but the oscillation probability can be measured as a function of the neutrino energy. This is shown on the right plot of Fig. 18. In this case, the position of the first maximum contains information on the mass splitting:

$$E_{\max}(\text{GeV}) = 1.27 \frac{\Delta m^2(\text{eV}^2)L(\text{km})}{\pi/2}. \quad (6.24)$$

An optimal neutrino oscillation experiment in vacuum is such that the ratio of the neutrino energy and baseline are tuned to be of the same order as the mass splitting, $E/L \sim \Delta m^2$. If $E/L \gg \Delta m^2$, the oscillation phase is small and the oscillation probability is approximately $P(\nu_\alpha \rightarrow \nu_\beta) \propto \sin^2 2\theta(\Delta m^2)^2$, so the mixing angle and mass splitting cannot be disentangled. The opposite limit $E/L \ll \Delta m^2$ is the fast oscillation regime, where one can only measure an energy or baseline-smeared oscillation probability

$$\langle P(\nu_\alpha \rightarrow \nu_\beta) \rangle \simeq \frac{1}{2} \sin^2 2\theta, \quad (6.25)$$

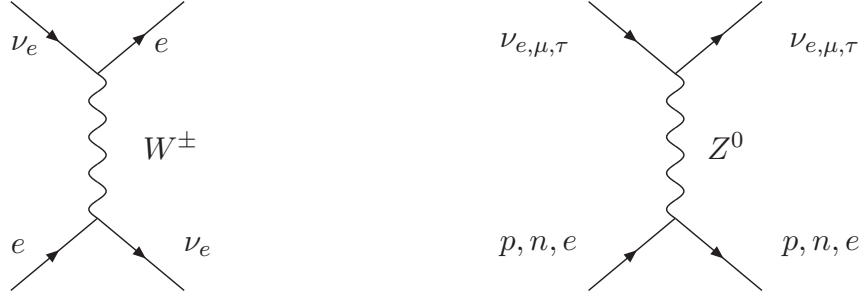
sensitivity to the mass splitting is lost in this limit. It is interesting, and reassuring, to note that this averaged oscillation regime gives the same result as the flavour transition probability in the case of incoherent propagation ($L \gg L_{\text{coh}}$):

$$P(\nu_\alpha \rightarrow \nu_\beta) = \sum_i |U_{\alpha i} U_{\beta i}|^2 = 2 \cos^2 \theta \sin^2 \theta = \frac{1}{2} \sin^2 2\theta. \quad (6.26)$$

Flavour transitions via incoherent propagation are sensitive to mixing but not to the neutrino mass splitting. The smoking gun for neutrino oscillations is not the flavour transition, which can occur in the presence of neutrino mixing without oscillations, but the peculiar L/E_ν dependence. An optimal experiment that intends to measure both the mixing and the mass splitting requires running $E/L \sim \Delta m^2$.

6.5 Neutrino propagation in matter

When neutrinos propagate in matter (earth, sun, etc.), their propagation is modified owing to coherent forward scattering on electrons and nucleons [23]:



The effective Hamiltonian density resulting from the charged current interaction is

$$\mathcal{H}_{CC} = 2\sqrt{2}G_F [\bar{e}\gamma_\mu P_L \nu_e][\bar{\nu}_e\gamma^\mu P_L e] = 2\sqrt{2}G_F [\bar{e}\gamma_\mu P_L e][\bar{\nu}_e\gamma^\mu P_L \nu_e]. \quad (6.27)$$

Since the medium is not polarized, the expectation value of the electron current is simply the number density of electrons:

$$\langle \bar{e}\gamma_\mu P_L e \rangle_{\text{unpol. medium}} = \delta_{\mu 0} \frac{N_e}{2}. \quad (6.28)$$

Including also the neutral current interactions in the same way, the effective Hamiltonian for neutrinos in the presence of matter is

$$\langle \mathcal{H}_{CC} + \mathcal{H}_{NC} \rangle_{\text{medium}} = \bar{\nu} V_m \gamma^0 (1 - \gamma_5) \nu \quad (6.29)$$

$$V_m = \begin{pmatrix} \frac{G_F}{\sqrt{2}} (N_e - \frac{N_n}{2}) & 0 & 0 \\ 0 & \frac{G_F}{\sqrt{2}} (-\frac{N_n}{2}) & 0 \\ 0 & 0 & \frac{G_F}{\sqrt{2}} (-\frac{N_n}{2}) \end{pmatrix}, \quad (6.30)$$

where N_n is the number density of neutrons. Due to the neutrality of matter, the proton and electron contributions to the neutral current potential cancel.

The plane wave solutions to the modified Dirac equation satisfy a different dispersion relation

$$E^2 = |\mathbf{p}|^2 + M_\nu^2 \pm 4EV_m, \quad (6.31)$$

where \pm is for neutrinos/antineutrinos. The phases of neutrino oscillation phenomena change.

The effect of matter can be simply accommodated in an effective mass matrix:

$$\tilde{M}_\nu^2 = M_\nu^2 \pm 4EV_m. \quad (6.32)$$

The effective mixing matrix \tilde{V}_{MNS} is the one that takes us from the original flavour basis to that which diagonalizes this effective mass matrix:

$$\begin{pmatrix} \tilde{m}_1^2 & 0 & 0 \\ 0 & \tilde{m}_2^2 & 0 \\ 0 & 0 & \tilde{m}_3^2 \end{pmatrix} = \tilde{V}_{\text{MNS}}^\dagger \left(M_\nu^2 \pm 4E \begin{pmatrix} V_e & 0 & 0 \\ 0 & V_\mu & 0 \\ 0 & 0 & V_\tau \end{pmatrix} \right) \tilde{V}_{\text{MNS}}. \quad (6.33)$$

The effective mixing angles and masses depend on the energy.

The matter potential in the center of the sun is $V_m \sim 10^{-12}$ eV and in the earth $V_m \sim 10^{-13}$ eV. In spite of these tiny values, these effects are non-negligible in neutrino oscillations.

6.6 Neutrino oscillations in constant matter

In the case of two flavours, the effective mass and mixing angle have relatively simple expressions:

$$\Delta\tilde{m}^2 = \sqrt{(\Delta m^2 \cos 2\theta \mp 2\sqrt{2}E G_F N_e)^2 + (\Delta m^2 \sin 2\theta)^2}, \quad (6.34)$$

$$\sin^2 2\tilde{\theta} = \frac{(\Delta m^2 \sin 2\theta)^2}{(\Delta\tilde{m}^2)^2}, \quad (6.35)$$

where the sign \mp corresponds to neutrinos/antineutrinos. The corresponding oscillation amplitude has a resonance [24], when the neutrino energy satisfies

$$\sqrt{2} G_F N_e \mp \frac{\Delta m^2}{2E} \cos 2\theta = 0 \quad \Rightarrow \quad \sin^2 2\tilde{\theta} = 1, \quad \Delta\tilde{m}^2 = \Delta m^2 \sin 2\theta. \quad (6.36)$$

The oscillation amplitude is therefore maximal, independently of the value of the vacuum mixing angle.

We also note that

- oscillations vanish at $\theta = 0$, because the oscillation length becomes infinite for $\theta = 0$;
- the resonance is only there for ν or $\bar{\nu}$ but not both;
- the resonance condition depends on the $\text{sign}(\Delta m^2 \cos 2\theta)$:

$$\text{resonance observed in } \nu \rightarrow \text{sign}(\Delta m^2 \cos 2\theta) > 0,$$

$$\text{resonance observed in } \bar{\nu} \rightarrow \text{sign}(\Delta m^2 \cos 2\theta) < 0.$$

The origin of this resonance is a would-be level crossing in the case of vanishing mixing. In the case of two families, for $\theta = 0$, the mass eigenstates as a function of the electron number density, at fixed neutrino energy, are depicted in Fig. 19 for $\Delta m^2 > 0$. As soon as the mixing is lifted from zero, no matter how small, the crossing cannot take place. The resonance condition corresponds to the minimum level-splitting point.

6.7 Neutrino oscillations in variable matter

In the sun the density of electrons is not constant. However, if the variation is sufficiently slow, the eigenstates will change slowly with the density, and we can assume that the neutrino produced in an

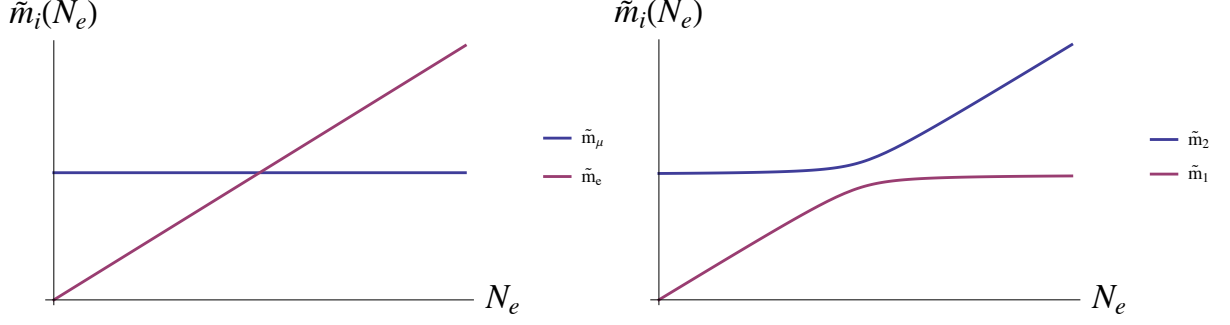


Fig. 19: Mass eigenstates as a function of the electron number density at fixed neutrino energy for $\theta = 0$ (left) and $\theta \neq 0$ (right).

eigenstate in the center of the sun, remains in the same eigenstate along the trajectory. This is the so-called *adiabatic approximation*.

We consider here two-family mixing for simplicity. At any point in the trajectory, it is possible to diagonalize the Hamiltonian fixing the matter density to that at the given point. The resulting eigenstates can be written as

$$|\tilde{\nu}_1\rangle = |\nu_e\rangle \cos \tilde{\theta} - |\nu_\mu\rangle \sin \tilde{\theta}, \quad (6.37)$$

$$|\tilde{\nu}_2\rangle = |\nu_e\rangle \sin \tilde{\theta} + |\nu_\mu\rangle \cos \tilde{\theta}. \quad (6.38)$$

Neutrinos are produced close to the centre $x = 0$ where the electron density is $N_e(0)$. Let us suppose that it satisfies

$$2\sqrt{2}G_F N_e(0) \gg \Delta m^2 \cos 2\theta. \quad (6.39)$$

Then the diagonalization of the mass matrix at this point gives

$$\tilde{\theta} \simeq \frac{\pi}{2} \Rightarrow |\nu_e\rangle \simeq |\tilde{\nu}_2\rangle, \quad (6.40)$$

in such a way that an electron neutrino is mostly the second mass eigenstate. When neutrinos exit the sun, at $x = R_\odot$, the matter density falls to zero, $N_e(R_\odot) = 0$, and the local effective mixing angle is the one in vacuum, $\tilde{\theta} = \theta$. If θ is small, the eigenstate $\tilde{\nu}_2$ is mostly ν_μ according to Eq. (6.38).

Therefore an electron neutrino produced at $x = 0$ is mostly the eigenstate $\tilde{\nu}_2$, but this eigenstate outside the sun is mostly ν_μ . There is maximal $\nu_e \rightarrow \nu_\mu$ conversion if the adiabatic approximation is a good one. This is the famous MSW effect [23, 24]. The conditions for this to happen are:

- *Resonant condition:* the density at the production is above the critical one

$$N_e(0) > \frac{\Delta m^2 \cos 2\theta}{2\sqrt{2}EG_F}. \quad (6.41)$$

- *Adiabaticity:* the splitting of the levels is large compared to energy injected in the system by the

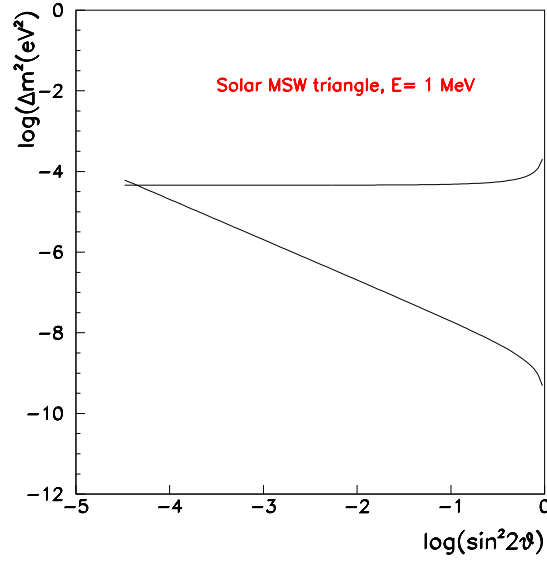


Fig. 20: MSW triangle: in the region between the two lines the resonance and adiabaticity conditions are both satisfied for neutrinos of energy 1 MeV.

variation of $N_e(r)$. A measurement of this is given by γ which should be much larger than one:

$$\gamma = \frac{\sin^2 2\theta}{\cos 2\theta} \frac{\Delta m^2}{2E} \frac{1}{|\nabla \log N_e(r)|} > \gamma_{\min} > 1, \quad (6.42)$$

where $\nabla = \partial/\partial r$.

At fixed energy both conditions give the famous MSW triangles, if plotted on the plane $(\log(\sin^2 2\theta), \log(\Delta m^2))$:

$$\log(\Delta m^2) < \log\left(\frac{2\sqrt{2}G_F N_e(0)E}{\cos 2\theta}\right) \quad (6.43)$$

$$\log(\Delta m^2) > \log\left(\gamma_{\min} 2E \nabla \log N_e \frac{\cos 2\theta}{\sin^2 2\theta}\right). \quad (6.44)$$

For example, taking $N_e(r) = N_c \exp(-r/R_0)$, $R_0 = R_\odot/10.54$, $N_c = 1.6 \times 10^{26} \text{ cm}^{-3}$, $E = 1 \text{ MeV}$, these curves are shown in Fig. 20.

It should be stressed that neutrino oscillations are not responsible for the flavour transition of solar neutrinos. The survival probability of the solar ν_e in the adiabatic approximation is the incoherent sum of the contribution of each of the mass eigenstates:

$$P(\nu_e \rightarrow \nu_e) = \sum_i |\langle \nu_e | \tilde{\nu}_i(R_\odot) \rangle|^2 |\langle \tilde{\nu}_i(0) | \nu_e \rangle|^2, \quad (6.45)$$

where $\tilde{\nu}_i(r)$ is the i -th mass eigenstate for the electron number density, $N_e(r)$, at a distance r from the center of the sun. If the mass eigenstates contribute incoherently, how can we measure the neutrino mass splitting? The answer is that the resonance condition of Eq. (6.41) depends on the neutrino energy. If we

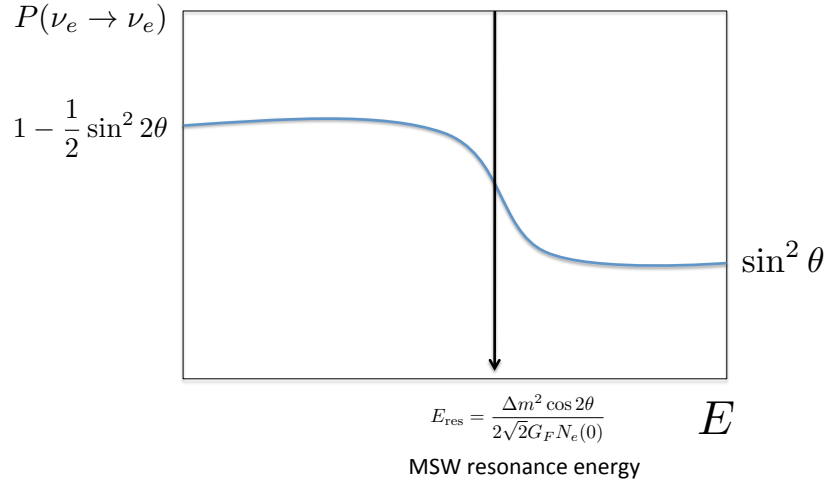


Fig. 21: Schematic survival probability of solar neutrinos as a function of the energy.

define

$$E_{\text{res}} \equiv \frac{\Delta m^2 \cos 2\theta}{2\sqrt{2}G_F N_e(0)}, \quad (6.46)$$

the MSW effect will affect neutrinos with $E > E_{\text{res}}$, while for $E < E_{\text{res}}$, the oscillation probability is close to that in vacuum for averaged oscillations. The spectrum of the solar neutrino flux includes energies both above and below E_{res} :

$$\begin{aligned} P(\nu_e \rightarrow \nu_e) &\simeq 1 - \frac{1}{2} \sin^2 2\theta, & E \ll E_{\text{res}} \\ P(\nu_e \rightarrow \nu_e) &\simeq \sin^2 \theta, & E \gg E_{\text{res}} \end{aligned} \quad (6.47)$$

The sensitivity to Δm^2 relies on the ability to locate the resonant energy. This behaviour is schematically depicted in Fig. 21.

7 Evidence for neutrino oscillations

Nature has been kind enough to provide us with two natural sources of neutrinos (the sun and the atmosphere) where neutrino flavour transitions have been observed in a series of ingenious experiments, that started back in the 1960s with the pioneering experiment of R. Davies. This effort was rewarded with the Nobel prize of 2002 to R. Davies and M. Koshiba *for the detection of cosmic neutrinos*.

7.1 Solar neutrinos

The sun, like all stars, is an intense source of neutrinos produced in the chain of nuclear reactions that burn hydrogen into helium:



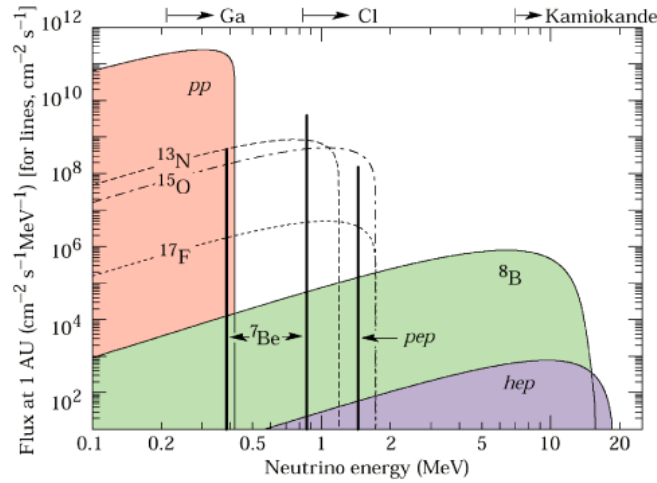


Fig. 22: Spectrum of solar neutrinos [26]. The arrows indicate the threshold of the different detection techniques.

The theory of stellar nucleosynthesis was established at the end of the 30's by H. Bethe [25]. The spectrum of the solar ν_e , for massless neutrinos, is shown in Fig. 22. The prediction of this flux, obtained by J. Bahcall and collaborators [26], is the result of a detailed simulation of the solar interior and has been improved over many years. It is the so-called standard solar model (SSM).

Neutrinos coming from the sun have been detected with several experimental techniques that have a different neutrino energy threshold as indicated in Fig. 22. On the one hand, the radiochemical techniques, used in the experiments Homestake (chlorine, ^{37}Cl) [27], Gallex/GNO [28] and Sage [29] (using gallium, ^{71}Ga , and germanium, ^{71}Ge , respectively), can count the total number of neutrinos with a rather low threshold ($E_\nu > 0.81$ MeV in Homestake and $E_\nu > 0.23$ MeV in Gallex and Sage), but they cannot get any information on the directionality, the energy of the neutrinos, nor the time of the event.

On the other hand, Kamiokande [30] pioneered a new technique to observe solar neutrinos using water Cherenkov detectors that can measure the recoil electron in elastic neutrino scattering on electrons: $\nu_e + e^- \rightarrow \nu_e + e^-$. This is a real-time experiment that provides information on the directionality and the energy of the neutrinos. The threshold on the other hand is much higher, ~ 5 MeV. All these experiments have consistently observed a number of solar neutrinos between 1/3 and 1/2 of the number expected in the SSM and for a long time this was referred to as the *solar neutrino problem or deficit*.

The progress in this field over the last two decades has been enormous culminating in a solution to this puzzle that no longer relies on the predictions of the SSM. There have been three milestones.

1998: The experiment Super-Kamiokande [31] measured the solar neutrino deficit with unprecedented precision, using the elastic reaction (ES):

$$(ES) \quad \nu_e + e^- \rightarrow \nu_e + e^- \quad E_{\text{thres}} > 5 \text{ MeV}. \quad (7.2)$$

The measurement of the direction of the events demonstrated that the neutrinos measured definitely come from the sun: the left plot of Fig. 23 shows the distribution of the events as a function of the zenith angle

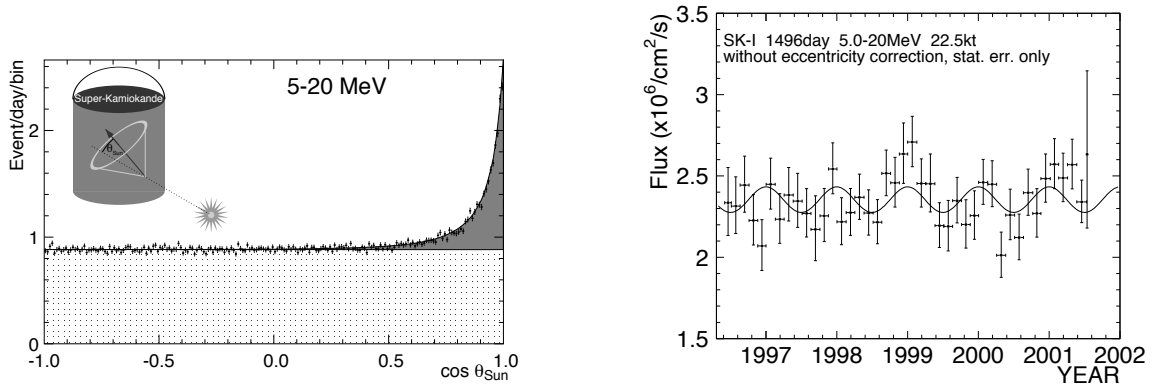


Fig. 23: Left: distribution of solar neutrino events as a function of the zenith angle of the sun. Right: seasonal variation of the solar neutrino flux in Super-Kamiokande (from Ref. ([32])).

of the sun. A seasonal variation of the flux is expected since the distance between the earth and the sun varies seasonally. The right plot of Fig. 23 shows that the measured variation is in perfect agreement with that expectation.

2001: The SNO experiment [33, 34] measured the flux of solar neutrinos using also the two reactions:

$$(CC) \quad \nu_e + d \rightarrow p + p + e^- \quad E_{\text{thres}} > 5 \text{ MeV} \quad (7.3)$$

$$(NC) \quad \nu_x + d \rightarrow p + n + \nu_x \quad x = e, \mu, \tau \quad E_{\text{thres}} > 2.2 \text{ MeV} \quad (7.4)$$

Since the CC reaction is only sensitive to electron neutrinos, while the NC one is sensitive to all the types that couple to the Z^0 boson, the comparison of the fluxes measured with both reactions can establish if there are ν_μ and ν_τ in the solar flux independently of the normalization given by the SSM. The result is shown on the Nobel-prize-winning plot Fig. 24. These measurements demonstrate that the sun shines (ν_μ, ν_τ) about twice more than it shines ν_e , which constitutes the first direct demonstration of flavour transitions in the solar flux! Furthermore the NC flux that measures all active species in the solar flux, is compatible with the total ν_e flux expected according to the SSM.

All solar neutrino data can be interpreted in terms of neutrino masses and mixings. The solar ν_e deficit can be explained for a $\Delta m_{\text{solar}}^2 \simeq 7-8 \times 10^{-5} \text{ eV}^2$ and a relatively large mixing angle. The fortunate circumstance that

$$\Delta m_{\text{solar}}^2 \sim \langle E_\nu(1 \text{ MeV}) \rangle / L(100 \text{ km}) \quad (7.5)$$

implies that one could look for this oscillation measuring reactor neutrinos at baselines of ~ 100 km. This was the third milestone.

2002: The solar oscillation is confirmed with reactor neutrinos in the KamLAND experiment [35]. This has 1 kilo ton of liquid scintillator which measures the flux of reactor neutrinos produced in a cluster of nuclear plants around the Kamioka mine in Japan. The average distance is $\langle L \rangle = 175$ km. Neutrinos

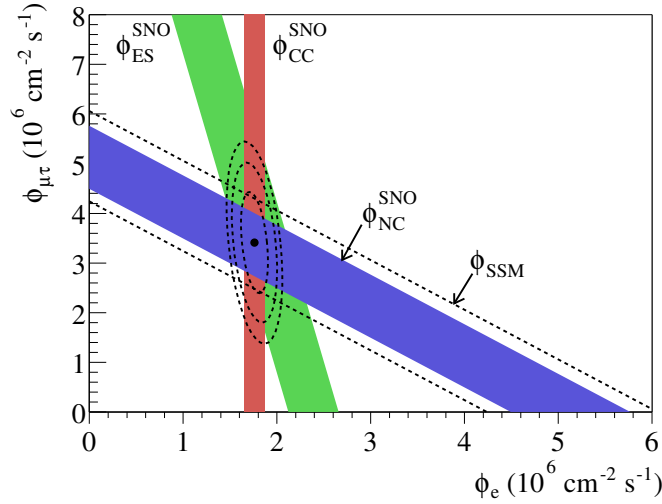


Fig. 24: Flux of ν_μ and ν_τ versus the flux of ν_e in the solar neutrino flux as measured from the three reactions observable in the SNO experiment. The dashed band shows the prediction of the SSM, which agrees perfectly with the flux measured with the NC reaction (from Ref. [34]).

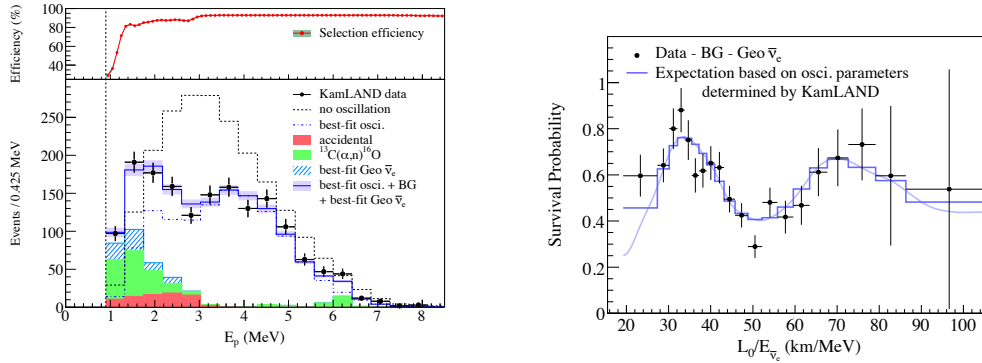


Fig. 25: Spectral distribution of the $\bar{\nu}_e$ events in KamLAND (left) and E_ν/L dependence (right). The data are compared to the expectation in the absence of oscillations and to the best fit oscillation hypothesis (from Ref. [36]).

are detected via inverse β -decay which has a threshold energy of about 2.6 MeV:

$$\bar{\nu}_e + p \rightarrow e^+ + n \quad E_{\text{th}} > 2.6 \text{ MeV} . \quad (7.6)$$

Figure 25 shows the KamLAND results [36] on the antineutrino spectrum, as well as the survival probability as a function of the ratio E_ν/L .

The low-energy contribution of geo-neutrinos is clearly visible. This measurement could have important implications in geophysics.

Concerning the sensitivity to the oscillation parameters, Fig. 26 shows the present determination of the solar oscillation parameters from KamLAND and other solar experiments. The precision in the determination of $\Delta m_{\text{solar}}^2$ is spectacular and shows that solar neutrino experiments are entering the era of

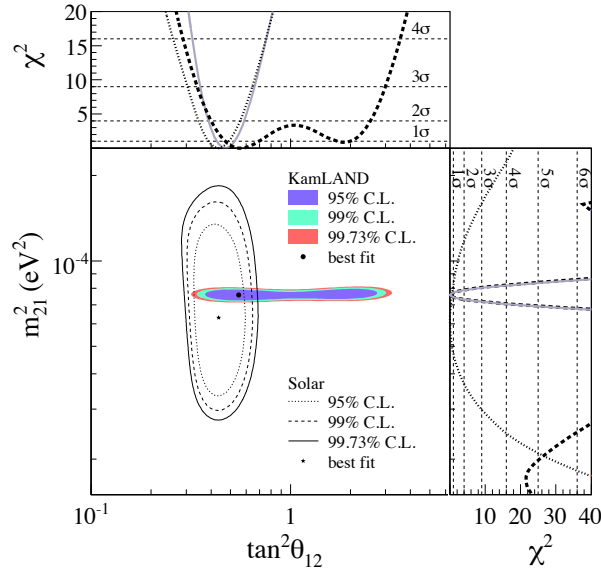


Fig. 26: Analysis of all solar and KamLAND data in terms of oscillations (from Ref. [36]).

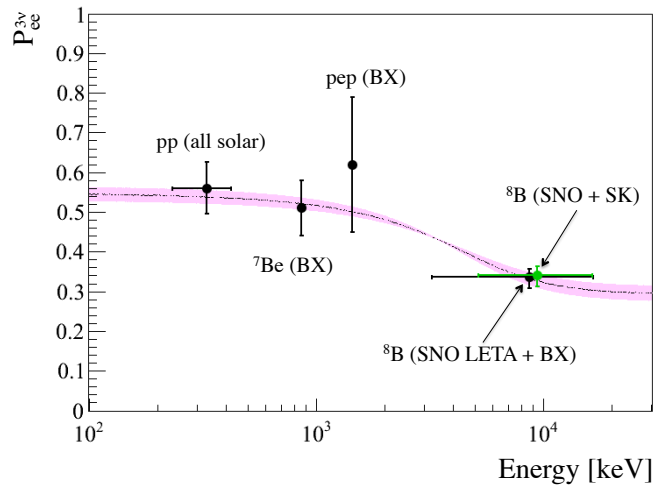


Fig. 27: Comparison of solar neutrino fluxes measured by the different solar neutrino experiments (from Ref. [37]).

precision physics.

The last addition to this success story is the Borexino experiment [37]. This is the lowest-threshold real-time solar neutrino experiment and the only one capable of measuring the flux of the monochromatic ${}^7\text{Be}$ neutrinos and pep neutrinos. Their recent results are shown in Fig. 27. The result is in agreement with the oscillation interpretation of other solar and reactor experiments and it adds further information to disfavour alternative exotic interpretations of the data.

In summary, solar neutrinos experiments have made fundamental discoveries in particle physics and are now becoming useful for other applications, such as a precise understanding of the sun and the

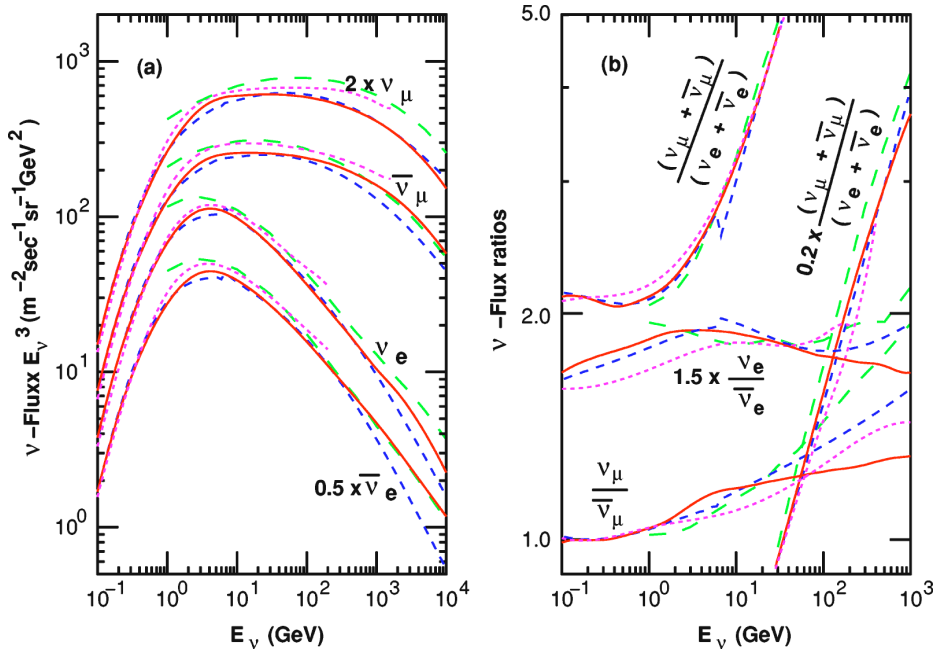


Fig. 28: Comparison of the predictions of different Monte Carlo simulations of the atmospheric neutrino fluxes averaged over all directions (left) and of the flux ratios $(\nu_\mu + \bar{\nu}_\mu)/(\nu_e + \bar{\nu}_e)$, $\nu_\mu/\bar{\nu}_\mu$, and $\nu_e/\bar{\nu}_e$ (right). The solid line corresponds to a recent full 3D simulation. Taken from the last reference in Ref. [38].

earth.

7.2 Atmospheric neutrinos

Neutrinos are also produced in the atmosphere when primary cosmic rays impinge on it producing K , π that subsequently decay. The fluxes of such neutrinos can be predicted within a 10–20% accuracy to be those in the left plot of Fig. 28.

Clearly, atmospheric neutrinos are an ideal place to look for neutrino oscillation since the E_ν/L span several orders of magnitude, with neutrino energies ranging from a few hundred MeV to 10^3 GeV and distances between production and detection varying from 10– 10^4 km, as shown in Fig. 29 (right).

Many of the uncertainties in the predicted fluxes cancel when the ratio of muon to electron events is considered. The first indication of a problem was found when a deficit was observed precisely in this ratio by several experiments: Kamiokande, IMB, Soudan2 and Macro.

In 1998, Super-Kamiokande clarified the origin of this anomaly [39]. This experiment can distinguish muon and electron events, measure the direction of the outgoing lepton (the zenith angle with respect to the earth's axis) which is correlated to that of the neutrino (the higher the energy the higher the correlation), in such a way that they could measure the variation of the flux as a function of the distance travelled by the neutrinos. Furthermore, they considered different samples of events: sub-GeV (lepton with energy below 1 GeV), multi-GeV (lepton with energy above 1 GeV), together with stopping and through-going muons that are produced on the rock surrounding Super-Kamiokande. The different

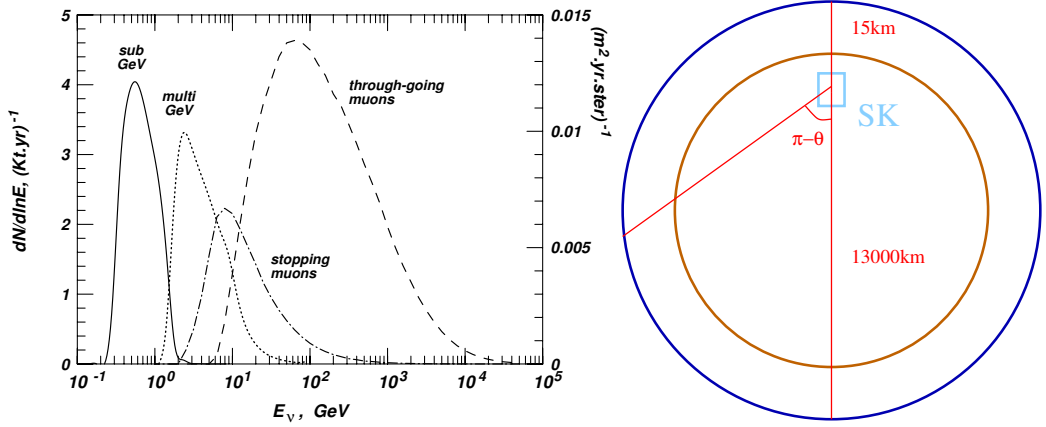


Fig. 29: Left: Parent neutrino energies of the different samples considered in Super-Kamiokande: sub-GeV, multi-GeV, stopping and through-going muons. Right: Distances travelled by atmospheric neutrinos as a function of the zenith angle.

samples correspond to different parent neutrino energies as can be seen in Fig. 29 (left).

The number of events for the different samples as a function of the zenith angle of the lepton are shown in the Nobel-prize-winning plot Fig. 30.

While the electron events observed are in rough agreement with predictions, a large deficit of muon events was found with a strong dependence on the zenith angle: the deficit was almost 50% for those events corresponding to neutrinos coming from below $\cos\theta = -1$, while there is no deficit for those coming from above. The perfect fit to the oscillation hypothesis is rather non-trivial given the sensitivity of this measurement to the E_ν (different samples) and L (zenith angle) dependence. The significance of the E_ν/L dependence has also been measured by the Super-Kamiokande Collaboration [41], as shown in Fig. 31. The best fit value of the oscillation parameters indicate $\Delta m^2 \simeq 3 \times 10^{-3} \text{ eV}^2$ and maximal mixing.

Appropriate neutrino beams to search for the atmospheric oscillation can easily be produced at accelerators if the detector is located at a long baseline of a few hundred kilometres, and also with reactor neutrinos in a baseline of $\mathcal{O}(1\text{km})$, since

$$|\Delta m_{\text{atmos}}^2| \sim \frac{E_\nu(1 - 10 \text{ GeV})}{L(10^2 - 10^3 \text{ km})} \sim \frac{E_\nu(1 - 10 \text{ MeV})}{L(0.1 - 1 \text{ km})}. \quad (7.7)$$

A *conventional* accelerator neutrino beam, as the one used in the LSS experiment, is produced from protons hitting a target and producing π and K :

$$p \rightarrow \text{Target} \rightarrow \pi^+, K^+ \rightarrow \nu_\mu (\% \nu_e, \bar{\nu}_\mu, \bar{\nu}_e) \quad (7.8)$$

$$\nu_\mu \rightarrow \nu_x. \quad (7.9)$$

Those of a selected charge are focused and are left to decay in a long decay tunnel producing a neutrino beam of mostly muon neutrinos (or antineutrinos) with a contamination of electron neutrinos of a few per cent. The atmospheric oscillation can be established by studying, as a function of the energy, either the disappearance of muon neutrinos, the appearance of electron neutrinos or, if the energy of the beam

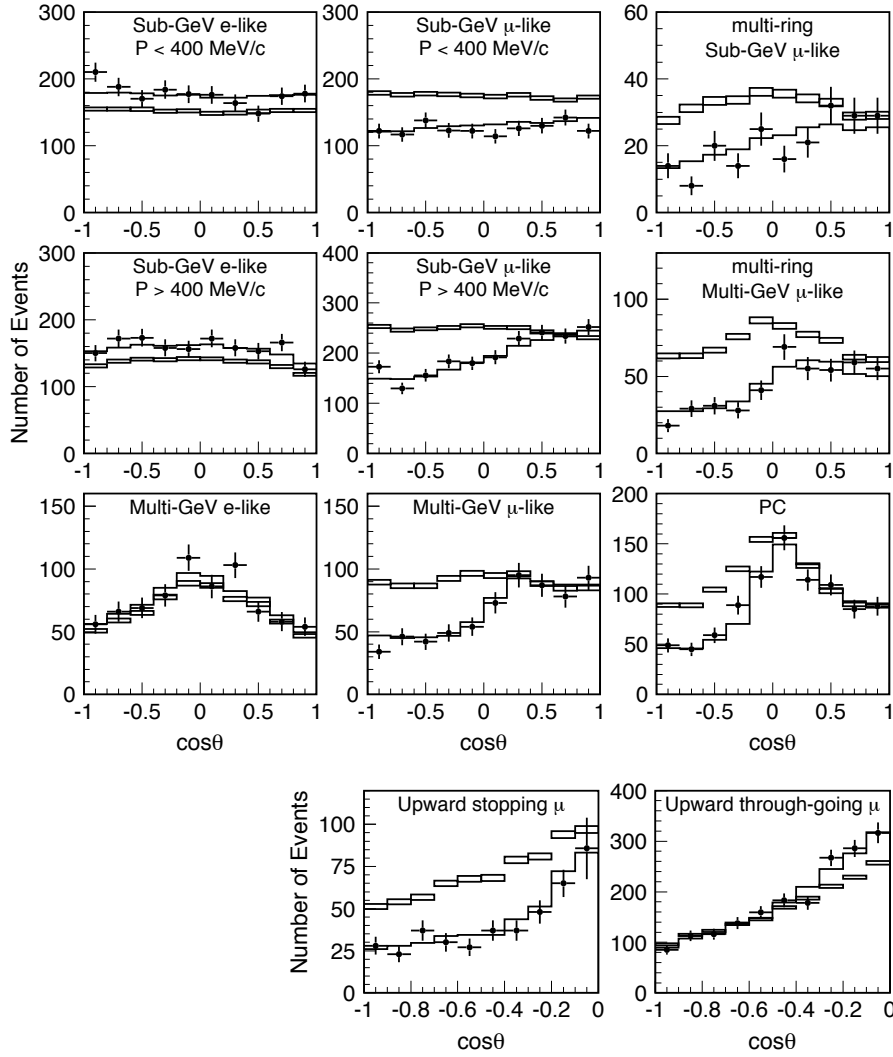


Fig. 30: Zenith angle distribution for fully-contained single-ring e -like and μ -like events, multi-ring μ -like events, partially contained events, and upward-going muons. The points show the data and the boxes show the Monte Carlo events without neutrino oscillations. The solid lines show the best-fit expectations for $\nu_\mu \leftrightarrow \nu_\tau$ oscillations (from Ref. [40]).

is large enough, the appearance of τ neutrinos.

Three conventional beams confirmed the atmospheric oscillation from the measurement of the disappearance of ν_μ neutrinos: K2K ($L = 235$ km) [42], MINOS ($L = 730$ km) [43] and from the appearance of ν_τ , OPERA ($L = 730$ km) [44]. Fig. 32 shows the measurement of the ν_μ survival probability as a function of the reconstructed neutrino energy in the MINOS experiment.

Three reactor neutrino experiments, Daya Bay [46], RENO [47] and Double Chooz [48], have discovered that the electron neutrino flavour also oscillates with the atmospheric wavelength: electron antineutrinos from reactors disappear at distances of $\mathcal{O}(1$ km), but with a small amplitude. See Fig. 33.

Finally the T2K and NOVA experiments have measured the appearance of ν_e and $\bar{\nu}_e$ in an accelerator $\nu_\mu/\bar{\nu}_\mu$ beam [49, 50] in the atmospheric range. The agreement of all these measurements with the

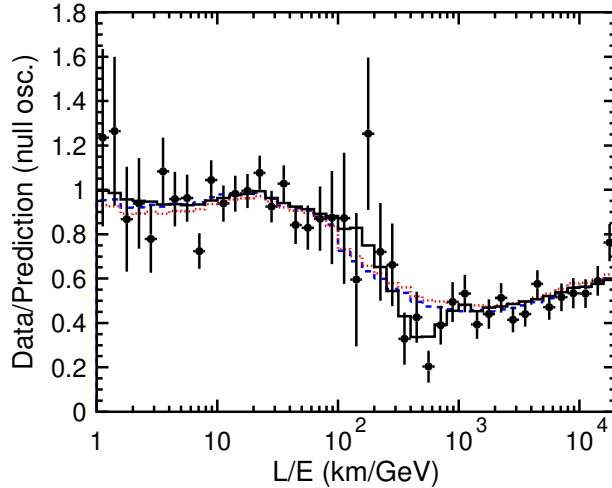


Fig. 31: Ratio of the data to the non-oscillated Monte Carlo events (points) with the best-fit expectation for 2-flavour $\nu_\mu \leftrightarrow \nu_\tau$ oscillations (solid line) as a function of E_ν/L (from Ref. [41]).

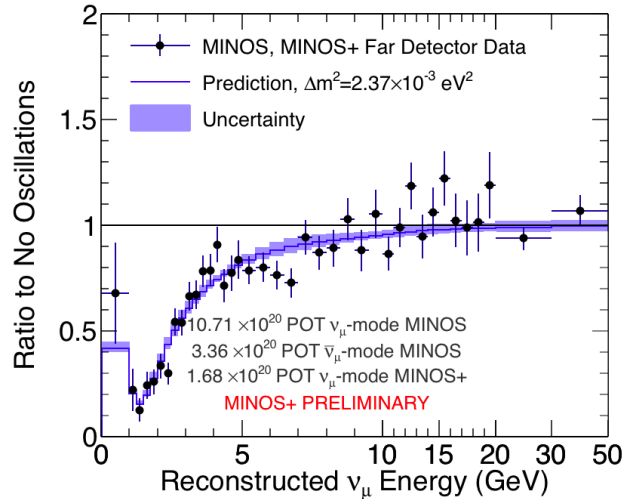


Fig. 32: Ratio of measured to expected (in absence of oscillations) neutrino events in MINOS as a functions of neutrino energy compared to the best fit oscillation solution (from Ref. [45]).

original atmospheric oscillation signal is excellent.

8 The three-neutrino mixing scenario

As we have seen, the evidence summarized in the previous section points to two distinct neutrino mass square differences related to the solar and atmospheric oscillation frequencies:

$$\underbrace{|\Delta m_{\text{solar}}^2|}_{\sim 8 \cdot 10^{-5} \text{ eV}^2} \ll \underbrace{|\Delta m_{\text{atmos}}^2|}_{\sim 2.5 \cdot 10^{-3} \text{ eV}^2} \quad (8.1)$$

The mixing of the three standard neutrinos ν_e, ν_μ, ν_τ can accommodate both. The two independent neutrino mass square differences are conventionally assigned to the solar and atmospheric ones in the

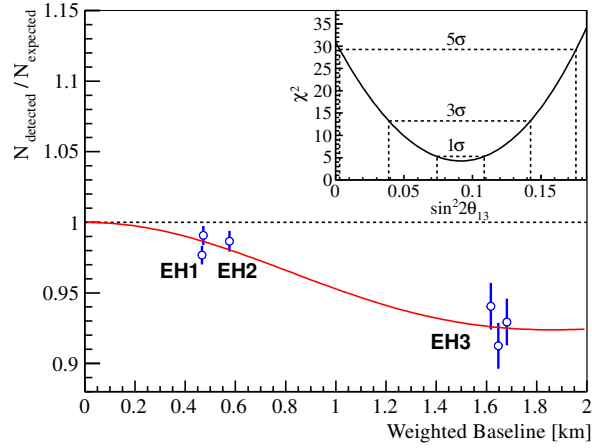


Fig. 33: Ratio of measured to expected reactor neutrino events as function of the baseline in the Daya Bay experiment (from Ref. [46]).

following way:

$$\Delta m_{13}^2 = m_3^2 - m_1^2 = \Delta m_{\text{atmos}}^2, \quad \Delta m_{12}^2 = m_2^2 - m_1^2 = \Delta m_{\text{solar}}^2. \quad (8.2)$$

The PMNS mixing matrix depends on three angles and one or more CP phases (see Eq. (4.7) for the standard parametrization). Only one CP phase, the so-called Dirac phase δ , appears in neutrino oscillation probabilities.

With this convention, the mixing angles θ_{23} and θ_{12} in the parametrization of Eq. (4.7) correspond approximately to the ones measured in atmospheric and solar oscillations, respectively. This is because solar and atmospheric anomalies approximately decouple as independent 2-by-2 mixing phenomena thanks to the hierarchy between the two mass splittings, $|\Delta m_{\text{atmos}}^2| \gg |\Delta m_{\text{solar}}^2|$, on the one hand, and the fact that the angle θ_{13} , which measures the electron component of the third mass eigenstate element $\sin \theta_{13} = (U_{\text{PMNS}})_{e3}$, is small.

To see this, let us first consider the situation in which $E_\nu/L \sim |\Delta m_{\text{atmos}}^2|$. We can thus neglect the solar mass square difference in front of the atmospheric one and E_ν/L . The oscillation probabilities obtained in this limit are given by

$$P(\nu_e \rightarrow \nu_\mu) \simeq s_{23}^2 \sin^2 2\theta_{13} \sin^2 \left(\frac{\Delta m_{13}^2 L}{4E_\nu} \right), \quad (8.3)$$

$$P(\nu_e \rightarrow \nu_\tau) \simeq c_{23}^2 \sin^2 2\theta_{13} \sin^2 \left(\frac{\Delta m_{13}^2 L}{4E_\nu} \right), \quad (8.4)$$

$$P(\nu_\mu \rightarrow \nu_\tau) \simeq c_{13}^4 \sin^2 2\theta_{23} \sin^2 \left(\frac{\Delta m_{13}^2 L}{4E_\nu} \right). \quad (8.5)$$

The results for antineutrinos are the same (there is no CP violation if one mass difference is neglected). All flavours oscillate therefore with the atmospheric frequency, but only two angles enter these formulae: θ_{23} and θ_{13} . The latter is the only one that enters the disappearance probability for ν_e or $\bar{\nu}_e$ in this regime

since

$$P(\nu_e \rightarrow \nu_e) = P(\bar{\nu}_e \rightarrow \bar{\nu}_e) = 1 - P(\nu_e \rightarrow \nu_\mu) - P(\nu_e \rightarrow \nu_\tau) \simeq \sin^2 2\theta_{13} \sin^2 \left(\frac{\Delta m_{13}^2 L}{4E_\nu} \right). \quad (8.6)$$

This is precisely the measurement of reactor neutrino experiments like Chooz, Daya Bay, RENO and Double Chooz. Therefore the oscillation amplitude of these experiments is a direct measurement of the angle θ_{13} , which has been measured to be small.

Note that in the limit $\theta_{13} \rightarrow 0$, the only probability that survives in Eq. (8.5) is the $\nu_\mu \rightarrow \nu_\tau$ one, which has the same form as a 2-family mixing formula Eq. (6.22) if we identify

$$(\Delta m_{\text{atmos}}^2, \theta_{\text{atmos}}) \rightarrow (\Delta m_{13}^2, \theta_{23}). \quad (8.7)$$

Therefore the close-to-maximal mixing angle observed in atmospheric neutrinos and the accelerator neutrino experiments like MINOS is identified with θ_{23} .

Instead if we consider experiments in the solar range, $E_\nu/L \sim \Delta m_{\text{solar}}^2$, the atmospheric oscillation is too rapid and gets averaged out. The survival probability for electrons in this limit is given by:

$$P(\nu_e \rightarrow \nu_e) = P(\bar{\nu}_e \rightarrow \bar{\nu}_e) \simeq c_{13}^4 \left(1 - \sin^2 2\theta_{12} \sin^2 \left(\frac{\Delta m_{12}^2 L}{4E_\nu} \right) \right) + s_{13}^4. \quad (8.8)$$

Again it depends only on two angles, θ_{12} and θ_{13} , and in the limit in which the latter is zero, the survival probability measured in solar experiments has the form of two-family mixing if we identify

$$(\Delta m_{\text{solar}}^2, \theta_{\text{solar}}) \rightarrow (\Delta m_{12}^2, \theta_{12}). \quad (8.9)$$

The results that we have shown in the previous section of solar and atmospheric experiments have been analysed in terms of 2-family mixing. The previous argument indicates that when fits are done in the context of 3-family mixing nothing changes too much.

On the other hand, the fact that reactor experiments have already measured the disappearance of reactor $\bar{\nu}_e$ in the atmospheric range implies that the effects of $\theta_{13} \simeq 9^\circ$ are not negligible, and therefore a proper analysis of all the oscillation data requires performing global fits in the 3-family scenario. Figure 34 shows the $\Delta\chi^2$ as a function of each of the six parameters from one recent global analysis [51]. See also Refs. [52, 53].

There are two parameters in which we observe two distinct minima, these correspond to degeneracies that cannot be resolved with present data. The first corresponds to the neutrino mass ordering or hierarchy: present data cannot distinguish between the normal (NH or NO) and inverted ordering (IH or IO) represented in Fig. 35.

Note that we denote by $\Delta m_{13}^2 = \Delta m_{\text{atmos}}^2$ the atmospheric splitting for NO and $\Delta m_{23}^2 = -\Delta m_{\text{atmos}}^2$ for IO. The second degeneracy corresponds to the octant choice of θ_{23} . Present data are mostly sensitive to $\sin^2 2\theta_{23}$. If this angle is not maximal, there are two possible choices that are roughly equivalent $\theta_{23} \leftrightarrow \pi/4 - \theta_{23}$. Due to this degeneracy, the largest angle is also the one less accurate. The

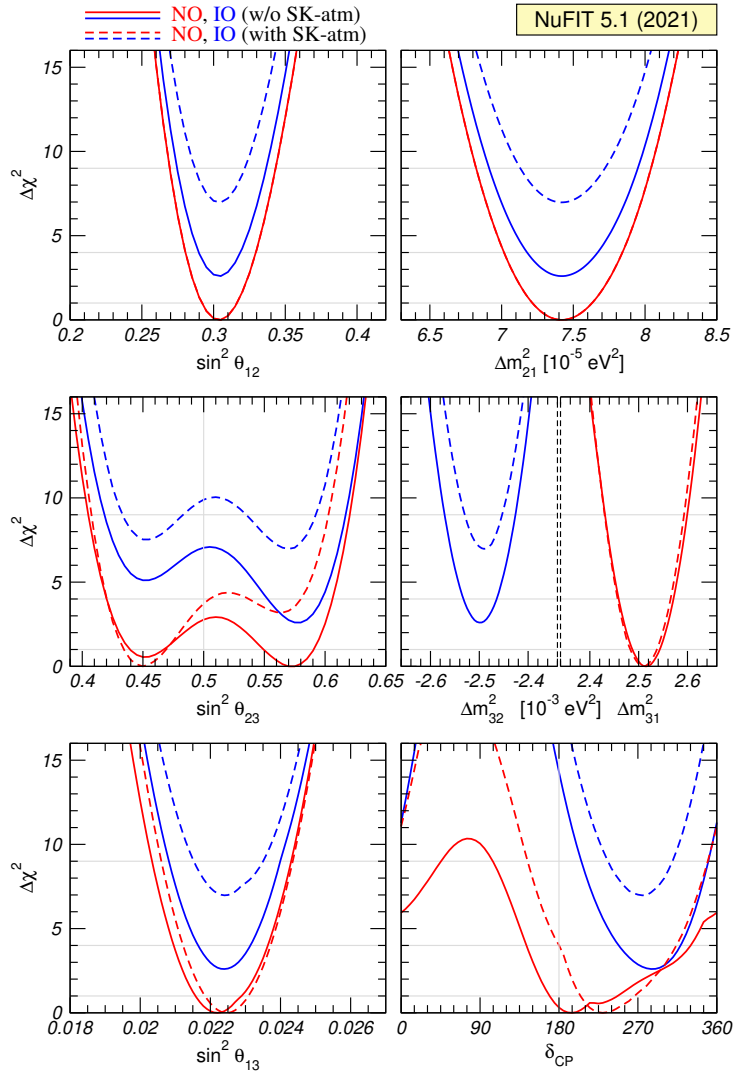


Fig. 34: $\Delta\chi^2$ of the fits to the standard 3ν -mixing scenario including all available neutrino oscillation data (from Ref. [51]). The solid lines do not include SK atmospheric data, while the dashed ones do.

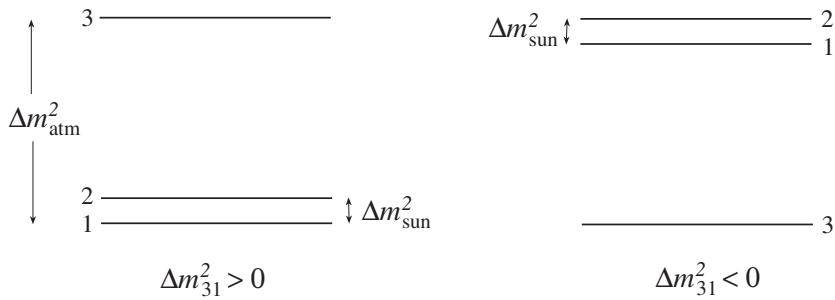


Fig. 35: Possible neutrino spectra consistent with solar and atmospheric data.

1 σ limits for NO are:

$$\begin{aligned} \theta_{23}/^\circ &= 49.2_{-1.3}^{+1}, & \theta_{12}/^\circ &= 33.4_{-0.74}^{+0.77}, & \theta_{13}/^\circ &= 8.57(13), \\ \Delta m_{12}^2 &= 7.42(21) \times 10^{-5} \text{ eV}^2, & \Delta m_{13}^2 &= 2.515(28) \times 10^{-3} \text{ eV}^2. \end{aligned} \quad (8.10)$$

The CP phase δ remains roughly unconstrained at 3σ , while there is about half of the region excluded at 2σ . As we will see, the dependence on the phase requires sensitivity to both frequencies simultaneously.

9 Prospects in determining unknown neutrino parameters

An ambitious experimental program is underway to pin down the remaining unknowns and reach a 1% precision in the lepton flavour parameters. The neutrino ordering, the octant of θ_{23} and the CP violating phase, δ , can be searched for in neutrino oscillation experiments with improved capabilities. The determination of the absolute neutrino mass scale relies on tritium beta decay experiments or cosmology.

9.1 Neutrino ordering

Concerning the neutrino ordering, the best hope to identify the spectrum exploits the MSW effect in the propagation of GeV neutrinos through earth's matter. In the case of three neutrinos propagating in matter, the ν mass eigenstates as a function of the electron density for vanishing θ_{12}, θ_{13} are depicted in Fig. 36 for NO and IO. For NO we see that there are two level crossings giving rise to two MSW resonances. The first one is essentially the one relevant for solar neutrinos, as it affects the smallest mass splitting, with the resonance condition:

$$E_{\text{res}}^{(1)} = \frac{\Delta m_{12}^2 \cos 2\theta_{12}}{2\sqrt{2}G_F N_e}. \quad (9.1)$$

The second one affects the largest mass splitting

$$E_{\text{res}}^{(2)} = \frac{\Delta m_{13}^2 \cos 2\theta_{13}}{2\sqrt{2}G_F N_e}. \quad (9.2)$$

For IO, only the first resonance appears in the ν channel.

For $\bar{\nu}$ the dependence on N_e of the first eigenstate has a negative slope and therefore there is no resonance for NO and only the atmospheric resonance appears for IO.

The existence of the atmospheric resonance implies a large enhancement of the oscillation probability $P(\nu_e \leftrightarrow \nu_\mu)$ for NO for energies near the resonant energy and at sufficiently long baseline. For IO the enhancement occurs in $P(\bar{\nu}_e \leftrightarrow \bar{\nu}_\mu)$ instead. For the typical matter densities of the earth's crust and mantle and the value of the atmospheric mass splitting, the resonant energy for neutrinos travelling through earth is $\simeq 6$ GeV, an energy that can be reached in accelerator neutrino beams. The measurement of the neutrino ordering becomes almost a digital measurement sending a conventional ν beam sufficiently far as shown in Fig. 37, which shows the oscillation probability $P(\nu_\mu \rightarrow \nu_e)$ as a function of the neutrino energy at a distance corresponding to the baseline from CERN-Kamioka (8770 km).

The first experiment that will be sensitive to this effect is the NOvA experiment, optimized like

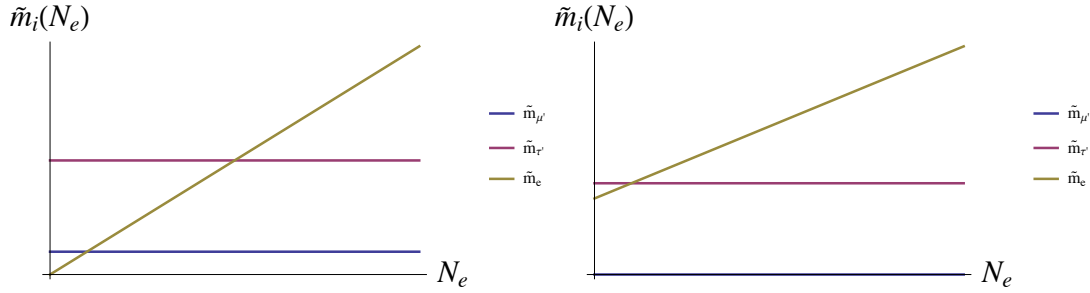


Fig. 36: Level crossings for ν in the three neutrino scenario for NO (left) and IO (right) at vanishing θ_{12} and θ_{13} .

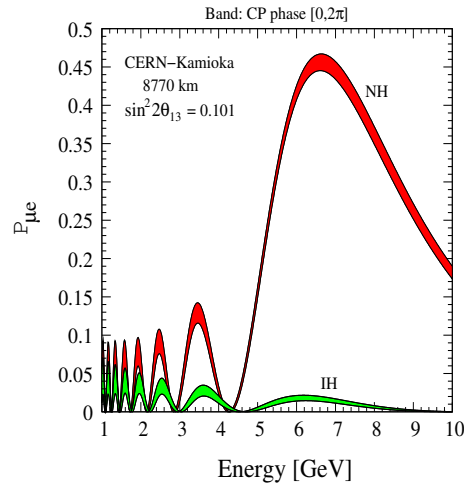


Fig. 37: Resonant increase of the $P_{\mu e}$ for NH as a function of neutrino energy for L corresponding to the distance CERN-Kamioka for NH/IH. The bands corresponds to the uncertainty in δ (from Ref. [54]).

T2K to see the ν_e appearance signal, with a baseline of 810km, which is however a bit short to see a large enhancement. Nevertheless if lucky NOvA could discriminate the ordering at 3σ .

The atmospheric resonance must also affect atmospheric neutrinos at the appropriate energy and baseline. Unfortunately the atmospheric flux contains both neutrinos and antineutrinos in similar numbers, and the corresponding events cannot be told apart, because present atmospheric neutrino detectors cannot measure the lepton charge. If we superimpose the neutrino and antineutrino signals, both orderings will give rise to an enhancement in the resonance region, since either the neutrino or antineutrino channel will have a resonance. Nevertheless with sufficient statistics, there is some discrimination power and in fact the biggest neutrino telescopes, IceCube and KM3NeT have proposed to instrument more finely some part of their detectors (PINGU and ORCA projects) to perform this measurement. Also the next generation of atmospheric neutrino detectors, such as Hyper-Kamiokande, with a factor $\mathcal{O}(20)$ more mass than the present Super-Kamiokande, or the INO detector that is designed to measure the muon charge in atmospheric events, could discriminate between the two orderings.

A very different strategy has been proposed for reactor neutrino experiments (e.g. JUNO project). The idea is to measure very precisely the reactor neutrinos at a baseline of roughly 50 km, where the depletion of the flux due to the solar oscillation is maximal. At this optimal distance, one can get a superb

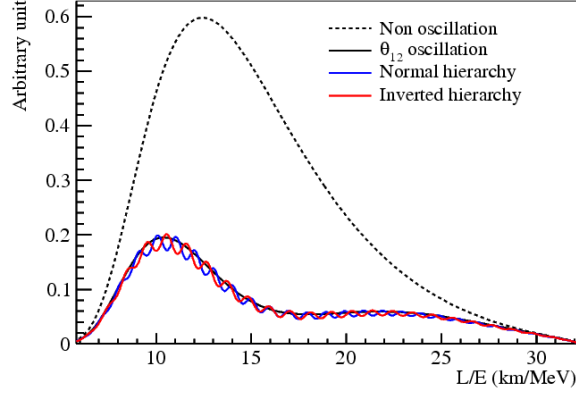


Fig. 38: Reactor neutrino spectrum in JUNO for NO/IO (from Ref. [57]).

measurement of the solar oscillation parameters, $(\theta_{12}, \Delta m_{12}^2)$, and, with sufficient energy resolution, one could detect the modulation of the signal due to the atmospheric oscillation [55, 56]. Figure 38 shows how this modulation is sensitive to the neutrino ordering. A leap ahead is however needed to reach the required energy resolution that would enable this measurement.

9.2 Leptonic CP violation

As we have seen, the CP phase, δ , in the mixing matrix induces CP violation in vacuum neutrino oscillations, that is a difference between $P(\nu_\alpha \rightarrow \nu_\beta)$ and $P(\bar{\nu}_\alpha \rightarrow \bar{\nu}_\beta)$, for $\alpha \neq \beta$. As we saw in the general expression of Eq. (6.20), CP violation is possible if there are imaginary entries in the mixing matrix that make $\text{Im}[W_{\alpha\beta}^{jk}] \neq 0$. By CPT, disappearance probabilities cannot violate CP however, because under CPT

$$P(\nu_\alpha \rightarrow \nu_\beta) = P(\bar{\nu}_\beta \rightarrow \bar{\nu}_\alpha), \quad (9.3)$$

so in order to observe a CP or T-odd asymmetry the initial and final flavour must be different, $\alpha \neq \beta$:

$$A_{\alpha\beta}^{CP} \equiv \frac{P(\nu_\alpha \rightarrow \nu_\beta) - P(\bar{\nu}_\alpha \rightarrow \bar{\nu}_\beta)}{P(\nu_\alpha \rightarrow \nu_\beta) + P(\bar{\nu}_\alpha \rightarrow \bar{\nu}_\beta)}, \quad A_{\alpha\beta}^T \equiv \frac{P(\nu_\alpha \rightarrow \nu_\beta) - P(\nu_\beta \rightarrow \nu_\alpha)}{P(\nu_\alpha \rightarrow \nu_\beta) + P(\nu_\beta \rightarrow \nu_\alpha)}. \quad (9.4)$$

In the case of 3-family mixing it is easy to see that the CP(T)-odd terms in the numerator are the same for all transitions $\alpha \neq \beta$:

$$A_{\nu_\alpha \nu_\beta}^{\text{CP(T)-odd}} = \frac{\overbrace{\sin \delta c_{13} \sin 2\theta_{13} \sin 2\theta_{12}}^{\text{solar}} \overbrace{\frac{\Delta m_{12}^2 L}{4E_\nu}}^{\text{atmos}} \sin 2\theta_{23} \sin^2 \frac{\Delta m_{13}^2 L}{4E_\nu}}{P_{\nu_\alpha \nu_\beta}^{\text{CP-even}}}. \quad (9.5)$$

As expected, the numerator is GIM suppressed in all the Δm_{ij}^2 and all the angles, because if any of them is zero, the CP-odd phase becomes unphysical. Therefore an experiment which is sensitive to CP violation must be sensitive to both mass splittings simultaneously. In this situation, it is not clear a priori what the optimization of E/L should be.

It can be shown that including only statistical errors, the signal-to-noise ratio for this asymmetry is

maximized for $\langle E_\nu \rangle / L \sim \Delta m_{\text{atmos}}^2$. In this case, only two small parameters remain in the CP-odd terms: the solar splitting, $\Delta m_{\text{solar}}^2$ (i.e., compared to the other scales, $\Delta m_{\text{atmos}}^2$ and $\langle E_\nu \rangle / L$), and the angle θ_{13} . The asymmetry is then larger in the sub-leading transitions: $\nu_e \rightarrow \nu_\mu (\nu_\tau)$, because the CP-even terms in the denominator are also suppressed by the same small parameters. A convenient approximation for the $\nu_e \leftrightarrow \nu_\mu$ transitions is obtained expanding to second order in both small parameters [58]:

$$\begin{aligned}
 P_{\nu_e \nu_\mu (\bar{\nu}_e \bar{\nu}_\mu)} &= s_{23}^2 \sin^2 2\theta_{13} \sin^2 \left(\frac{\Delta m_{13}^2 L}{4E_\nu} \right) \equiv P^{\text{atmos}} \\
 &+ c_{23}^2 \sin^2 2\theta_{12} \sin^2 \left(\frac{\Delta m_{12}^2 L}{4E_\nu} \right) \equiv P^{\text{solar}} \\
 &+ \tilde{J} \cos \left(\pm \delta - \frac{\Delta m_{13}^2 L}{4E_\nu} \right) \frac{\Delta m_{12}^2 L}{4E_\nu} \sin \left(\frac{\Delta m_{13}^2 L}{4E_\nu} \right) \equiv P^{\text{inter}}, \quad (9.6)
 \end{aligned}$$

where $\tilde{J} \equiv c_{13} \sin 2\theta_{13} \sin 2\theta_{12} \sin 2\theta_{23}$. The first term corresponds to the atmospheric oscillation, the second one is the solar one and there is an interference term which has the information on the phase δ and depends on both mass splittings.

These results correspond to vacuum propagation, but usually these experiments require the propagation of neutrinos in the earth's matter. The oscillation probabilities in matter can also be approximated by a similar series expansion [58]. The result has the same structure as in vacuum:

$$\begin{aligned}
 P_{\nu_e \nu_\mu (\bar{\nu}_e \bar{\nu}_\mu)} &= s_{23}^2 \sin^2 2\theta_{13} \left(\frac{\Delta_{13}}{B_\pm} \right)^2 \sin^2 \left(\frac{B_\pm L}{2} \right) \\
 &+ c_{23}^2 \sin^2 2\theta_{12} \left(\frac{\Delta_{12}}{A} \right)^2 \sin^2 \left(\frac{A L}{2} \right) \\
 &+ \tilde{J} \frac{\Delta_{12}}{A} \sin \left(\frac{A L}{2} \right) \frac{\Delta_{13}}{B_\pm} \sin \left(\frac{B_\pm L}{2} \right) \cos \left(\pm \delta - \frac{\Delta_{13} L}{2} \right), \quad (9.7)
 \end{aligned}$$

where

$$B_\pm = |A \pm \Delta_{13}|, \quad \Delta_{ij} = \frac{\Delta m_{ij}^2}{2E_\nu}, \quad A = \sqrt{2} G_F N_e. \quad (9.8)$$

The oscillation probability for neutrinos and antineutrinos now differ not just because of leptonic CP violation, but also due to the matter effects, that as we have seen can be resonant. In particular, the atmospheric term which is the dominant one, shows the expected resonant enhancement in the neutrino or antineutrino oscillation probability (depending on the ordering).

The sensitivity to the interference term requires very good knowledge of the leading atmospheric term and the present degeneracies (the octant and the neutrino ordering) directly affect the leading term compromising therefore the δ sensitivity. Either both uncertainties are solved before this measurement, or there must be sufficient sensitivity from the energy dependence of the signal to resolve all unknowns simultaneously.

A rough optimization of L for fixed E/L for discovering CP violation is shown in Fig. 39. It shows the signal-to-noise as a function of the true value of δ , assuming only statistical errors, but including the expected dependence of the cross sections and fluxes. At very short baselines, the sensitivity is compromised due to the lack of knowledge of the neutrino ordering. In a wide intermediate region

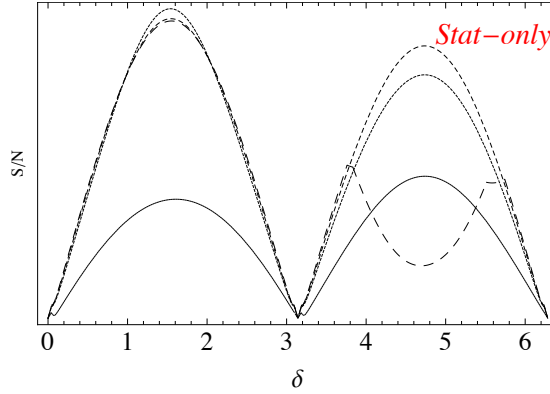


Fig. 39: Signal-to-noise for the discovery of CP violation at fixed $E/L \sim \Delta m_{\text{atm}}^2$ as a function of the true value of δ for $L = 295\text{km}$ (long-dashed), $L = 650\text{km}$ (short-dashed), $L = 1300\text{km}$ (dotted), $L = 2300\text{km}$ (solid). The ordering is assumed to be unknown.

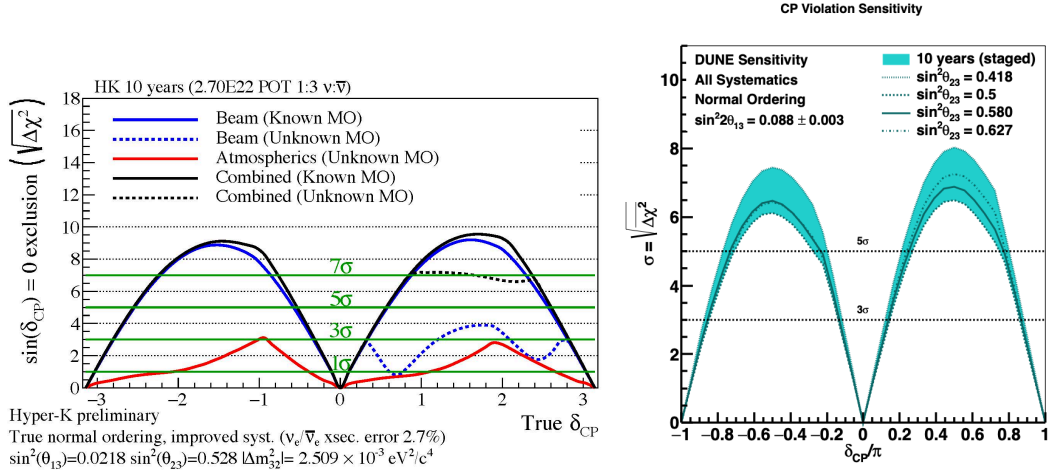


Fig. 40: Sensitivity to CP violation as a function of the true value of δ in Hyper-Kamiokande (left) [59] and DUNE (right) [60]. Solid (dashed) lines on the left plot correspond to the mass ordering (MO) known(unknown).

around $\mathcal{O}(1000)\text{km}$ the sensitivity is optimal, and at much larger baselines the sensitivity deteriorates because the matter effects completely hide CP-violation.

Several projects have been proposed to search for leptonic CP violation, including conventional beams, but also novel neutrino beams from muon decays (neutrino factories), from radioactive ion decays (β -beams) or from spallation sources (ESS). The relatively large value of θ_{13} has refocused the interest in using the less challenging conventional beams and two projects are presently being developed: the Hyper-Kamiokande detector, an up-scaled version of Super-Kamiokande that will measure atmospheric neutrinos with unprecedented precision, and also intercept a neutrino beam from JPARC at a relatively short baseline $L = 295\text{km}$, and the DUNE project that involves a liquid argon neutrino detector and a neutrino beam from Fermilab to the Soudan mine at a baseline of $L = 1500\text{km}$. The expected sensitivities to CP violation of both projects are shown in Fig. 40.

9.3 Absolute neutrino mass scale

Neutrino oscillation experiments are only sensitive to neutrino mass differences, so at present we do not have information on the absolute neutrino mass scale, only upper limits. The sum of all neutrino masses is tightly constrained by cosmological measurements of the cosmic microwave background (CMB) [61]:

$$\sum_i m_i \leq 0.12 \text{ eV}. \quad (9.9)$$

As we have seen the kinematical effects of neutrino masses in this range can also modify the end-point spectrum of beta decay. More precisely, this measurement can constrain the combination

$$m_{\nu_e} \equiv \sqrt{\sum_i |U_{ei}|^2 m_i^2}. \quad (9.10)$$

The strongest upper limit of 0.8 eV as we saw has been set by the Katrin experiment [7].

In Fig. 41 we show the allowed regions on the plane m_{ν_e} vs $\sum_i m_i$ from the known neutrino masses and mixings. The limit from cosmology on the right axis is already more stringent (although cosmological model dependent) than the present and future expected sensitivity of the Katrin experiment.

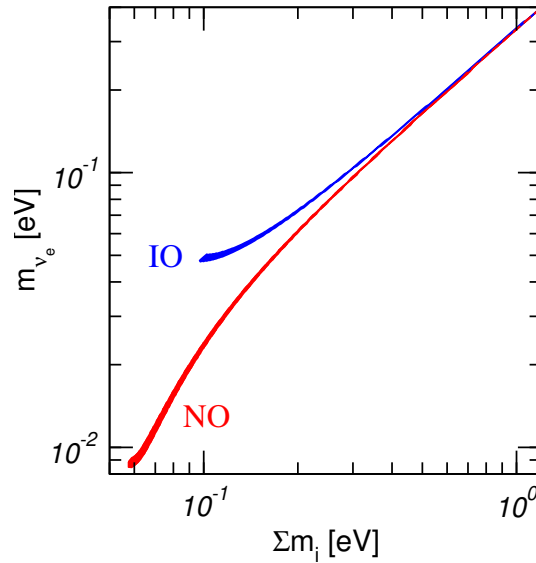


Fig. 41: Allowed region for m_{ν_e} for IO (blue contour) and NO (red contour) from a global analysis of neutrino data (from Ref. [51]) on the plane m_{ν_e} vs the sum of all neutrino masses.

10 Outliers: the LSND anomaly

The long-standing puzzle brought by the LSND experiment is still unresolved. This experiment [62] observed a surplus of electron events in a muon neutrino beam from π^+ decaying in flight (DIF) and a surplus of positron events in a neutrino beam from μ^+ decaying at rest (DAR). The interpretation of this data in terms of neutrino oscillations, that is a non-vanishing $P(\nu_\mu \rightarrow \nu_e)$, gives the range shown by a coloured band in Fig. 43.

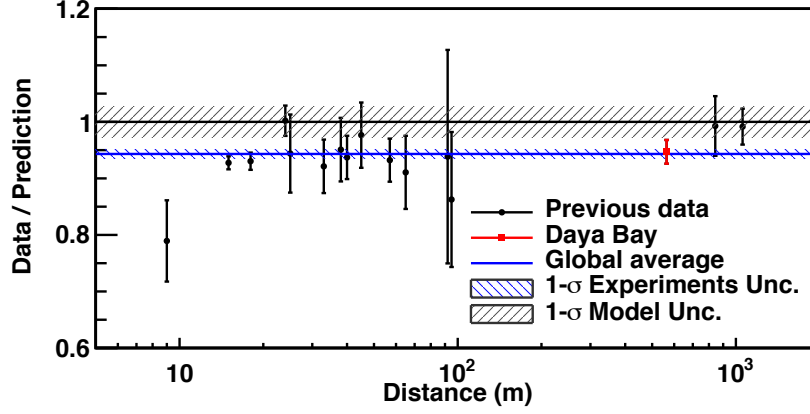


Fig. 42: Reactor neutrino flux measured by various near detectors compared with the recent flux predictions (from Ref. [70]).

$$\begin{aligned}
 \pi^+ &\rightarrow \mu^+ \nu_\mu \\
 \nu_\mu &\rightarrow \nu_e \quad \text{DIF } (28 \pm 6 / 10 \pm 2) \\
 \mu^+ &\rightarrow e^+ \nu_e \bar{\nu}_\mu \\
 \bar{\nu}_\mu &\rightarrow \bar{\nu}_e \quad \text{DAR } (64 \pm 18 / 12 \pm 3)
 \end{aligned}$$

A significant fraction of this region was already excluded by the experiment KARMEN [63] that has unsuccessfully searched for $\bar{\nu}_\mu \rightarrow \bar{\nu}_e$ in a similar range.

The experiment MiniBOONE was designed to further investigate the LSND signal, with inconclusive results [64]. They did not confirm the LSND anomaly, but found a significant excess at lower energies [65]. Recently the MicroBoone experiment [66], designed to have improved discrimination capabilities of NC background, did not find evidence for the MiniBOONE anomaly.

On the other hand, the results of various short baseline (tens of meters) reactor neutrino experiments were revised, after an update on the reactor neutrino flux predictions [67–69], which increased these fluxes by a few per cent. While the measured neutrino flux was found to be in agreement with predictions before, after this revision some reactor neutrinos seem to disappear before reaching near detectors, $L = \mathcal{O}(10)\text{m}$. This is the so-called reactor anomaly shown in Fig. 42. This result brought some excitement because if this disappearance is due to oscillations, it might reinforce the oscillation interpretation of the LSND anomaly.

The required mass splitting to describe both anomalies is $\Delta m_{\text{LSND}}^2 \simeq 1\text{eV}^2$, which is much larger than the solar and atmospheric, and therefore requires the existence of at least a fourth neutrino mass eigenstate, i . If such a state can explain the LSND anomaly, it must couple to both electrons and muons. Unfortunately the smoking gun would require that also accelerator ν_μ disappear with the same wavelength and this has not been observed:

$$\begin{aligned}
 P(\nu_\mu \rightarrow \nu_e) &\propto |U_{ei}U_{\mu i}|^2 && \text{LSND} \\
 1 - P(\nu_e \rightarrow \nu_e) &\propto |U_{ei}|^4 && \text{reactor} \\
 1 - P(\nu_\mu \rightarrow \nu_\mu) &\propto |U_{\mu i}|^4 && \text{not observed}
 \end{aligned}$$

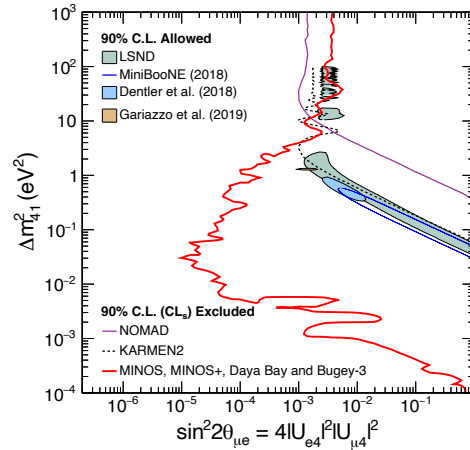


Fig. 43: Sterile neutrino search combining disappearance of ν_μ 's and ν_e (from Ref. [71]). At 90% CL only the region to the left of the red line is allowed, excluding most of the regions favoured by LSND, MiniBoone and the global fits.

The strongest constraint on the disappearance of ν_μ in the LSND range has been recently set by MINOS+ and the tension between appearance and disappearance measurements is shown in Fig. 43.

Very recently a new update on the flux predictions has been presented and the significance of the reactor anomaly has decreased. In parallel a plethora of new short baseline reactor neutrino experiments (Prospect, DANSS, Stereo, NEOS, NEUTRINO-4) have taken data exploiting the L dependence of a putative oscillation signal. The results have for the most part not confirmed the oscillation of reactor neutrinos. A global analysis of all the reactor data results shows that at 2.6σ the results are compatible with the non-oscillation hypothesis. See Ref. [72] for a recent status and references.

11 Neutrinos and BSM physics

The new lepton flavour sector of the SM has opened new perspectives into the flavour puzzle. As we have seen neutrinos are massive but significantly lighter than the remaining charged fermions. Clearly the gap of Fig. 11 calls for an explanation. The leptonic mixing matrix is also very different to that in the quark sector. The neutrino mixing matrix is approximately given in Ref. [51]

$$|U_{\text{PMNS}}|_{3\sigma} \simeq \begin{pmatrix} 0.80 - 0.84 & 0.51 - 0.58 & 0.14 - 0.16 \\ 0.23 - 0.50 & 0.46 - 0.69 & 0.63 - 0.78 \\ 0.26 - 0.52 & 0.47 - 0.70 & 0.61 - 0.76 \end{pmatrix}. \quad (11.1)$$

The CKM matrix is presently constrained [73] to be:

$$|V_{\text{CKM}}| \simeq \begin{pmatrix} 0.97435(16) & 0.22500(67) & 0.00369(11) \\ 0.22486(67) & 0.97349(16) & 0.04182(85) \\ 0.00857(20) & 0.04110(83) & 0.999118(31) \end{pmatrix}. \quad (11.2)$$

There is a striking difference between the two (and not only in the precision of the entries). The CKM matrix is close to the unit matrix:

$$V_{\text{CKM}} \simeq \begin{pmatrix} 1 & O(\lambda) & O(\lambda^3) \\ O(\lambda) & 1 & O(\lambda^2) \\ O(\lambda^3) & O(\lambda^2) & 1 \end{pmatrix}, \quad \lambda \sim 0.2, \quad (11.3)$$

while the leptonic one has large off-diagonal entries. With a similar level of precision, it is close to the tri-bimaximal mixing pattern [74]

$$U_{\text{PMNS}} \simeq V_{\text{tri-bi}} \simeq \begin{pmatrix} \sqrt{\frac{2}{3}} & \sqrt{\frac{1}{3}} & 0 \\ -\sqrt{\frac{1}{6}} & \sqrt{\frac{1}{3}} & \sqrt{\frac{1}{2}} \\ \sqrt{\frac{1}{6}} & -\sqrt{\frac{1}{3}} & \sqrt{\frac{1}{2}} \end{pmatrix}.$$

Discrete flavour symmetries have been extensively studied as the possible origin of this pattern.

While we do not have yet a compelling explanation of the different mixing patterns, we do have one for the gap between neutrino and other fermion masses. We saw that if the light neutrinos are Majorana particles and get their mass via the Weinberg interaction of Fig. 12, they are signalling BSM physics. As we have seen neutrino masses are then

$$m_\nu = \lambda \frac{v^2}{\Lambda}, \quad (11.4)$$

where Λ represents the mass of the neutrino mass mediators, i.e. the heavy particles that give rise to the Weinberg interaction. The more massive these particles are, the lighter neutrinos become. This is the famous *seesaw* mechanism depicted in Fig. 44.

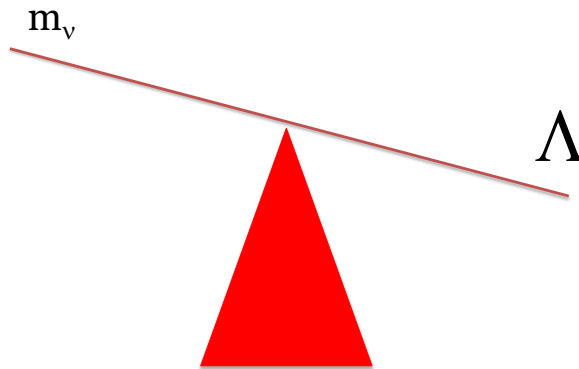


Fig. 44: Seesaw mechanism: the higher the scale Λ of new physics is, the lighter neutrino masses become.

λ on the other hand is the strength of the coupling of the new states with the lepton and Higgs doublets. Both parameters are in principle undetermined and only the combination $\frac{\lambda}{\Lambda}$ is fixed by neutrino masses. If we assume that the *natural* choice for λ is $\mathcal{O}(1)$, then neutrino masses require $\Lambda \sim M_{\text{GUT}}$,

that is a grand unification scale. This is an intriguing fact, however it leads to the famous hierarchy problem [75, 76]:

$$m_H^2 \sim \Lambda^2. \quad (11.5)$$

The recent discovery of the Higgs field and in particular the value of its mass $m_H = 125$ GeV [77] suggests that the SM is as healthy as ever. In spite of the Landau poles present in the theory, the value of the SM couplings surprisingly conspire to make the model consistent up to the Planck scale [78].

On the other hand, the SM contains other small couplings, for example the electron Yukawa coupling is $Y_e \sim \mathcal{O}(10^{-6})$. It is then a fair question to ask how small can λ be not to worsen the flavour hierarchies in the charged lepton and quark sectors. Unfortunately the answer to this question depends on the underlying model. We can for example consider the three types of seesaw models, which correspond to the models that give rise to the Weinberg operator from the exchange of a massive particle, as depicted in Fig. 45:

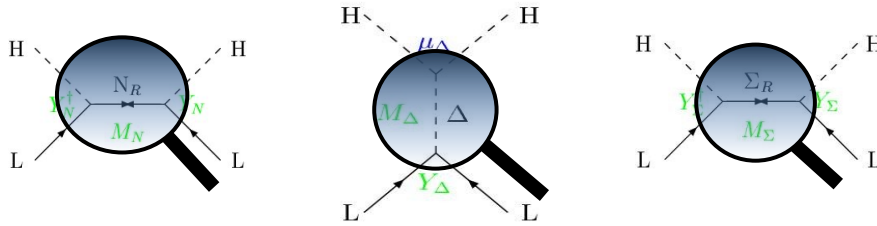


Fig. 45: Magnifying-glass view of the Weinberg operator in seesaw models of Type I (left), Type II (middle), Type III (right).

- type I see-saw: SM+ heavy singlet fermions, N , with mass M_N [79–82],
- type II see-saw: SM + heavy triplet scalar, Δ , with mass M_Δ [83–87],
- type III see-saw: SM + heavy triple fermions, Σ with mass M_Σ [88, 89],

In each of these cases $\Lambda = M_{N/\Delta/\Sigma}$ and the matching of the underlying theory to the Weinberg interaction fixes λ . For Type I and III:

$$\text{TypeI/III} : \lambda = \mathcal{O}(Y_{N/\Sigma}^2), \quad (11.6)$$

where $Y_{N,\Sigma}$ is the neutrino Yukawa coupling. In the case of Type II also the scalar trilinear coupling enters. If we now plot the hierarchies in the Yukawa couplings as opposed to the masses for Type I and III, we see that assuming a $Y_{N,\Sigma} \sim Y_e$, the scale Λ can be close to the electroweak scale, as shown in Fig. 46.

It is also possible that Weinberg’s interaction is generated by new physics at higher orders, such as in the famous Zee model [90] and related ones [91, 92]. In this case, neutrino masses have an additional suppression by loop factors $1/(16\pi^2)$ and generically higher powers of the couplings of the underlying theory.

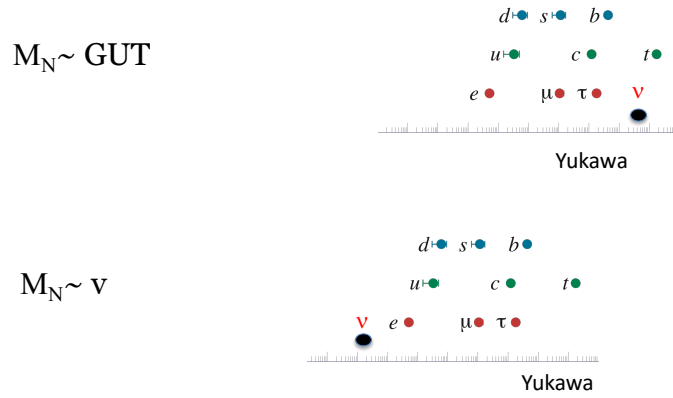


Fig. 46: Yukawa hierarchies in the Type I and III seesaw model if $M_N \sim M_{GUT}$ or $\sim v$.

Summarizing, for $\Lambda \in [v, M_{GUT}]$, neutrino masses do not imply larger hierarchies than already present in the minimal SM. Determining the scale Λ is one of the crucial problems in neutrino physics that we will try to elucidate in the future.

If $\Lambda \gg 100 \text{ MeV}$, there is a model-independent prediction: neutrinoless double-beta decay is possible with an amplitude proportional to the combination

$$m_{ee} = \sum_{i=1,3} (U_{PMNS})_{ei}^2 m_i. \quad (11.7)$$

The information we already have about neutrino masses and mixings constrains this quantity to be in any of the bands in Fig. 47 depending on the neutrino mass ordering.

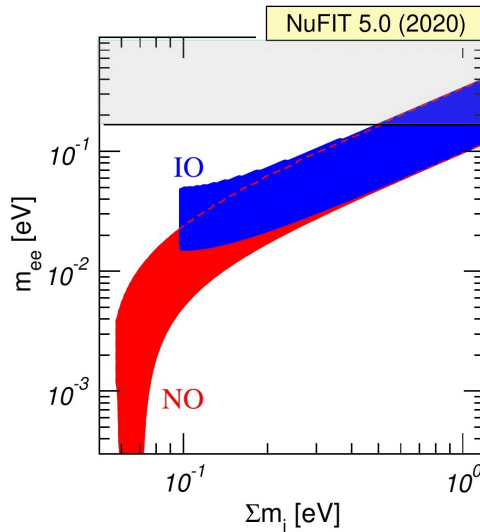


Fig. 47: Allowed region for m_{ee} for IO (blue contour) and NO (red contour) from a global analysis of neutrino data (from Ref. [51]) on the plane m_{ee} vs the sum of all neutrino masses. We have added by the shaded region the exclusion from present neutrinoless double-beta decay searches.

Obviously if Λ is below the energies of present colliders, the new particles may be directly acces-

sible. The dynamics of this new physics sector breaks lepton number and generically might induce the generation of the baryon asymmetry in the universe or may be connected to dark matter. Unfortunately both predictions: the production of these new states in colliders and their connection to baryogenesis or dark matter are model dependent. The type I seesaw model is the better studied case so we will consider this scenario in the following discussion.

11.1 One example: Type I seesaw model

It is arguably the most minimal extension of the SM explaining neutrino masses [79–82]. It involves the addition of $n_R \geq 2$ singlet Weyl fermions, ν_R , to the SM. With $n_R = 2$ two light neutrinos can be massive, which is the minimum compatible with neutrino mass measurements, i.e. two neutrino mass differences. The minimum number of singlets required to give non-zero mass to the three light neutrinos is $n_R = 3$, as shown in Fig. 48.

$(\mathbf{1}, \mathbf{2})_{-\frac{1}{2}}$	$(\mathbf{3}, \mathbf{2})_{-\frac{1}{6}}$	$(\mathbf{1}, \mathbf{1})_{-1}$	$(\mathbf{3}, \mathbf{1})_{-\frac{2}{3}}$	$(\mathbf{3}, \mathbf{1})_{-\frac{1}{3}}$	$(\mathbf{1}, \mathbf{1})_0$
$\begin{pmatrix} \nu_e \\ e \end{pmatrix}_L$	$\begin{pmatrix} u^i \\ d^i \end{pmatrix}_L$	e_R	u^i_R	d^i_R	ν^1_R
$\begin{pmatrix} \nu_\mu \\ \mu \end{pmatrix}_L$	$\begin{pmatrix} c^i \\ s^i \end{pmatrix}_L$	μ_R	c^i_R	s^i_R	ν^2_R
$\begin{pmatrix} \nu_\tau \\ \tau \end{pmatrix}_L$	$\begin{pmatrix} t^i \\ b^i \end{pmatrix}_L$	τ_R	t^i_R	b^i_R	ν^3_R

Fig. 48: Particle content of the SM+Type I seesaw model with three light massive neutrinos.

The most general renormalizable Lagrangian which satisfies Lorentz and the gauge symmetries is given by:

$$\mathcal{L}_{\text{TypeI}} = \mathcal{L}_{\text{SM}} - \sum_{\alpha, i} \bar{L}^\alpha Y_\nu^{\alpha i} \tilde{\Phi} \nu_R^i - \sum_{i, j} \frac{1}{2} \bar{\nu}_R^{ic} M_N^{ij} \nu_R^j + \text{h.c.}, \quad (11.8)$$

where the new parameters involved are a $3 \times n_R$ neutrino Yukawa matrix and a $n_R \times n_R$ symmetric Majorana mass matrix for the singlet fields. Upon spontaneous symmetry breaking these couplings become mass terms, that can be written in the Majorana basis (ν_L^c, ν_R) as

$$\mathcal{L}_{\text{TypeI}} \rightarrow \mathcal{L}_{\text{SM}} - \frac{1}{2} \begin{pmatrix} \bar{\nu}_L & \bar{\nu}_R^c \end{pmatrix} \begin{pmatrix} 0 & m_D \\ m_D^T & M_N \end{pmatrix} \begin{pmatrix} \nu_L^c \\ \nu_R \end{pmatrix} + \text{h.c.} + \dots \quad (11.9)$$

where

$$m_D = Y_\nu \frac{v}{\sqrt{2}}. \quad (11.10)$$

Note that Dirac neutrinos are a particular case of the model for $n_R = 3$. If we invoke a global lepton number symmetry, under which ν_R have charge $+1$, this forces $M_N = 0$, the singlets are exactly equivalent to the right-handed neutrinos in the Dirac case described in sec. 3.1. In the opposite limit $M_N \gg v$, the singlets can be integrated out and give rise to the Weinberg interaction as well as others at $d = 6$, etc. For intermediate M_N , the spectrum of this theory contains in general $3 + n_R$ Majorana neutrinos, which are admixtures of the active ones and the extra singlets.

It is easy to diagonalize the mass matrix in Eq. (11.9) in an expansion in m_D/M_N . The result to leading order in this expansion is

$$U^T \begin{pmatrix} 0 & m_D \\ m_D^T & M_N \end{pmatrix} U \simeq \begin{pmatrix} -m_D \frac{1}{M_N} m_D^T & 0 \\ 0 & M_N \end{pmatrix} + \mathcal{O}(\theta^2), \quad U = \begin{pmatrix} 1 & \theta \\ -\theta^\dagger & 1 \end{pmatrix}, \quad (11.11)$$

where

$$\theta = m_D^* \frac{1}{M_N}. \quad (11.12)$$

The matrix represents the active component of the heavy neutrino states and therefore controls their gauge interactions. To this order therefore the light neutrino and heavy neutrino masses are given by

$$m_l = \text{Diag} \left[-m_D \frac{1}{M_N} m_D^T \right], \quad M_h = \text{Diag}[M_N]. \quad (11.13)$$

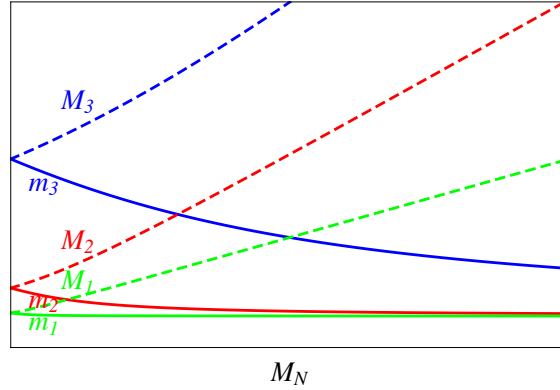


Fig. 49: Spectrum of the type I seesaw model for $n_R = 3$ as a function of a common M_N .

Figure 49 depicts the spectrum for the case of $n_R = 3$ as a function of a common M_N . In the limit $M_N \rightarrow 0$ the states degenerate in pairs to form Dirac fermions. As M_N increases three states get more massive proportional to M_N . These are often referred to as heavy neutral leptons (HNL), while three get lighter proportional to M_N^{-1} , as expected from the seesaw mechanism. The number of new free parameters is large. For the case $n_R = 3$ there are 18 fundamental parameters in the lepton sector: six of them are masses, six mixing angles and six phases. The counting of parameters for general n_R is shown in Table 4. Out of these 18 parameters we have determined only five: two mass differences and three neutrino mixing angles.

A very convenient parametrization in this model was introduced by Casas–Ibarra [93], which

Table 4: Number of physical parameters in the see-saw model with n families and the same number of right-handed Majorana neutrinos at high and low energies

	Yukawas	Field redefinitions	No. m	No. θ	No. ϕ
see-saw $E \geq M_i$	$Y_l, Y_\nu, M_R = M_R^T$ $5n^2 + n$	$U(n)^3$ $\frac{3(n^2-n)}{2}, \frac{3(n^2+n)}{2}$	$3n$	$n^2 - n$	$n^2 - n$
see-saw $E \ll M_i$	$Y_l, \alpha_\nu^T = \alpha_\nu$ $3n^2 + n$	$U(n)^2$ $n^2 - n, n^2 + n$	$2n$	$\frac{n^2-n}{2}$	$\frac{n^2-n}{2}$

allows to write in all generality (up to corrections of $\mathcal{O}(\theta^2)$) the Lagrangian parameters in terms of those of the light neutrino masses and mixings, and others related to the HNLs. In particular the phenomenology of this model depends on the spectrum of neutrino mass eigenstates, that we denote by $(\nu_1, \nu_2, \nu_3, N_1, N_2, \dots, N_{n_R})$, and their admixture in the flavour neutrino states :

$$\begin{pmatrix} \nu_e \\ \nu_\mu \\ \nu_\tau \end{pmatrix} = U_{ll} \begin{pmatrix} \nu_1 \\ \nu_2 \\ \nu_3 \end{pmatrix} + U_{lh} \begin{pmatrix} N_1 \\ N_2 \\ \dots \\ N_{n_R} \end{pmatrix}. \quad (11.14)$$

In the Casas–Ibarra parametrization we have

$$\begin{aligned} U_{ll} &= U_{\text{PMNS}} + \mathcal{O}(\theta^2), \\ U_{lh} &= iU_{\text{PMNS}}\sqrt{m_l}R\frac{1}{\sqrt{M_h}} + \mathcal{O}(\theta^2), \end{aligned} \quad (11.15)$$

where R is a general complex orthogonal matrix, $R^T R = 1$, which together with the heavy neutrino masses, M_h , parametrizes the parameter space inaccessible to neutrino oscillation experiments. Note that U_{ll} is the mixing matrix that we measure in neutrino oscillation experiments, assuming the heavy states are too heavy to play a role. This matrix is however no longer unitary,³ but the unitarity violations are parametrically of $\mathcal{O}(\theta^2) \sim m_l/M_h$.

Equations (11.15) indicate that in this model there is a strong correlation between flavour mixings of the heavy states, U_{lh} , and the ratio of light-to-heavy neutrino masses. However the presence of the unknown matrix R , which is not bounded, implies that the naive seesaw scaling, $|U_{lh}|^2 \sim m_l/M_h$, that would hold exactly for one neutrino family, is far too naive for $n_R > 1$. In fact there are regions of parameter space where these mixings can be much larger than suggested by the naive scaling, and these are precisely the regions with more phenomenological interest, as we will see below.

Let us discuss some phenomenological implications of the different choices of the scale M_N .

³The Casas–Ibarra parametrization needs to be modified in the presence of large unitarity violations. A similar parametrization valid to all orders in θ is given in Ref. [94].

11.1.1 Neutrinoless double-beta decay

The amplitude for this process receives contributions from the light and heavy states:

$$m_{ee} \equiv \sum_{i=1}^3 (U_{\text{PMNS}})_{ei}^2 m_i + \sum_{j=1}^{n_R} (U_{lh})_{ej}^2 M_j \frac{\mathcal{M}^{\beta\beta 0\nu}(M_j)}{\mathcal{M}^{\beta\beta 0\nu}(0)}, \quad (11.16)$$

where the ratio of matrix elements $\mathcal{M}^{\beta\beta 0\nu}$ for heavy and light mediators satisfy [95]:

$$\frac{\mathcal{M}^{\beta\beta 0\nu}(M_j)}{\mathcal{M}^{\beta\beta 0\nu}(0)} \propto \left(\frac{100 \text{ MeV}}{M_j} \right)^2, \quad M_j \rightarrow \infty. \quad (11.17)$$

If all the heavy state masses $\gg 100$ MeV, the second term is suppressed and the amplitude contains only the light neutrino masses and mixings, which is constrained as shown before in Fig. 47. A plethora of experiments using different technologies have been proposed to reach a sensitivity in m_{ee} in the range of 10^{-2} eV, which could be sufficient to explore the full parameter space in the case of the IO. The importance of this measurement can hardly be overstated. A non-zero m_{ee} will imply that neutrinos are Majorana and therefore a new physics scale must exist, that lepton number is violated, and might give very valuable information on the lightest neutrino mass, and even help establishing the neutrino mass ordering. On the other hand, if the heavy states are not too heavy, within 100 MeV–few GeV, they could also contribute to the process significantly and even dominate over the light neutrino contribution for both orderings [96–98].

11.1.2 Cosmology and the seesaw scale

For $M_N \leq 100$ MeV, the heavy states in seesaw models can sizeably modify the history of the Universe: the abundance of light elements, the fluctuations in the CMB and the galaxy distribution at large scales. This is the case because these extra states contribute to the expansion either as a significant extra component of dark matter (Ω_m) or radiation (ΔN_{eff}).

The singlet states in this mass range are produced at T below the electroweak phase transition via mixing. The state i will reach thermal equilibrium if their interaction rate, $\Gamma_{s_i}(T)$, is larger than the Hubble parameter at some T . If this is the case, the extra species will contribute like one extra neutrino for $T > M_i$ or like an extra component of dark matter for $T < M_i$. The latest results from Planck strongly constrain an extra radiation component at CMB:

$$N_{\text{eff}}(\text{CMB}) = 3.2 \pm 0.5. \quad (11.18)$$

and also measures the dark matter component to be $\Omega_m = 0.308 \pm 0.012$. Similar bounds are obtained from the abundance of light elements, BBN. These bounds exclude the possibility of having essentially any extra fully thermalized neutrino that is sufficiently long-lived to survive BBN. It can be shown that the ratio $\frac{\Gamma_{s_i}(T)}{H(T)}$ reaches a maximum at T_{max} [99, 100] and

$$\frac{\Gamma_{s_i}(T_{\text{max}})}{H(T_{\text{max}})} \sim \frac{\sum_{\alpha} |(U_{lh})_{\alpha i}|^2 M_i}{\sqrt{g_*(T_{\text{max}})}}. \quad (11.19)$$

The naive seesaw scaling $U_{lh}^2 M_h \sim m_l$, would seem to imply that the thermalization condition depends only on the light neutrino masses and is independent on the seesaw scale. In fact a detailed study shows that indeed this naive expectation holds.

For $n_R = 2$, the heavy states must be $M_i \geq 100$ MeV [101], so that they might decay before BBN. For $n_R = 3$ two things can happen [102]. If the lightest neutrino mass, $m_{\text{lightest}} \geq 3 \times 10^{-3}$ eV, all the three heavy states thermalize and $M_i \geq 100$ MeV. If $m_{\text{lightest}} \leq 3 \times 10^{-3}$ eV two states must be above this limit, but one of the states with mass M_1 might not thermalize and therefore be sufficiently diluted. M_1 may take any value provided m_{lightest} , which is presently unconstrained, and is tuned accordingly.

11.1.3 Warm dark matter

For $m_{\text{lightest}} \leq 10^{-5}$ eV, M_1 might be $\mathcal{O}(\text{keV})$, and a viable warm dark matter candidate [103, 104]. This scenario is the so-called ν MSM model [104]. The most spectacular signal of this type of dark matter is a monochromatic X-ray line from the decay of this keV neutrino. There has been some evidence for an unexplained X-ray line in galaxy clusters that might be compatible with a 7 keV neutrino [105, 106]. These results are under intense scrutiny. If interpreted in terms of a keV neutrino, the mixing however is too small and some extra mechanism is needed to enhance the production so that it matches the required dark matter density, such as the presence of large primordial lepton asymmetries [107].

11.1.4 Direct searches for heavy neutral leptons

Naturalness arguments suggest that maybe the scale of M_N is not far from the electroweak scale. States with masses in this range could be produced in the lab [108]. The production of the HNL is mediated by charged or neutral currents or Higgs interactions with strength given by the U_{hl} coupling, see Fig. 50. The most important production mechanisms, from meson decays, at e^+e^- collisions at the Z peak or at hadron colliders, are shown in Fig. 51.

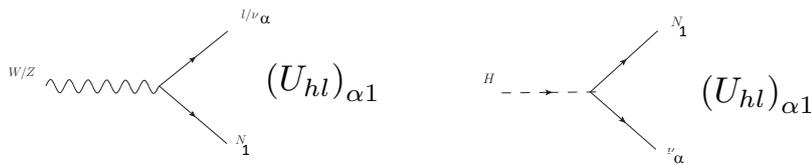


Fig. 50: Interactions of HNL in Type I seesaw model.

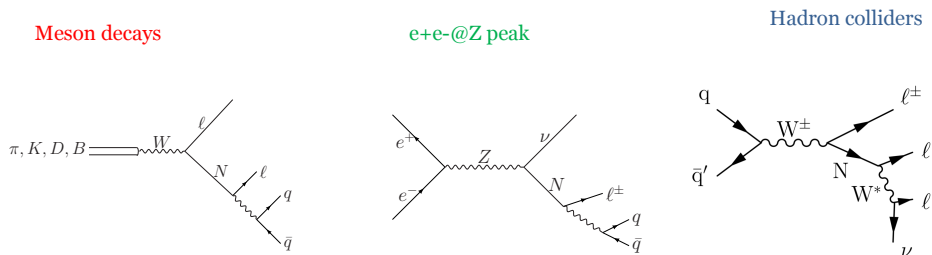


Fig. 51: Production processes of HNLs from meson decays, e^+e^- colliders and hadron colliders.

The present experimental bounds on the e mixings of these heavy states are shown in Figs. 52, on the plane $\sum_{\alpha=e,\mu,\tau} |(U_{hl})_{\alpha i}|^2$ versus M_i . The shaded regions correspond to existing constraints and the unshaded ones to prospects of various new experiments. For masses below a few GeV, the best constraints come from peak searches in meson decays. In particular the new beam dump experiment SHiP [109] can improve considerably the sensitivity in the region between the Kaon and B meson mass. Above the B meson mass and below the Z boson mass, searches in FCCee at the Z peak would improve present limits by several orders of magnitude [110]. The best existing limits in this range come from the LEP experiment DELPHI [111] and LHC searches from displaced vertices [112, 113]. The HNL in this range are very long lived and lead to displaced decays [114–116] that have a negligible SM background.

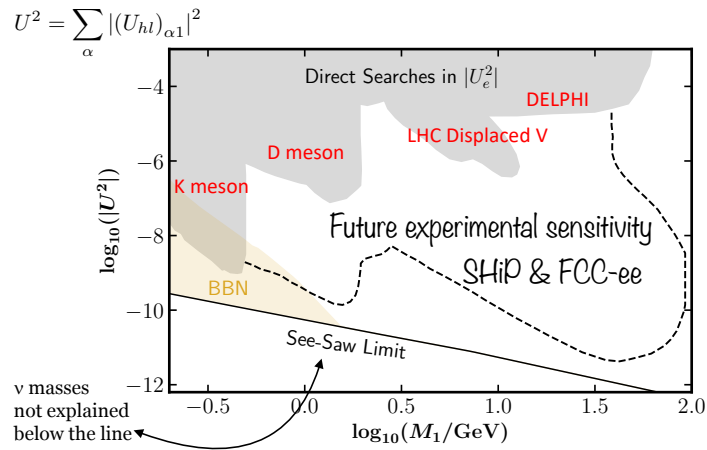


Fig. 52: Constraints from present and future experiments on a HNLs. Shaded regions are existing bounds on the HNL electron mixing as a function of the HNL mass, from the various processes that are sensitive to different mass ranges. The dashed line is the future sensitivity of SHiP at lower masses and FCCee at higher ones. Below the seesaw line neutrino masses cannot be explained. The exclusion from BBN is also added. Figure is courtesy of S. Sandner.

For masses above the W and Z masses, the best constraints are presently coming from LHC searches [117–119].

12 Low-scale leptogenesis

The Universe is made of matter. The matter–antimatter asymmetry is measured to be [61]

$$\eta_B \equiv \frac{N_b - N_{\bar{b}}}{N_\gamma} \sim 6.21(16) \times 10^{-10}. \quad (12.1)$$

One generic implication of neutrino mass models is that they provide a new mechanism to explain this asymmetry dynamically.

It has been known for a long time that all the ingredients to generate such an asymmetry from a symmetric initial state are present in the laws of particle physics. These ingredients were first put forward by Sakharov [120]:

1. Baryon number violation

$B + L$ is anomalous in the SM [121] both with and without massive neutrinos. At high T in the early

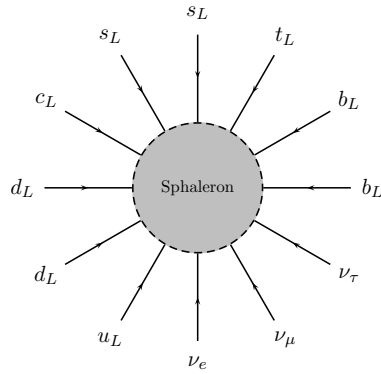


Fig. 53: Artistic view of a sphaleron.

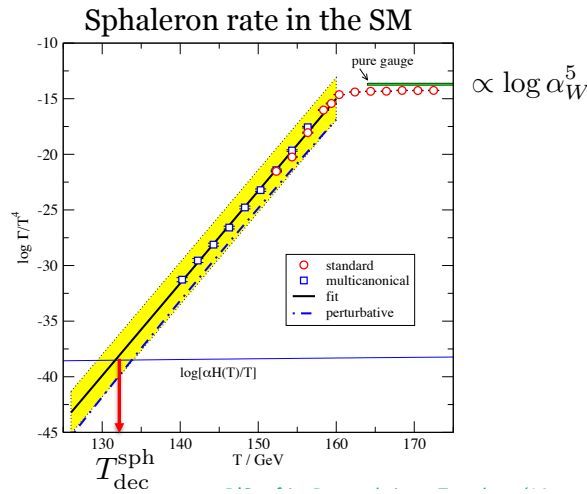


Fig. 54: Sphaleron rate in the SM normalized by T^4 as function of the temperature, from [123]. The horizontal line corresponds to the Hubble expansion rate.

Universe, $B + L$ violating transitions are in thermal equilibrium [122] due to the thermal excitation of configurations with topological charge called sphalerons, see Fig. 53.

These processes violate baryon and lepton numbers by the same amount:

$$\Delta B = \Delta L. \quad (12.2)$$

In seesaw models, there is generically an additional source of L violation (and $B - L$). If a lepton charge is generated at temperatures where the sphalerons are still in thermal equilibrium, a baryon charge can be generated.

The sphaleron rate in the SM has been computed accurately after the discovery of the Higgs boson [123]. The rate normalized to the fourth power of the temperature is shown in Fig. 54 around the electroweak phase transition. At $T \geq 160\text{GeV}$ the rate is $\propto \alpha_W^5 T^4$, while it drops exponentially at lower temperatures. The Hubble rate is indicated by the horizontal line. The temperature where the sphaleron rate equals the Hubble expansion rate is the sphaleron decoupling temperature, $T_{\text{dec}}^{\text{sph}}$, below which no baryon number violation is possible.

2. C and CP violation

Any lepton or baryon asymmetry can only be generated if there is C and CP violation. Seesaw models generically include new sources of CP violation. As we have seen in type I seesaw model with $n_R = 3$ there are six new CP phases in the lepton sector. They can be absorbed in the Yukawa matrix, Y_ν of Eq. (11.8). Even though CP violation is connected to imaginary phases, CP violating observables such as the baryon asymmetry depends on many flavour parameters. A very useful concept is that of the flavour CP invariants [124]. Let us consider for example the minimal SM. Since quark Yukawa couplings are the only source of CP violation and they are small, we expect that any CP violating asymmetry generated at high temperatures (above the quark masses) can be expanded as a polynomial in the up and down Yukawa couplings, Y_u and Y_d . Furthermore we expect that this polynomial is independent of the flavour basis used⁴ and it is not real, that is it must have a non-zero imaginary part. The lowest order polynomial of Y_u and Y_d that satisfies these conditions is the famous Jarlskog invariant [124]

$$\Delta_{\text{CP}}^{\text{quarks}} = \text{Im} \left[\det \left([Y_u Y_u^\dagger, Y_d Y_d^\dagger] \right) \right] \propto J \prod_{i < j} (m_{d_i}^2 - m_{d_j}^2) \prod_{i < j} (m_{u_i}^2 - m_{u_j}^2), \quad (12.3)$$

with

$$J \equiv \text{Im}[V_{ij}^* V_{ii} V_{ji}^* V_{jj}] = c_{23} s_{23} c_{12} s_{12} c_{13}^2 s_{13} \sin \delta. \quad (12.4)$$

We can then naively estimate the baryon asymmetry generated at the EW transition in the SM as

$$Y_B \propto \frac{\Delta_{\text{CP}}^{\text{quarks}}}{T_{\text{EW}}^{12}} \sim 10^{-20}, \quad (12.5)$$

where the denominator is fixed by dimensional analysis. This simple analysis shows that the CP violation in the minimal SM is far too small to explain the baryon asymmetry at the electroweak phase transition. A detailed computation arrives to the same conclusion [125].

In the case of the Type I seesaw extension of the SM we have also CP violation in the lepton sector encoded in the flavour parameters: Majorana mass matrix of the singlets, M_N , and the neutrino and charge lepton Yukawas, Y_ν and Y_l . The lowest order invariant involving Y_ν and M_N is [126, 127]:

$$\Delta_{\text{CP}}^{\text{leptons}} = \text{Im} \left(\text{Tr}[Y_\nu^\dagger Y_\nu M^\dagger M M^* (Y_\nu^\dagger Y_\nu)^* M] \right), \quad (12.6)$$

or including also the lepton Yukawa

$$\tilde{\Delta}_{\text{CP}}^{\text{leptons}} = \text{Im} \left(\text{Tr}[Y_\nu^\dagger Y_\nu M^\dagger M Y_\nu^\dagger Y_l Y_l^\dagger Y_\nu] \right) \equiv \sum_{\alpha} y_{l\alpha}^2 \Delta_{\alpha}. \quad (12.7)$$

Even at low scales, these invariants are potentially much larger than those in the quark sector [128].

3. Departure from thermal equilibrium

In order for a CP asymmetry to arise, it is necessary that the relevant processes occur out of thermal equilibrium since otherwise the abundances are fixed by the thermal Fermi–Dirac distributions and are

⁴A unitary rotation in flavour space of left and right chiral fields leaves all the terms in the Lagrangian invariant except the Yukawa couplings.

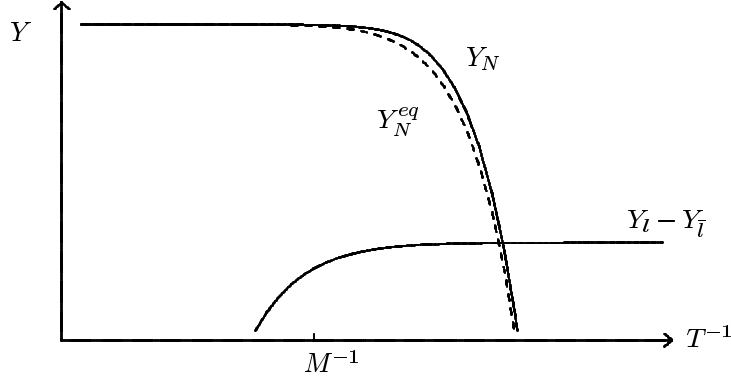


Fig. 55: High scale seesaw: abundance of the heavy Majorana singlets at the decoupling temperature and the lepton number generated in the decay.

equal for particles and antiparticles. Out-of-equilibrium conditions can happen in the evolution of the universe in the presence of first-order phase transitions, or due to the presence of sufficiently weakly coupled sectors that cannot keep up with the expansion of the universe. This happens when the interaction rates become smaller than the Hubble expansion rate, $\Gamma(T) \leq H(T)$. This must happen at T above the sphaleron decoupling, $T_{\text{dec}}^{\text{sph}}$ to be effective in generating baryons.

No particle in the minimal SM satisfies this condition within the standard cosmological model, not even neutrinos, that decouple much below sphaleron decoupling. On the other hand, the SM predicts the existence of a phase transition from the broken phase at low temperatures to a symmetric phase above, i.e. the EW phase transition. The critical temperature, T_{EW} , is closely related to the sphaleron decoupling temperature. The EW transition has been shown to be a crossover transition and therefore with insufficient departure from thermal equilibrium [129].

In the Type I seesaw extension at low scales however, some of the states are more weakly interacting than neutrinos and therefore can fulfil the requirement $\Gamma_{N_i}(T) \leq H_u(T)$, for $T \geq T_{\text{dec}}^{\text{sph}}$.

In the high scale scenario $M_i \gg v$, the non-equilibrium condition is met at freeze out of the heavy neutrino states. These are thermally produced and freeze out at temperatures similar to their masses [128]. A net lepton asymmetry can be produced if the decay rate is slower than the expansion of the Universe at $T \sim M_i$, as shown in Fig. 55.

In contrast, in the low-scale scenario, for $M_i < v$, the out-of-equilibrium condition is met at freeze-in [104, 130, 131], that is some of the states never reach thermal equilibrium above $T_{\text{dec}}^{\text{sph}}$. A non-vanishing lepton and baryon asymmetry can survive and, if this is the case, sphaleron transitions can no longer wash it out. It turns out that these conditions can be met naturally in type I seesaw models for masses in the range [0.1, 100] GeV. The relevant CP asymmetries arise in the production of the heavy seesaw states via the interference of CP-odd phases from the Yukawa couplings with CP-even phases from propagation and oscillations, see Fig. 56. A quantum treatment of the corresponding kinetic equations is mandatory in this case and quite complex.

A perturbative solution to the kinetic equations [132] allows to extract the analytical solution for Y_B in terms of the CP invariants, and using the Casas–Ibarra parametrization can then be expressed in terms of the neutrino masses and mixings, CP phases and HNL parameters.

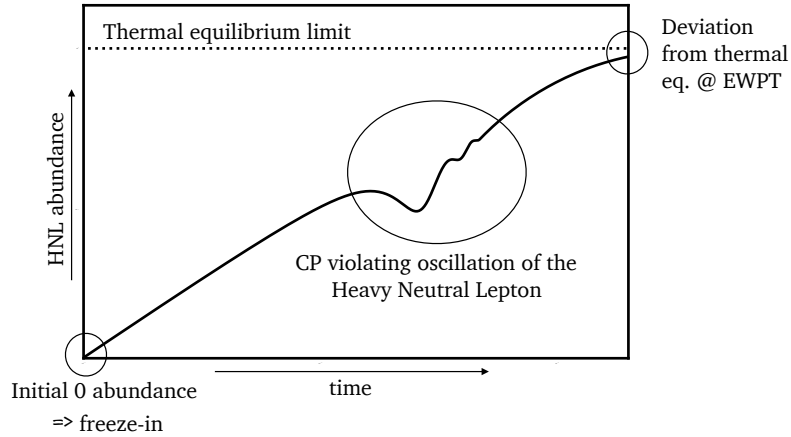


Fig. 56: Low-scale seesaw: abundance of the heavy Majorana singlets at T_{EW} .

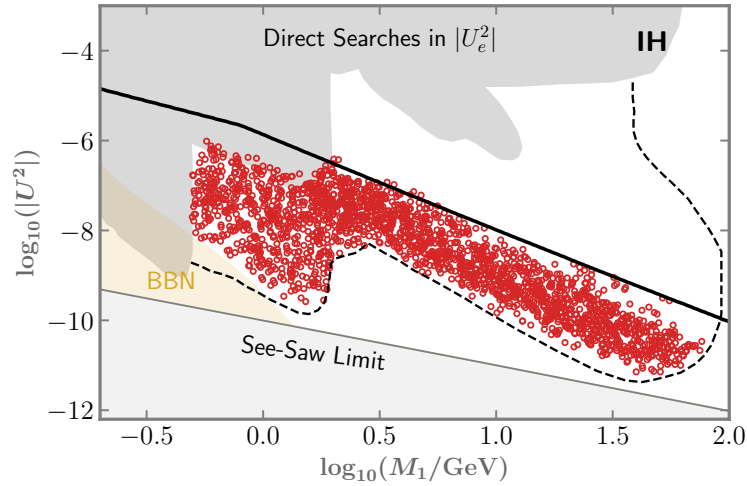


Fig. 57: Numerical scan of points on the plane of mixing versus mass of the HNL where the baryon asymmetry can be explained and within the sensitivity region of SHiP and/or FCCee (dashed line) in the minimal Type I seesaw ($n_R = 2$). The line is obtained analytically from a perturbative solution of the kinetic equations that can be expressed in terms of CP flavour invariants and maximized over unknown parameters. From Ref. [132].

In Fig. 57 we show the region on the plane U^2 v.s. M_i , where the baryon asymmetry and neutrino masses can be accounted for within the range of sensitivity of the future SHiP and FCCee projects. The solid line is the analytical upper bound to explain the baryon asymmetry based on the analytical solutions, and maximizing the asymmetry over the unknown parameters. This demonstrates the discovery potential of the future projects.

Other interesting correlations between Y_B and other observables are shown in Fig. 58. On the left, we show the HNL flavoured mixings for masses in the range accessible to FCC when neutrino masses are explained for both hierarchies. On the right plot the constrain of generating the correct baryon asymmetry is added. The correct baryon asymmetry therefore restricts the flavour of the HNL mixings as well as the PMNS CP phases (only two for $n_R = 2$), as shown in Fig. 59 for both hierarchies.

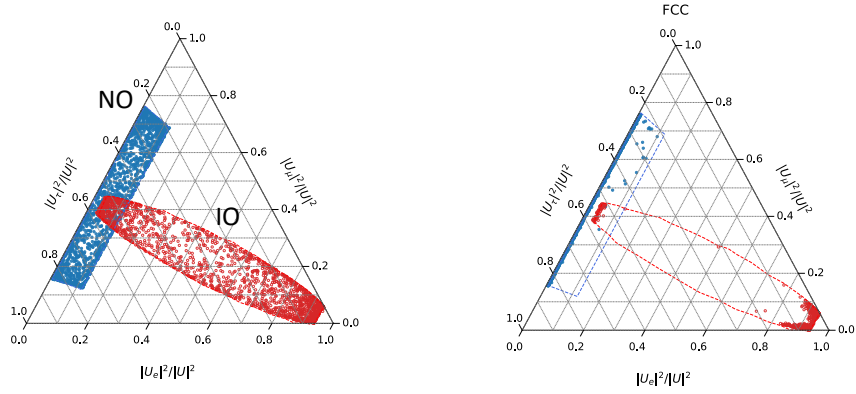


Fig. 58: Normalized mixings to e, μ, τ of HNLs with masses in the range of FCCee and mild degeneracy. Only the constrain from neutrino masses is imposed on the left plot, while also the Y_B is imposed on the right plot. The two regions correspond to neutrino orderings. From Ref. [132].

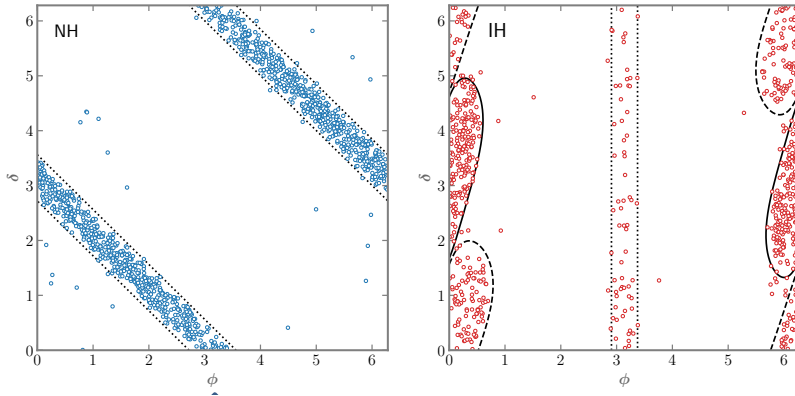


Fig. 59: Numerical scan of points that explain Y_B on the plane of the Dirac CP violating phase, δ , and the Majorana phase, ϕ in the minimal Type I seesaw ($n_R = 2$). From Ref. [132].

An interesting question is whether the baryon asymmetry can be predicted quantitatively from the measurements of CP violation in neutrino oscillations or from the CP violation in the neutrino mass matrix. Unfortunately this is not the case generically, because the asymmetry depends on more parameters than those in the light neutrino mass matrix. However, if the model is sufficiently constrained very strong correlations can occur.

For example, in the minimal Type I seesaw model, $n_R = 2$, and in the assumption that the two eigenvalues of the matrix M_N are degenerate, there are only two physical CP violating phases, that can then be parametrized by the two in the light neutrino mass matrix. They determine both Y_B and CP violation in neutrino oscillations. In this case, the measurement of the HNL mixings to electrons, muons and τ 's can pin down the CP phase in neutrino oscillations and Y_B up to discrete degeneracies, as shown in Fig. 60. If the phase δ is also measured, a prediction of Y_B is possible from laboratory measurements.

This simple example demonstrates the interplay between Y_B and other observables in neutrino physics.

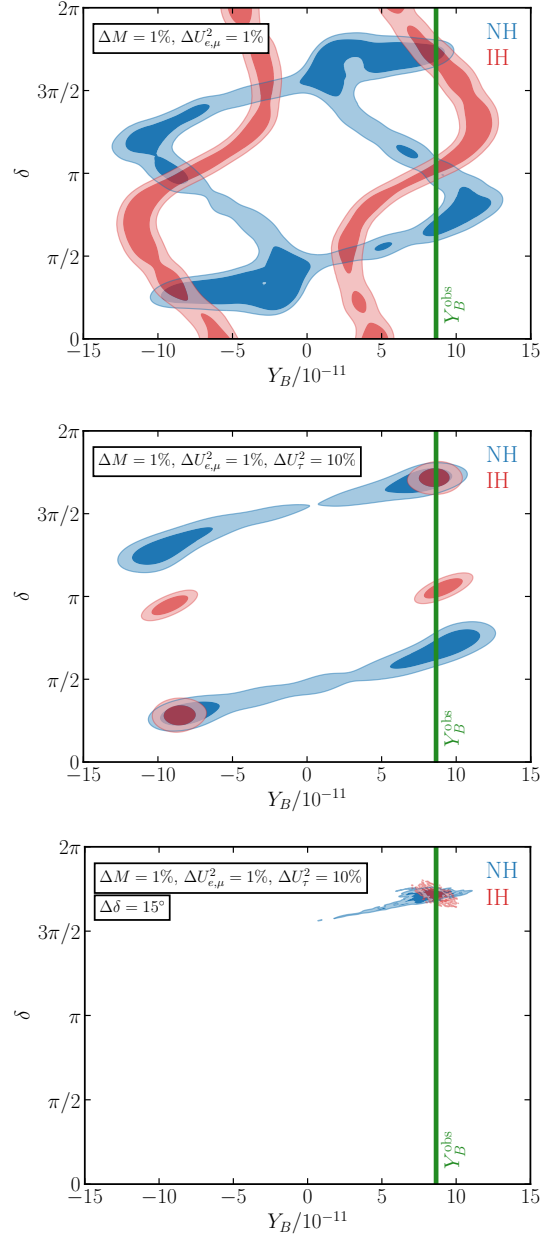


Fig. 60: Assuming the minimal Type I seesaw model with $n_R = 2$, and degenerate singlets within the FCCee range, with parameters that can explain neutrino masses and Y_B . Upper Plot: determination of δ and Y_B from a putative measurement of HNL mixings to electrons and muons and masses with accuracies as indicated, and for NO (blue) and IO (blue). Middle Plot: adding also a measurement of the HNL mixing to τ 's. Bottom Plot: adding also a measurement of the phase δ from future neutrino oscillation experiments. From Ref. [133].

13 Conclusions

The results of many beautiful experiments in the last decade have demonstrated that neutrinos are massive and mix. The standard 3ν scenario can explain all available data, except that of the unconfirmed signal of LSND. The lepton flavour sector of the Standard Model is expected to be at least as complex as the quark one, even though we know it only partially.

The structure of the neutrino spectrum and mixing is quite different from the one that has been observed for the quarks: there are large leptonic mixing angles and the neutrino masses are much smaller than those of the remaining leptons. These peculiar features of the lepton sector strongly suggest that leptons and quarks constitute two complementary approaches to understanding the origin of flavour in the Standard Model. In fact, the smallness of neutrino masses can be naturally understood if there is new physics beyond the electroweak scale.

Many fundamental questions remain to be answered in future neutrino experiments, and these can have very important implications for our understanding of the Standard Model and of what lies beyond: Are neutrinos Majorana particles? Are neutrino masses the result of a new physics scale? Is CP violated in the lepton sector? Could neutrinos be the seed of the matter–antimatter asymmetry in the Universe?

A rich experimental programme lies ahead where fundamental physics discoveries are very likely (almost warranted). We can only hope that neutrinos will keep up with their old tradition and provide a window to what lies beyond the Standard Model.

References

- [1] E. Fermi. Trends to a theory of β radiation. (In Italian). *Nuovo Cim.* **11** (1934) 1–19, [doi:10.1007/BF02959820](https://doi.org/10.1007/BF02959820).
- [2] H. Bethe and R. Peierls. The “neutrino”. *Nature*, **133** (1934) 532, [doi:10.1038/133532a0](https://doi.org/10.1038/133532a0).
- [3] B. Pontecorvo. Inverse β process, reprinted in K. Winter, *Neutrino physics* 2nd ed. (Cambridge Univ. Press, Cambridge, 2008), pp. 23–28, version from [Centro Pontecorvo](#).
- [4] F. Reines and C. L. Cowan. The neutrino. *Nature* **178** (1956) 446–449, [doi:10.1038/178446a0](https://doi.org/10.1038/178446a0).
- [5] C. L. Cowan *et al.*, Detection of the free neutrino: A confirmation, *Science* **124** (1956) 103–104, [doi:10.1126/science.124.3212.103](https://doi.org/10.1126/science.124.3212.103).
- [6] G. Danby *et al.*, Observation of high-energy neutrino reactions and the existence of two kinds of neutrinos, *Phys. Rev. Lett.* **9** (1962) 36–44, [doi:10.1103/PhysRevLett.9.36](https://doi.org/10.1103/PhysRevLett.9.36).
- [7] M. Aker *et al.*, Direct neutrino-mass measurement with sub-electronvolt sensitivity, *Nature Phys.* **18**(2) (2022) 160–166, [doi:10.1038/s41567-021-01463-1](https://doi.org/10.1038/s41567-021-01463-1).
- [8] K. Assamagan *et al.*, Upper limit of the muon-neutrino mass and charged pion mass from momentum analysis of a surface muon beam, *Phys. Rev.* **D53** (1996) 6065–6077, [doi:10.1103/PhysRevD.53.6065](https://doi.org/10.1103/PhysRevD.53.6065).
- [9] R. Barate *et al.*, An upper limit on the tau-neutrino mass from three-prong and five-prong tau decays, *Eur. Phys. J.* **C2** (1998) 395–406, [doi:10.1007/s100529800850](https://doi.org/10.1007/s100529800850).
- [10] S. Schael *et al.*, Precision electroweak measurements on the Z resonance, *Phys. Rept.* **427** (2006) 257–454, [doi:10.1016/j.physrep.2005.12.006](https://doi.org/10.1016/j.physrep.2005.12.006).
- [11] P. Janot and S. Jadach, Improved Bhabha cross section at LEP and the number of light neutrino species, *Phys. Lett.* **B803** (2020) 135319, [doi:10.1016/j.physletb.2020.135319](https://doi.org/10.1016/j.physletb.2020.135319).
- [12] G. Voutsinas *et al.*, Beam-beam effects on the luminosity measurement at LEP and the number of light neutrino species, *Phys. Lett.* **B800** (2020) 135068, [doi:10.1016/j.physletb.2019.135068](https://doi.org/10.1016/j.physletb.2019.135068).
- [13] S. Weinberg, Baryon and lepton nonconserving processes, *Phys. Rev. Lett.* **43** (1979) 1566–1570, [doi:10.1103/PhysRevLett.43.1566](https://doi.org/10.1103/PhysRevLett.43.1566).
- [14] S. Weinberg, Phenomenological Lagrangians, *Physica* **A96** (1979) 327–340, [doi:10.1016/0378-4371\(79\)90223-1](https://doi.org/10.1016/0378-4371(79)90223-1).
- [15] W. Buchmuller and D. Wyler, Effective Lagrangian analysis of new interactions and flavor conservation, *Nucl. Phys.* **B268** (1986) 621–653, [doi:10.1016/0550-3213\(86\)90262-2](https://doi.org/10.1016/0550-3213(86)90262-2).
- [16] Z. Maki, M. Nakagawa, and S. Sakata, Remarks on the unified model of elementary particles, *Prog. Theor. Phys.* **28** (1962) 870–880, [doi:10.1143/PTP.28.870](https://doi.org/10.1143/PTP.28.870).
- [17] B. Pontecorvo, Neutrino experiments and the problem of conservation of leptonic charge, *Sov. Phys. JETP* **26** (1968) 984–988 [*Zh. Eksp. Teor. Fiz.* **53** (1967) 1717], [Inspire](#).
- [18] P.A. Zyla *et al.*, Review of particle physics, *PTEP* **2020**(8) (2020) 083C01, [doi:10.1093/ptep/ptaa104](https://doi.org/10.1093/ptep/ptaa104).
- [19] B. Pontecorvo, Mesonium and anti-mesonium, *Sov. Phys. JETP* **6** (1957) 429 [*Zh. Eksp. Teor. Fiz.* **33** (1957) 549], [Inspire](#).

- [20] E.K. Akhmedov and A.Yu. Smirnov, Paradoxes of neutrino oscillations, *Phys. Atom. Nucl.* **72** (2009) 1363–1381, doi:[10.1134/S1063778809080122](https://doi.org/10.1134/S1063778809080122), arXiv:0905.1903.
- [21] E.K. Akhmedov and J. Kopp, Neutrino oscillations: quantum mechanics vs. quantum field theory, *JHEP* **04** (2010) 008, doi:[10.1007/JHEP04\(2010\)008](https://doi.org/10.1007/JHEP04(2010)008), [Erratum: *JHEP* **10** (2013) 052, doi:[10.1007/JHEP10\(2013\)052](https://doi.org/10.1007/JHEP10(2013)052)].
- [22] M. Cerdá, Neutrino oscillations in quantum field theory. Master thesis, University of Valencia, 2011.
- [23] L. Wolfenstein, Neutrino oscillations in matter, *Phys. Rev.* **D17** (1978) 2369–2374, doi:[10.1103/PhysRevD.17.2369](https://doi.org/10.1103/PhysRevD.17.2369).
- [24] S.P. Mikheev and A.Yu. Smirnov, Resonance amplification of oscillations in matter and spectroscopy of solar neutrinos, *Sov. J. Nucl. Phys.* **42** (1985) 913–917 [*Yad. Fiz.* **42**, 1441 (1985)].
- [25] H.A. Bethe, Energy production in stars, *Phys. Rev.* **55** (1939) 434–456, doi:[10.1103/PhysRev.55.434](https://doi.org/10.1103/PhysRev.55.434).
- [26] J.N. Bahcall, M.H. Pinsonneault, and S. Basu, Solar models: current epoch and time dependences, neutrinos, and helioseismological properties, *Astrophys. J.* **555** (2001) 990–1012, doi:[10.1086/321493](https://doi.org/10.1086/321493).
- [27] B.T. Cleveland *et al.*, Measurement of the solar electron neutrino flux with the Homestake chlorine detector, *Astrophys. J.* **496** (1998) 505–526, doi:[10.1086/305343](https://doi.org/10.1086/305343).
- [28] W. Hampel *et al.*, GALLEX solar neutrino observations: results for GALLEX IV, *Phys. Lett.* **B447** (1999) 127–133, doi:[10.1016/S0370-2693\(98\)01579-2](https://doi.org/10.1016/S0370-2693(98)01579-2).
- [29] J.N. Abdurashitov *et al.*, Solar neutrino flux measurements by the Soviet-American Gallium Experiment (SAGE) for half the 22 year solar cycle, *J. Exp. Theor. Phys.* **95** (2002) 181–193 [*Zh. Eksp. Teor. Fiz.* **122** (2002) 211], doi:[10.1134/1.1506424](https://doi.org/10.1134/1.1506424), arXiv:astro-ph/0204245.
- [30] Y. Fukuda *et al.*, Solar neutrino data covering solar cycle 22, *Phys. Rev. Lett.* **77** (1996) 1683–1686, doi:[10.1103/PhysRevLett.77.1683](https://doi.org/10.1103/PhysRevLett.77.1683).
- [31] Y. Fukuda *et al.*, Measurement of the solar neutrino energy spectrum using neutrino electron scattering, *Phys. Rev. Lett.* **82** (1999) 2430–2434, doi:[10.1103/PhysRevLett.82.2430](https://doi.org/10.1103/PhysRevLett.82.2430), arXiv:hep-ex/9812011.
- [32] J. Hosaka *et al.*, Solar neutrino measurements in Super-Kamiokande-I, *Phys. Rev.* **D73** (2006) 112001, doi:[10.1103/PhysRevD.73.112001](https://doi.org/10.1103/PhysRevD.73.112001), arXiv:hep-ex/0508053.
- [33] Q.R. Ahmad *et al.*, Measurement of the rate of $\nu_e + d \rightarrow p + p + e^-$ interactions produced by 8B solar neutrinos at the Sudbury Neutrino Observatory, *Phys. Rev. Lett.* **87** (2001) 071301, doi:[10.1103/PhysRevLett.87.071301](https://doi.org/10.1103/PhysRevLett.87.071301), arXiv:nucl-ex/0106015.
- [34] Q.R. Ahmad *et al.*, Direct evidence for neutrino flavor transformation from neutral current interactions in the Sudbury Neutrino Observatory, *Phys. Rev. Lett.* **89** (2002) 011301, doi:[10.1103/PhysRevLett.89.011301](https://doi.org/10.1103/PhysRevLett.89.011301), arXiv:nucl-ex/0204008.
- [35] K. Eguchi *et al.*, First results from KamLAND: evidence for reactor anti-neutrino disappearance, *Phys. Rev. Lett.* **90** (2003) 021802, doi:[10.1103/PhysRevLett.90.021802](https://doi.org/10.1103/PhysRevLett.90.021802), arXiv:hep-ex/0212021.

- [36] S. Abe *et al.*, Precision measurement of neutrino oscillation parameters with KamLAND, *Phys. Rev. Lett.* **100** (2008) 221803, [doi:10.1103/PhysRevLett.100.221803](https://doi.org/10.1103/PhysRevLett.100.221803), [arXiv:0801.4589](https://arxiv.org/abs/0801.4589).
- [37] G. Bellini *et al.*, Final results of Borexino Phase-I on low energy solar neutrino spectroscopy, *Phys. Rev.* **D89** (2014) 112007, [doi:10.1103/PhysRevD.89.112007](https://doi.org/10.1103/PhysRevD.89.112007), [arXiv:1308.0443](https://arxiv.org/abs/1308.0443).
- [38] M. Honda *et al.*, A new calculation of the atmospheric neutrino flux in a 3-dimensional scheme, *Phys. Rev. D* **70** (2004) 043008, [doi:10.1103/PhysRevD.70.043008](https://doi.org/10.1103/PhysRevD.70.043008), [arXiv:astro-ph/0404457](https://arxiv.org/abs/astro-ph/0404457).
- [39] Y. Fukuda *et al.*, Evidence for oscillation of atmospheric neutrinos, *Phys. Rev. Lett.* **81** (1998) 1562–1567, [doi:10.1103/PhysRevLett.81.1562](https://doi.org/10.1103/PhysRevLett.81.1562), [arXiv:hep-ex/9807003](https://arxiv.org/abs/hep-ex/9807003).
- [40] Y. Ashie *et al.*, Measurement of atmospheric neutrino oscillation parameters by Super-Kamiokande I, *Phys. Rev.* **D71** (2005) 112005, [doi:10.1103/PhysRevD.71.112005](https://doi.org/10.1103/PhysRevD.71.112005), [arXiv:hep-ex/0501064](https://arxiv.org/abs/hep-ex/0501064).
- [41] Y. Ashie *et al.*, Evidence for an oscillatory signature in atmospheric neutrino oscillation, *Phys. Rev. Lett.* **93** (2004) 101801, [doi:10.1103/PhysRevLett.93.101801](https://doi.org/10.1103/PhysRevLett.93.101801), [arXiv:hep-ex/0404034](https://arxiv.org/abs/hep-ex/0404034).
- [42] M.H. Ahn *et al.*, Measurement of neutrino oscillation by the K2K experiment, *Phys. Rev.* **D74** (2006) 072003, [doi:10.1103/PhysRevD.74.072003](https://doi.org/10.1103/PhysRevD.74.072003), [arXiv:hep-ex/0606032](https://arxiv.org/abs/hep-ex/0606032).
- [43] D.G. Michael *et al.*, Observation of muon neutrino disappearance with the MINOS detectors and the NuMI neutrino beam, *Phys. Rev. Lett.* **97** (2006) 191801, [doi:10.1103/PhysRevLett.97.191801](https://doi.org/10.1103/PhysRevLett.97.191801), [arXiv:hep-ex/0607088](https://arxiv.org/abs/hep-ex/0607088).
- [44] N. Agafonova *et al.*, Discovery of τ neutrino appearance in the CNGS neutrino beam with the OPERA experiment, *Phys. Rev. Lett.* **115** (2015) 121802, [doi:10.1103/PhysRevLett.115.121802](https://doi.org/10.1103/PhysRevLett.115.121802), [arXiv:1507.01417](https://arxiv.org/abs/1507.01417).
- [45] A. Holin, Results from the MINOS experiment and new MINOS+ data, *PoS NFACT2014* (2014) 028, [doi:10.22323/1.226.0028](https://doi.org/10.22323/1.226.0028), [arXiv:1507.08564](https://arxiv.org/abs/1507.08564).
- [46] F.P. An *et al.*, Observation of electron-antineutrino disappearance at Daya Bay, *Phys. Rev. Lett.* **108** (2012) 171803, [doi:10.1103/PhysRevLett.108.171803](https://doi.org/10.1103/PhysRevLett.108.171803), [arXiv:1203.1669](https://arxiv.org/abs/1203.1669).
- [47] J.K. Ahn *et al.*, Observation of reactor electron antineutrino disappearance in the RENO experiment, *Phys. Rev. Lett.* **108** (2012) 191802, [doi:10.1103/PhysRevLett.108.191802](https://doi.org/10.1103/PhysRevLett.108.191802).
- [48] Y. Abe *et al.*, Indication for the disappearance of reactor electron antineutrinos in the Double Chooz experiment, *Phys. Rev. Lett.* **108** (2012) 131801, [doi:10.1103/PhysRevLett.108.131801](https://doi.org/10.1103/PhysRevLett.108.131801).
- [49] K. Abe *et al.*, Observation of electron neutrino appearance in a muon neutrino beam, *Phys. Rev. Lett.* **112** (2014) 061802, [doi:10.1103/PhysRevLett.112.061802](https://doi.org/10.1103/PhysRevLett.112.061802).
- [50] P. Adamson *et al.*, First measurement of electron neutrino appearance in NOvA, *Phys. Rev. Lett.* **116** (2016) 151806, [doi:10.1103/PhysRevLett.116.151806](https://doi.org/10.1103/PhysRevLett.116.151806).
- [51] I. Esteban *et al.*, The fate of hints: updated global analysis of three-flavor neutrino oscillations, *JHEP* **09** (2020) 178, [doi:10.1007/JHEP09\(2020\)178](https://doi.org/10.1007/JHEP09(2020)178).
- [52] P.F. de Salas *et al.*, 2020 global reassessment of the neutrino oscillation picture, *JHEP* **02** (2021) 071, [doi:10.1007/JHEP02\(2021\)071](https://doi.org/10.1007/JHEP02(2021)071).

- [53] F. Capozzi *et al.*, Global constraints on absolute neutrino masses and their ordering, *Phys. Rev. D* **95** (2017) 096014, doi:[10.1103/PhysRevD.95.096014](https://doi.org/10.1103/PhysRevD.95.096014). [Addendum: *Phys. Rev.* **D101** (2020) 116013, doi:[10.1103/PhysRevD.101.116013](https://doi.org/10.1103/PhysRevD.101.116013)].
- [54] S.K. Agarwalla and P. Hernandez, Probing the neutrino mass hierarchy with Super-Kamiokande, *JHEP* **10** (2012) 086, doi:[10.1007/JHEP10\(2012\)086](https://doi.org/10.1007/JHEP10(2012)086).
- [55] S.T. Petcov and M. Piai, The LMA MSW solution of the solar neutrino problem, inverted neutrino mass hierarchy and reactor neutrino experiments, *Phys. Lett.* **B533** (2002) 94–106, doi:[10.1016/S0370-2693\(02\)01591-5](https://doi.org/10.1016/S0370-2693(02)01591-5).
- [56] S. Choubey, S.T. Petcov, and M. Piai, Precision neutrino oscillation physics with an intermediate baseline reactor neutrino experiment, *Phys. Rev.* **D68** (2003) 113006, doi:[10.1103/PhysRevD.68.113006](https://doi.org/10.1103/PhysRevD.68.113006).
- [57] F. An *et al.*, Neutrino physics with JUNO, *J. Phys.* **G43** (2016) 030401, doi:[10.1088/0954-3899/43/3/030401](https://doi.org/10.1088/0954-3899/43/3/030401).
- [58] A. Cervera *et al.*, Golden measurements at a neutrino factory, *Nucl. Phys.* **B579** (2000) 17–55, doi:[10.1016/S0550-3213\(00\)00221-2](https://doi.org/10.1016/S0550-3213(00)00221-2). [Erratum: *Nucl. Phys.* **B593** (2001) 731, doi:[10.1016/S0550-3213\(00\)00606-4](https://doi.org/10.1016/S0550-3213(00)00606-4)].
- [59] J. Bian *et al.*, Hyper-Kamiokande experiment: A Snowmass white paper, in *Snowmass 2021*, March 2022, doi:[10.48550/arXiv.2203.02029](https://doi.org/10.48550/arXiv.2203.02029).
- [60] B. Abi *et al.*, Long-baseline neutrino oscillation physics potential of the DUNE experiment, *Eur. Phys. J.* **C80** (2020) 978, doi:[10.1140/epjc/s10052-020-08456-z](https://doi.org/10.1140/epjc/s10052-020-08456-z).
- [61] N. Aghanim *et al.*, Planck 2018 results. VI. Cosmological parameters, *Astron. Astrophys.* **641** (2020) A6, doi:[10.1051/0004-6361/201833910](https://doi.org/10.1051/0004-6361/201833910). [Erratum: *Astron. Astrophys.* **652** (2021) C4, doi:[10.1051/0004-6361/201833910e](https://doi.org/10.1051/0004-6361/201833910e)].
- [62] A. Aguilar-Arevalo *et al.*, Evidence for neutrino oscillations from the observation of $\bar{\nu}_e$ appearance in a $\bar{\nu}_\mu$ beam, *Phys. Rev.* **D64** (2001) 112007, doi:[10.1103/PhysRevD.64.112007](https://doi.org/10.1103/PhysRevD.64.112007).
- [63] B. Armbruster *et al.*, Upper limits for neutrino oscillations $\bar{\nu}_\mu \rightarrow \bar{\nu}_e$ from muon decay at rest, *Phys. Rev.* **D65** (2002) 112001, doi:[10.1103/PhysRevD.65.112001](https://doi.org/10.1103/PhysRevD.65.112001).
- [64] A.A. Aguilar-Arevalo *et al.*, Improved search for $\bar{\nu}_\mu \rightarrow \bar{\nu}_e$ oscillations in the MiniBooNE experiment, *Phys. Rev. Lett.* **110** (2013) 161801, doi:[10.1103/PhysRevLett.110.161801](https://doi.org/10.1103/PhysRevLett.110.161801).
- [65] A.A. Aguilar-Arevalo *et al.*, Significant excess of electron-like events in the MiniBooNE short-baseline neutrino experiment, *Phys. Rev. Lett.* **121** (2018) 221801, doi:[10.1103/PhysRevLett.121.221801](https://doi.org/10.1103/PhysRevLett.121.221801).
- [66] P. Abratenko *et al.*, Search for an excess of electron neutrino interactions in MicroBooNE using multiple final-state topologies, *Phys. Rev. Lett.* **128** (2022) 241801, doi:[10.1103/PhysRevLett.128.241801](https://doi.org/10.1103/PhysRevLett.128.241801).
- [67] T.A. Mueller *et al.*, Improved predictions of reactor antineutrino spectra, *Phys. Rev.* **C83** (2011) 054615, doi:[10.1103/PhysRevC.83.054615](https://doi.org/10.1103/PhysRevC.83.054615).
- [68] G. Mention *et al.*, The reactor antineutrino anomaly, *Phys. Rev.* **D83** (2011) 073006, doi:[10.1103/PhysRevD.83.073006](https://doi.org/10.1103/PhysRevD.83.073006).

- [69] P. Huber, Determination of antineutrino spectra from nuclear reactors, *Phys. Rev.* **C84** (2011) 024617, doi:10.1103/PhysRevC.84.024617. [Erratum: *Phys. Rev.* **C85** (2012) 029901, doi:10.1103/PhysRevC.85.029901].
- [70] F.P. An *et al.*, Measurement of the reactor antineutrino flux and spectrum at Daya Bay, *Phys. Rev. Lett.* **116** (2016) 061801, doi:10.1103/PhysRevLett.116.061801.
- [71] P. Adamson *et al.*, Improved constraints on sterile neutrino mixing from disappearance searches in the MINOS, MINOS+, Daya Bay, and Bugey-3 experiments, *Phys. Rev. Lett.* **125** (2020) 071801, doi:10.1103/PhysRevLett.125.071801.
- [72] C. Giunti *et al.*, Gallium anomaly: critical view from the global picture of ν_e and $\bar{\nu}_e$ disappearance, *JHEP* **10** (2022) 164, doi:10.1007/JHEP10(2022)164.
- [73] R.L. Workman *et al.*, Review of particle physics, *PTEP* **2022** (2022) 083C01, doi:10.1093/ptep/ptac097.
- [74] P.F. Harrison, D.H. Perkins, and W.G. Scott, Tri-bimaximal mixing and the neutrino oscillation data, *Phys. Lett.* **B530** (2002) 167, doi:10.1016/S0370-2693(02)01336-9.
- [75] F. Vissani, Do experiments suggest a hierarchy problem? *Phys. Rev.* **D57** (1998) 7027–7030, doi:10.1103/PhysRevD.57.7027.
- [76] J.A. Casas, J.R. Espinosa, and I. Hidalgo, Implications for new physics from fine-tuning arguments. 1. Application to SUSY and seesaw cases, *JHEP* **11** (2004) 057, doi:10.1088/1126-6708/2004/11/057.
- [77] G. Aad *et al.*, Combined measurement of the Higgs boson mass in pp collisions at $\sqrt{s} = 7$ and 8 TeV with the ATLAS and CMS experiments, *Phys. Rev. Lett.* **114** (2015) 191803, doi:10.1103/PhysRevLett.114.191803.
- [78] G. Degrandi *et al.*, Higgs mass and vacuum stability in the Standard Model at NNLO, *JHEP* **08** (2012) 098, doi:10.1007/JHEP08(2012)098.
- [79] P. Minkowski, $\mu \rightarrow e\gamma$ at a rate of one out of 10^9 muon decays?, *Phys. Lett.* **B67** (1977) 421–428, doi:10.1016/0370-2693(77)90435-X.
- [80] M. Gell-Mann, P. Ramond, and R. Slansky. Complex spinors and unified theories, *Conf. Proc.* **C790927** (1979) 315–321, doi:10.48550/arXiv.1306.4669.
- [81] T. Yanagida. Horizontal gauge symmetry and masses of neutrinos, *Conf. Proc.* **C7902131** (1979) 95–99, [Inspire](#).
- [82] R.N. Mohapatra and G. Senjanovic, Neutrino mass and spontaneous parity violation, *Phys. Rev. Lett.* **44** (1980) 912, doi:10.1103/PhysRevLett.44.912.
- [83] M. Magg and C. Wetterich, Neutrino mass problem and gauge hierarchy, *Phys. Lett.* **B94** (1980) 61, doi:10.1016/0370-2693(80)90825-4.
- [84] J. Schechter and J.W.F. Valle, Neutrino masses in $SU(2) \otimes U(1)$ theories, *Phys. Rev.* **D22** (1980) 2227, doi:10.1103/PhysRevD.22.2227.
- [85] C. Wetterich, Neutrino masses and the scale of $B - L$ violation, *Nucl. Phys.* **B187** (1981) 343, doi:10.1016/0550-3213(81)90279-0.

- [86] G. Lazarides, Q. Shafi, and C. Wetterich, Proton lifetime and fermion masses in an SO(10) model, *Nucl. Phys.* **B181** (1981) 287–300, doi:10.1016/0550-3213(81)90354-0.
- [87] R.N. Mohapatra and G. Senjanovic, Neutrino masses and mixings in gauge models with spontaneous parity violation, *Phys. Rev.* **D23** (1981) 165, doi:10.1103/PhysRevD.23.165.
- [88] R. Foot *et al.*, Seesaw neutrino masses induced by a triplet of leptons, *Z. Phys.* **C44** (1989) 441, doi:10.1007/BF01415558.
- [89] E. Ma, Pathways to naturally small neutrino masses, *Phys. Rev. Lett.* **81** (1998) 1171–1174, doi:10.1103/PhysRevLett.81.1171.
- [90] A. Zee, A theory of lepton number violation, neutrino Majorana mass, and oscillation, *Phys. Lett.* **B93** (1980) 389, doi:10.1016/0370-2693(80)90349-4. [Erratum: *Phys. Lett.* **B95** (1980) 461, doi:10.1016/0370-2693(80)90193-8].
- [91] A. Zee, Charged scalar field and quantum number violations, *Phys. Lett.* **B161** (1985) 141, doi:10.1016/0370-2693(85)90625-2.
- [92] K.S. Babu, Model of “calculable” Majorana neutrino masses, *Phys. Lett.* **B203** (1988) 132, doi:10.1016/0370-2693(88)91584-5.
- [93] J.A. Casas and A. Ibarra, Oscillating neutrinos and $\mu \rightarrow e\gamma$, *Nucl. Phys.* **B618** (2001) 171–204, doi:10.1016/S0550-3213(01)00475-8.
- [94] A. Donini *et al.*, The minimal 3 + 2 neutrino model versus oscillation anomalies, *JHEP* **07** (2012) 161, doi:10.1007/JHEP07(2012)161.
- [95] M. Blennow *et al.*, Neutrinoless double beta decay in seesaw models, *JHEP* **07** (2010) 096, doi:10.1007/JHEP07(2010)096.
- [96] A. Ibarra, E. Molinaro, and S.T. Petcov, TeV scale see-saw mechanisms of neutrino mass generation, the Majorana nature of the heavy singlet neutrinos, and $(\beta\beta)_{0\nu}$ -decay, *JHEP* **09** (2010) 108, doi:10.1007/JHEP09(2010)108.
- [97] M. Mitra, G. Senjanovic, and F. Vissani, Neutrinoless double beta decay and heavy sterile neutrinos, *Nucl. Phys.* **B856** (2012) 26–73, doi:10.1016/j.nuclphysb.2011.10.035.
- [98] J. Lopez-Pavon, E. Molinaro, and S.T. Petcov, Radiative corrections to light neutrino masses in low-scale type I seesaw scenarios and neutrinoless double beta decay, *JHEP* **11** (2015) 030, doi:10.1007/JHEP11(2015)030.
- [99] R. Barbieri and A. Dolgov, Bounds on sterile-neutrinos from nucleosynthesis, *Phys. Lett.* **B237** (1990) 440–445, doi:10.1016/0370-2693(90)91203-N.
- [100] K. Kainulainen, Light singlet neutrinos and the primordial nucleosynthesis, *Phys. Lett.* **B244** (1990) 191–195, doi:10.1016/0370-2693(90)90054-A.
- [101] P. Hernandez, M. Kekic, and J. Lopez-Pavon, Low-scale seesaw models versus N_{eff} , *Phys. Rev.* **D89** (2014) 073009, doi:10.1103/PhysRevD.89.073009.
- [102] P. Hernandez, M. Kekic, and J. Lopez-Pavon, N_{eff} in low-scale seesaw models versus the lightest neutrino mass, *Phys. Rev.* **D90** (2014) 065033, doi:10.1103/PhysRevD.90.065033.
- [103] S. Dodelson and L.M. Widrow, Sterile-neutrinos as dark matter, *Phys. Rev. Lett.* **72** (1994) 17–20, doi:10.1103/PhysRevLett.72.17.

- [104] T. Asaka and M. Shaposhnikov, The ν MSM, dark matter and baryon asymmetry of the universe, *Phys. Lett.* **B620** (2005) 17–26, doi:[10.1016/j.physletb.2005.06.020](https://doi.org/10.1016/j.physletb.2005.06.020).
- [105] E. Bulbul *et al.*, Detection of an unidentified emission line in the stacked X-ray spectrum of galaxy clusters, *Astrophys. J.* **789** (2014) 13, doi:[10.1088/0004-637X/789/1/13](https://doi.org/10.1088/0004-637X/789/1/13).
- [106] A. Boyarsky *et al.*, Unidentified line in X-ray spectra of the Andromeda galaxy and Perseus galaxy cluster, *Phys. Rev. Lett.* **113** (2014) 251301, doi:[10.1103/PhysRevLett.113.251301](https://doi.org/10.1103/PhysRevLett.113.251301).
- [107] X.-D. Shi and G.M. Fuller, A new dark matter candidate: Nonthermal sterile neutrinos, *Phys. Rev. Lett.* **82** (1999) 2832–2835, doi:[10.1103/PhysRevLett.82.2832](https://doi.org/10.1103/PhysRevLett.82.2832).
- [108] A. Atre *et al.*, The search for heavy Majorana neutrinos, *JHEP* **05** (2009) 030, doi:[10.1088/1126-6708/2009/05/030](https://doi.org/10.1088/1126-6708/2009/05/030).
- [109] C. Ahdida *et al.*, Sensitivity of the SHiP experiment to heavy neutral leptons, *JHEP* **04** (2019) 077, doi:[10.1007/JHEP04\(2019\)077](https://doi.org/10.1007/JHEP04(2019)077).
- [110] A. Blondel *et al.*, Search for heavy right-handed neutrinos at the FCC-ee, *Nucl. Part. Phys. Proc.* **273-275** (2016) 1883–1890, doi:[10.1016/j.nuclphysbps.2015.09.323](https://doi.org/10.1016/j.nuclphysbps.2015.09.323).
- [111] P. Abreu *et al.*, Search for neutral heavy leptons produced in Z decays, *Z. Phys.* **C74** (1997) 57–71, doi:[10.1007/s002880050459](https://doi.org/10.1007/s002880050459). [Erratum: *Z. Phys.* **C75**, 580 (1997)].
- [112] G. Aad *et al.*, Search for heavy neutral leptons in decays of W bosons using a dilepton displaced vertex in $\sqrt{s} = 13$ TeV pp collisions with the ATLAS detector, *Phys. Rev. Lett.* **131** (2023) 061803 doi:[10.1103/PhysRevLett.131.061803](https://doi.org/10.1103/PhysRevLett.131.061803).
- [113] A. Tumasyan *et al.*, Search for long-lived heavy neutral leptons with displaced vertices in proton-proton collisions at $\sqrt{s} = 13$ TeV, *JHEP* **07** (2022) 081, doi:[10.1007/JHEP07\(2022\)081](https://doi.org/10.1007/JHEP07(2022)081).
- [114] J.C. Helo, M. Hirsch, and S. Kovalenko, Heavy neutrino searches at the LHC with displaced vertices, *Phys. Rev.* **D89** (2014) 073005, doi:[10.1103/PhysRevD.89.073005](https://doi.org/10.1103/PhysRevD.89.073005).
- [115] E. Izaguirre and B. Shuve, Multilepton and lepton jet probes of sub-weak-scale right-handed neutrinos, *Phys. Rev.* **D91** (2015) 093010, doi:[10.1103/PhysRevD.91.093010](https://doi.org/10.1103/PhysRevD.91.093010).
- [116] A.M. Gago *et al.*, Probing the Type I seesaw mechanism with displaced vertices at the LHC, *Eur. Phys. J.* **C75** (2015) 470, doi:[10.1140/epjc/s10052-015-3693-1](https://doi.org/10.1140/epjc/s10052-015-3693-1).
- [117] F. del Aguila and J. A. Aguilar-Saavedra, Distinguishing seesaw models at LHC with multi-lepton signals, *Nucl. Phys.* **B813** (2009) 22–90, doi:[10.1016/j.nuclphysb.2008.12.029](https://doi.org/10.1016/j.nuclphysb.2008.12.029).
- [118] G. Aad *et al.*, Search for heavy neutral leptons in decays of W bosons produced in 13 TeV pp collisions using prompt and displaced signatures with the ATLAS detector, *JHEP* **10** (2019) 265, doi:[10.1007/JHEP10\(2019\)265](https://doi.org/10.1007/JHEP10(2019)265).
- [119] A.M. Sirunyan *et al.*, Search for heavy neutral leptons in events with three charged leptons in proton-proton collisions at $\sqrt{s} = 13$ TeV, *Phys. Rev. Lett.* **120** (2018) 221801, doi:[10.1103/PhysRevLett.120.221801](https://doi.org/10.1103/PhysRevLett.120.221801).
- [120] A.D. Sakharov, Violation of CP invariance, C asymmetry, and baryon asymmetry of the universe, *Pisma Zh. Eksp. Teor. Fiz.* **5** (1967) 32–35, [*Usp. Fiz. Nauk* **161**(1991) 61–64, *Sov. Phys. Usp.* **34** (1991) 392–393, doi:[10.1070/PU1991v034n05ABEH002497](https://doi.org/10.1070/PU1991v034n05ABEH002497)].

- [121] G. 't Hooft, Symmetry breaking through Bell–Jackiw anomalies, *Phys. Rev. Lett.* **37** (1976) 8–11, doi:10.1103/PhysRevLett.37.8.
- [122] V.A. Kuzmin, V.A. Rubakov, and M.E. Shaposhnikov, On the anomalous electroweak baryon number nonconservation in the early universe, *Phys. Lett.* **B155** (1985) 36, doi:10.1016/0370-2693(85)91028-7.
- [123] M. D’Onofrio, K. Rummukainen, and A. Tranberg, Sphaleron rate in the minimal Standard Model, *Phys. Rev. Lett.* **113** (2014) 141602, doi:10.1103/PhysRevLett.113.141602.
- [124] C. Jarlskog, Commutator of the quark mass matrices in the Standard Electroweak Model and a measure of maximal CP violation, *Phys. Rev. Lett.* **55** (1985) 1039, doi:10.1103/PhysRevLett.55.1039.
- [125] M.B. Gavela *et al.*, Standard Model CP violation and baryon asymmetry. Part 2: Finite temperature, *Nucl. Phys.* **B430** (1994) 382–426, doi:10.1016/0550-3213(94)00410-2.
- [126] G.C. Branco *et al.*, A Bridge between CP violation at low energies and leptogenesis, *Nucl. Phys.* **B617** (2001) 475–492, doi:10.1016/S0550-3213(01)00425-4.
- [127] E.E. Jenkins and A.V. Manohar, Algebraic structure of lepton and quark flavor invariants and CP violation, *JHEP* **10** (2009) 094, doi:10.1088/1126-6708/2009/10/094.
- [128] M. Fukugita and T. Yanagida, Baryogenesis without grand unification, *Phys. Lett.* **B174** (1986) 45, doi:10.1016/0370-2693(86)91126-3.
- [129] K. Kajantie *et al.*, Is there a hot electroweak phase transition at $m_H \gtrsim m_W$?, *Phys. Rev. Lett.* **77** (1996) 2887–2890, doi:10.1103/PhysRevLett.77.2887.
- [130] E.K. Akhmedov, V. Rubakov, and A.Y. Smirnov, Baryogenesis via neutrino oscillations, *Phys. Rev. Lett.* **81** (1998) 1359–1362, doi:10.1103/PhysRevLett.81.1359.
- [131] L. Canetti, M. Drewes, T. Frossard, and M. Shaposhnikov. Dark matter, baryogenesis and neutrino oscillations from right handed neutrinos. *Phys. Rev.*, D87:093006, 2013, 1208.4607.
- [132] P. Hernandez *et al.*, Bounds on right-handed neutrino parameters from observable leptogenesis. *JHEP*, 12 (2022) 012, doi:10.1007/JHEP11(2023)153.
- [133] S. Sandner *et al.*, Predicting the baryon asymmetry with degenerate right-handed neutrinos, *JHEP* **11** (2023) 153, 10.1007/JHEP11(2023)153